DOI:10.14753/SE.2015.1809

Complex Cell Surface Distribution of Voltage- and Ligand-Gated Ion Channels on Cortical Pyramidal Cells

Ph.D. Dissertation

Katalin Szigeti M.D.

János Szentágothai Doctoral School of Neurosciences
Semmelweis University

Supervisor: Zoltán Nusser, D.V.M., D.Sc.

Official reviewers:
Károly Altdorfer, M.D., Ph.D.
Bence Rácz, Ph.D.

Head of the Final Examination Committee:
László Hunyadi, M.D., D.Sc.

Members of the Final Examination Committee:
Katalin Halasy, D.Sc.
Árpád Dobolyi, D.Sc.

Budapest, 2015

DOI:10.14753/SE.2015.1809

TABLE OF CONTENTS

DOI:10.14753/SE.2015.1809

DOI:10.14753/SE.2015.1809

DOI:10.14753/SE.2015.1809

ABBREVIATIONS

ACSF	artificial cerebrospinal fluid
AIS	axon initial segment
AP	action potential
bAP	backpropagating action potential
BSA	bovine serum albumin
CaMKII	Ca^{2+}/calmodulin-dependent protein kinase II
CA.	*Cornu Ammonis*
CNS	central nervous system
Cre^-	Cre-recombinase negative
Cre^+	Cre-recombinase positive
DG	dentate gyrus
DPPX	dipeptidyl peptidase-like type II proteins (i.e. DPP6, DPP10)
E-face	exoplasmic face
EPSPs	excitatory post synaptic potentials
FSINs	fast-spiking interneurons
$GABA_ARs$	$GABA_A$ receptors
GCs	granule cells
HCN	hyperpolarization-activated and cyclic nucleotide-gated channel
I_A	A-type current
I_H	H-type current
IMP	intramembrane particle
INs	interneurons
IPSCs	inhibitory postsynaptic currents
IUPHAR	International Union of Pharmacology
K_{2P}	two-pore domain potassium channel
K_{Ca}	Ca^{2+}-activated potassium channels
KChIPs	voltage-gated potassium channel-interacting proteins

DOI:10.14753/SE.2015.1809

K_{ir}	inwardly rectifying potassium channel
K_v	voltage-gated potassium channel
mIPSCs	miniature inhibitory postsynaptic currents
NGS	normal goat serum
NL-2	neuroligin-2
P	postnatal day
PA	picric acid
PALM	photoactivation localization microscopy
PB	phosphate buffer
PCs	pyramidal cells
PFA	paraformaldehyde
PKA	protein kinase A
PKC	protein kinase C
P-face	protoplasmic face
PSD	post synaptic density
PV	parvalbumin
SD	standard deviation
SDS	sodium dodecylsulphate
SDS-FRL	sodium dodecylsulphate-digested freeze-fracture replica labelling
SLM	stratum lacunosum-molculare
SO	stratum oriens
SP	stratum pyramidale
SR	stratum radiatum
STED	stimulation emission depletion
STORM	stochastic optical reconstruction microscopy
TBS	Tris-buffered saline
$\gamma2^-$	γ2 subunit-negative
$\gamma2^+$	γ2 subunit-positive

DOI:10.14753/SE.2015.1809

1. INTRODUCTION

1.1. General introduction−The role of ion channels in controlling the activity of cortical neurons

Our ability to perceive the environment relies on rapid communication between neurons. Neurons are information processing units that make connections and organize into dynamic networks in order to accomplish various functions. Although a variety of neurons are involved in information processing, they generally fall into two functional classes: principal (or projection) neurons and local circuit interneurons (INs). Principal neurons (which are the main interest of my dissertation) are the most numerous cellular elements of the brain; they receive information from thousands of neurons, which they process and transmit to other neurons that are usually long distances away. To achieve this rapid signalling, the neuronal membrane contains many ion channels, which are responsible for the action potential (AP) generation and propagation (Hille, 2001). The theory of AP propagation was discovered by Hodgkin and Huxley (Hodgkin & Huxley, 1952) who described changes in membrane permeability for Na^+ and K^+ ions following changes in membrane potential. A few years later the term ’channel’ was given to these ion conducting pores of cell membranes (Armstrong & Hille, 1998; Hille *et al.*, 1999).

The activity of a single cell is controlled by the orchestrated function of different types of voltage- (i.e. Na^+, K^+, Ca^{2+}) and ligand-gated (i.e. AMPA, NMDA, GABA receptor) ion channels (Fig. 1.). While voltage-gated ion channels are responsible for conducting electrical signals through large distances along the cell membrane, the activation of excitatory or inhibitory synapses through the ligand-gated ion channels induces small, localized changes in the membrane potential. The various voltage-gated ion channels differently control the excitability of nerve cells. A particular significance has been attributed to voltage-gated potassium channels due to their role in controlling AP propagation and neurotransmitter release (Debanne *et al.*, 1997; Lambe & Aghajanian, 2001). In addition, the excitability of principal cells (i.e. pyramidal cells (PCs)) is shaped by the activity of local INs, which synapse on different subcellular compartments of the cell (Klausberger & Somogyi, 2008). Synaptically-generated

DOI:10.14753/SE.2015.1809

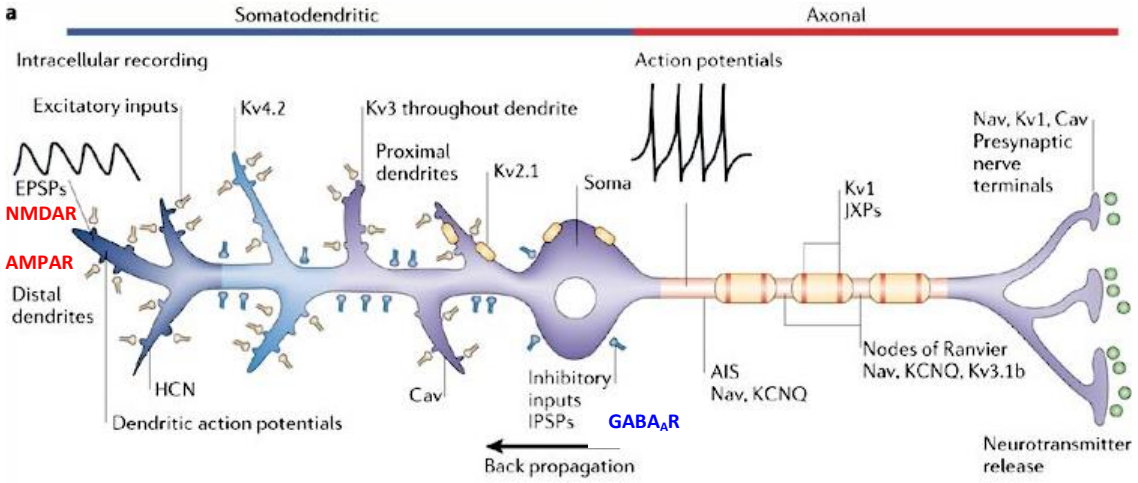

FIGURE 1. Functional role of voltage- and ligand-gated ion channels in controlling the excitability of principal cells. Sodium channels (Na_v) together with a subset of voltage-gated potassium channels (KCNQ, K_v1, $K_v3.1b$) are found in the axon initial segment (AIS), nodes of Ranvier, juxtaparanodes (JXPs) and nerve terminals where they contribute to action potential initiation, propagation and neurotransmitter release. Calcium channels (Ca_v) in nerve terminals regulate the transmitter release, while those in dendrites, together with the activation of NMDA and AMPA receptors contribute to local dendritic depolarization, which then propagates towards the soma. Dendritic HCN channels shape the postsynaptic response, while K_v4 channels control the action potential back-propagation. Inhibition of the nerve cell is mediated through $GABA_AR$ activation. *Modified from* (Lai & Jan, 2006).

signals are subjected to the regulatory influence of voltage-dependent ion channels that are activated by both anterograde, synaptically-induced membrane potential changes, and back-propagating action potentials (bAP) (Hoffman *et al.*, 1997; Magee, 1998; Migliore *et al.*, 1999; Cai *et al.*, 2004; Wang *et al.*, 2014).

Much of what we know about the distribution and influence of voltage-dependent ion channels comes from direct patch-pipette recordings from somata and apical dendrites within ~250 µm of the cell body (Hoffman *et al.*, 1997; Golding & Spruston, 1998; Chen & Johnston, 2005). For example, the A-type current (I_A), mediated by $K_v4.2$ subunits in hippocampal CA1 PCs, regulates the bAP (Hoffman *et al.*, 1997; Migliore *et al.*, 1999) and synaptic integration (Cai *et al.*, 2004; Makara *et al.*, 2009; Wang *et al.*, 2014). This, however, implies that the ion channels must be present in the plasma membrane and in close proximity to excitatory or inhibitory postsynaptic densities (PSDs). Interestingly, $K_v4.2$ channels have been localized to inhibitory postsynaptic specializations in the visual cortex and subiculum (Jinno *et al.*, 2005; Burkhalter *et al.*, 2006), which means that in these areas, $K_v4.2$ channels may be

DOI:10.14753/SE.2015.1809

modulated by synaptically released GABA, acting on $GABA_A$ receptors ($GABA_ARs$) clustered at the postsynaptic site. Conversely, the activation of $K_v4.2$ channels at GABAergic synapses clamps the postsynaptic membrane at or near the resting potential and weakens inhibition (Burkhalter *et al.*, 2006). However, $GABA_ARs$ have been found in the extrasynaptic plasma membrane as well (Somogyi *et al.*, 1989; Soltesz *et al.*, 1990; Nusser *et al.*, 1995; Kasugai *et al.*, 2010), where they are activated as a result of an increase in the ambient GABA concentration in the extracellular space (Farrant & Nusser, 2005) and together with voltage-gated ion channels can influence the membrane voltage of nerve cells. The question then arises, what determines the targeting of $GABA_ARs$ to either the synaptic or extrasynaptic plasma membrane? The current understanding is that the $GABA_AR$ γ2 subunit has an important role in clustering $GABA_ARs$ at inhibitory synapses (Essrich *et al.*, 1998; Schweizer *et al.*, 2003).

1.2. The role of potassium channels in controlling neuronal excitability

The concept of the excitable cell began with the discovery by Hodgkin and Huxley (Hodgkin & Huxley, 1952) of changes in the permeability of the squid giant axon membrane for Na^+ and K^+ ions during an AP. Using voltage-clamp recordings, they revealed an inward current generated by Na^+ entry into the cytoplasm, which was followed by an outward current mediated by K^+ ions. However, the direct evidence for the presence of ion-selective channels came from patch-clamp recordings, developed by Neher and Sakmann (Neher & Sakmann, 1976). With this technique, they were able to detect ionic currents through single acetylcholine receptor channels at the neuromuscular junction of frog skeletal muscle fibres. Later on, the emergence of cloning techniques revealed, the gene sequences of sodium, calcium and potassium channels and X-ray crystallography allowed the three-dimensional reconstruction of the channels (Doyle, 1998; Yu & Catterall, 2004; Long *et al.*, 2005; Yu *et al.*, 2005).

Ionic currents flowing through these channels result in changes in the membrane potential. If the membrane potential becomes more positive compared to the resting membrane potential and exceeds a threshold, an AP is generated, which then travels along the neurites of nerve cells. In a simplified view, the sodium channels are responsible for the rapid rising phase of the AP, while the falling phase is governed by

potassium channels. However, the existence of a huge number of genes encoding various ion channel subunits suggests a more complex contribution of individual ion channels to the AP initiation and propagation. Sodium and potassium channels in the dendrites are involved in the generation of local dendritic spikes (Spruston *et al.*, 1995; Larkum & Nevian, 2008; Kim *et al.*, 2012), while those in the axon initial segment (AIS) and nodes of Ranvier are responsible for AP generation and propagation, and juxtaparanodal potassium channels assist the AP conduction in myelinated axons (Chiu & Ritchie, 1981; Kole *et al.*, 2007; Shu *et al.*, 2007; Bender & Trussell, 2012; Kole & Stuart, 2012). Voltage-gated ion channels in axon terminals play roles in the regulation of neurotransmitter release (Dodson & Forsythe, 2004; Lai & Jan, 2006; Neher & Sakaba, 2008; Bucurenciu *et al.*, 2010).

Among ion channels, the potassium channels are the most numerous; there are over 70 genes encoding potassium channel subunits (Gutman *et al.*, 2003), suggesting that different subunits confer unique electrophysiological properties to each ion channel to fulfil distinct roles in regulating the excitability of nerve cells. The K_vs are exquisitely sensitive to small changes in membrane potential, some of them activating at low-voltage (K_v1, K_v4, K_v7), while others at high-voltage (K_v3, K_v2; Fig. 2.). Low-voltage-activated potassium channels open upon small depolarisations from around the

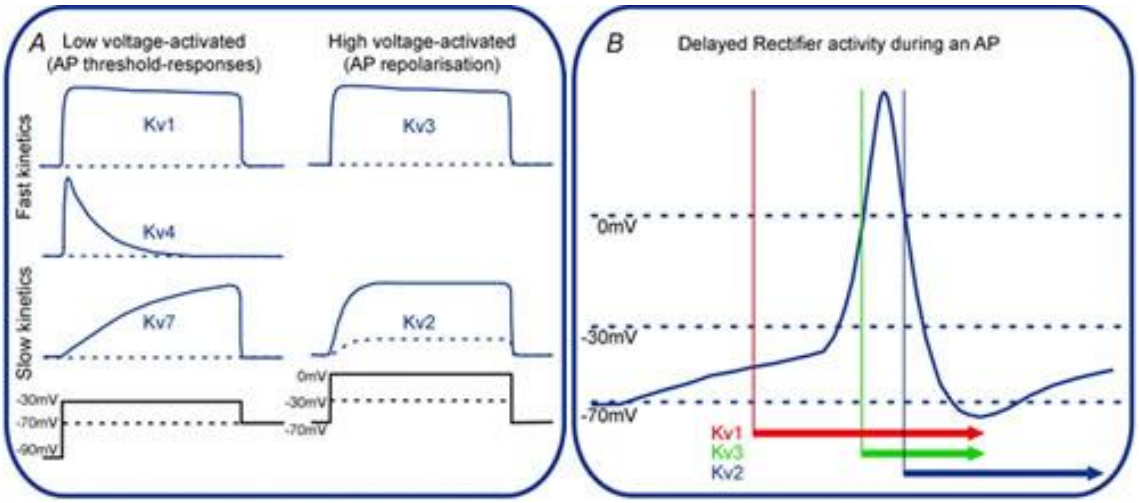

FIGURE 2. Functional classification of voltage-gated potassium channels. (A) Schematic representation of various potassium current waveforms evoked by voltage steps indicated in the bottom row. (B) Schematic drawing of an action potential shows that each channel activates over a characteristic period of an action potential waveform, as represented by the color-coded arrows. *Modified from* (Johnston *et al.*, 2010).

resting membrane potential, and therefore exert powerful control on the number of APs a cell fires upon the arrival of excitatory post synaptic potentials (EPSP). High-voltage-activated potassium channels are activated when an AP is generated, and due to their fast kinetics they control the duration of APs, and therefore regulate the repetitive firing properties of neurons. The resting membrane potential is generally set by the inward rectifying potassium channel (K_{ir}) family and by the two-pore domain potassium channel (K_{2P}) family (Enyedi & Czirjak, 2010; Luscher & Slesinger, 2010; Mathie *et al.*, 2010).

In addition to the functional heterogeneity, cell type and compartment-specific distribution of K_vs can influence the electrophysiological behaviour of nerve cells, and inhomogeneity in the distribution of ion channels can also have an impact. A good example for such non-uniform voltage-gated channel distribution is the hyperpolarization-activated and cyclic nucleotide-gated (HCN) channel, found in neocortical and hippocampal PCs. Electrophysiological experiments demonstrated that in CA1 PCs, dendritic H-type current (I_H) density increases as a function of distance from the soma (Magee, 1998), which is the result of a distance dependent increase in the HCN1 (Lorincz *et al.*, 2002) and HCN2 (Notomi & Shigemoto, 2004) subunit densities. This greatly influences the propagation of subthreshold voltage transients by decreasing the amplitude and duration of EPSPs and reducing the degree of temporal summation of the EPSPs. Similarly, the K_v4 channel-mediated I_A density shows a distance dependent increase along the somato-dendritic axis of CA1 PCs, which greatly attenuates the back-propagation of APs in the apical dendrites (Hoffman *et al.*, 1997; Migliore *et al.*, 1999).

1.2.1. Molecular diversity of potassium channels

Our knowledge of potassium channels originates from the genetic and molecular analysis of potassium channel genes in the fruit fly *Drosophila melanogaster*. These early studies resulted in the isolation of cDNAs encoding the potassium channel α subunit encoded at the Shaker gene locus in *Drosophila melanogaster*. Later on the identification of three additional genes, named Shab, Shal, and Shaw and finally the KCNQ, Eag, Erg and Elk genes were described in *Drosophila* (Jan & Jan, 1997). Using the Shaker cDNAs, Tempel et al. (Tempel *et al.*, 1987) isolated the first mammalian

potassium channel cDNA, the K_v1.1. This was followed by the isolation of many other genes, resulting in over 70 genes encoding potassium channel subunits in the mammalian brain (http://iuphar-db.org; Fig. 3.). The increasing number of subtypes necessitated the introduction of sequence homology-based nomenclature (Chandy, 1991) by the International Union of Pharmacology (IUPHAR), which was further complemented with the newly discovered subfamilies (Gutman *et al.*, 2003).

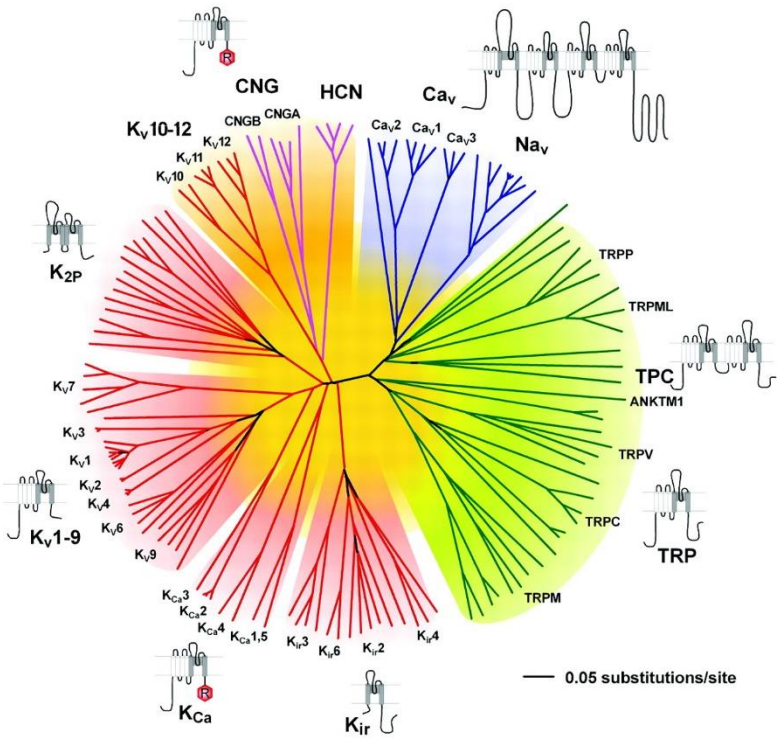

FIGURE 3. The voltage-gated ion channel superfamily. Polygenetic tree showing the 143 members of the structurally-related voltage-gated ion channel genes, with each group highlighted by a different colour. Note that potassium channels (red) form the most diverse group. (Yu *et al.*, 2005)

Four main potassium channel families have been identified (Fig. 4.). (1) The largest group is formed by the K_v channels, which are macromolecular protein complexes containing four transmembrane pore-forming subunit, termed α subunit. These individual potassium channel α subunits have six transmembrane segments (termed S1–S6) that co-assemble to form tetrameric complexes. The S1–S4 segments form the voltage-sensing domain and the S5–S6 segments make up the pore domain. Additional auxiliary subunits can be assembled to the channels, which can modulate their cell surface expression and kinetics (Vacher *et al.*, 2008). (2) The Ca^{2+}-activated

DOI:10.14753/SE.2015.1809

potassium channels (K_{Ca}) contain six or seven transmembrane domains to form tetramers, and open upon changes in the intracellular Ca^{2+} concentration. Some K_{Ca} channels also show voltage-dependent gating. (3) Members of the K_{2P} family are composed of four transmembrane domain and two P loops, and they form dimers. They are often called ”leak channels” because they are constantly active at the resting membrane potential of nerve cells and conduct a background potassium current to keep the cell membrane near the equilibrium potential for K^+. (4) The K_{ir} channels derive their name from their capacity to conduct K^+ inward more readily than outward. However, at physiological membrane potentials, these channels mediate K^+ efflux, therefore decreasing the excitability of neurons (Luscher & Slesinger, 2010). K_{ir} channels have the simplest transmembrane topology, having two transmembrane segments (M1 and M2) with a P loop. The channels are not gated by changes in trans-

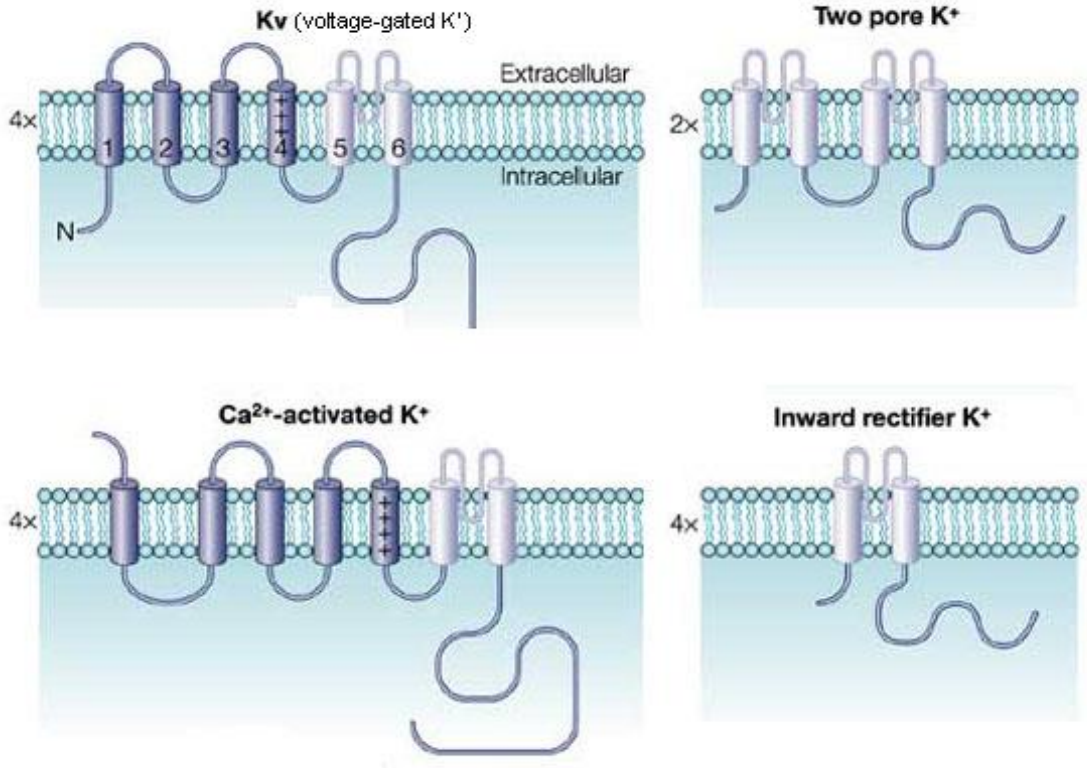

FIGURE 4. The main potassium channel families. Schematic drawings depicting the channel structures for the four main potassium channel categories. Voltage-gated, Ca^{2+}-activated (K_{Ca}), and inward rectifier (K_{ir}) potassium channels have four transmembrane domains while the two-pore potassium channels (K_{2P}) have two. *Modified from* (Swartz, 2004).

DOI:10.14753/SE.2015.1809

membrane voltage; a subtype of these channels, the $K_{ir}3$ subunits, are activated by G protein-coupled receptors (e.g. $GABA_B$, acetylcholine, dopamine, opioid, serotonin, somatostatin and adenosine receptors).

In conjunction with molecular cloning of potassium channels, technical improvement in the field of electrophysiology as well as the development of subunit specific antibodies represented the next step towards our understanding about the distribution of potassium channels. A combination of *in situ* hybridization histochemistry with immunohistochemical or immunofluorescence techniques using subunit-specific antibodies provided detailed descriptions of the regional, cellular and subcellular distribution of many of the potassium channel subunits (Trimmer & Rhodes, 2004; Lai & Jan, 2006; Vacher *et al.*, 2008).

1.2.2. The importance of K_v4.2 channels in the brain

The K_v4 channels received particular attention as they are responsible for the classical I_A, a transient potassium current with low activation threshold close to the resting membrane potential in most neurons (Birnbaum *et al.*, 2004). I_A has a major role in a large variety of dendritic processes, including the control of local sodium spike initiation and propagation (Losonczy *et al.*, 2008), the back-propagation of axonally-generated APs into the dendrites (Hoffman *et al.*, 1997; Migliore *et al.*, 1999), synaptic integration and plasticity (Margulis & Tang, 1998; Cash & Yuste, 1999; Watanabe *et al.*, 2002; Frick *et al.*, 2004; Kim & Hoffman, 2008; Makara *et al.*, 2009).

Early immunohistochemical studies demonstrated the widespread distribution of K_v4.2 and K_v4.3 subunits in the central nervous system (Serodio & Rudy, 1998). The mRNA for K_v4.2 was found at high levels in many principal cells, whereas K_v4.3 was found in a subset of principal cells and in many INs (Trimmer & Rhodes, 2004). Light microscopic immunohistochemical studies revealed strong K_v4.2 immunosignal in the dendritic layers of the hippocampal CA1 area (Maletic-Savatic *et al.*, 1995; Varga, 2000; Rhodes *et al.*, 2004; Jinno *et al.*, 2005), suggesting a unique role for K_v4.2 homotetramers in this region. This is further supported by a gene deletion study demonstrating that in hippocampal CA1 PCs dendritic I_A is exclusively mediated by the K_v4.2 subunit (Chen *et al.*, 2006). It has been noticed, that the intensity of the

immunoperoxidase or fluorescent signal is rather uniform across stratum radiatum (SR) with a slight decrease in the stratum lacunosum-moleculare (SLM). This is in sharp contrast with the finding of Hoffman et al. (Hoffman *et al.*, 1997), who by using dendritic patch-clamp recordings revealed a six-fold increase in the density of I_A as a function of distance from proximal to distal main apical dendrites. One possible explanation for the discrepancy between the density of I_A and that of $K_v4.2$ immunolabelling is, that the oblique dendrites or dendritic spines or axon terminals contain a high density of $K_v4.2$ subunit, which are superimposed and therefore mask the increasing, but lower density of $K_v4.2$ subunit in the main apical dendrites. Although $K_v4.2$ subunits have been localized to the dendritic region of the CA1 area with light microscopy, it is still unknown if the increased current density in the apical dendrites of CA1 PCs is indeed the result of an increased channel number.

1.2.3. The importance of $K_{ir}3$ channels in the brain

Potassium channels formed by the $K_{ir}3$ subunits are the effectors of many G-protein coupled receptors and are potent regulators of neuronal excitability. Mammals express four $K_{ir}3$ channel subunits: $K_{ir}3.1$-3.4. In the brain, $K_{ir}3.1$-3.3 subunits are common, (Lujan *et al.*, 2009; Luscher & Slesinger, 2010), whereas $K_{ir}3.4$ expression is low and therefore does not make a substantial contribution to cerebral $K_{ir}3$ currents (Wickman *et al.*, 2000). Out of the three main neuronal $K_{ir}3$ subunits, the $K_{ir}3.2$ subunit is unique in that it can form homotetramers as well as heterotetramers with other $K_{ir}3$ subunits (e.g. $K_{ir}3.1$–$K_{ir}3.2$ and $K_{ir}3.2$–$K_{ir}3.3$; (Kofuji *et al.*, 1995; Lesage *et al.*, 1995; Slesinger *et al.*, 1996)). It is an essential part of the functional channel, determining its cell surface localization (Ma *et al.*, 2002). Biochemical and molecular studies have shown that the $K_{ir}3.1$–$K_{ir}3.2$ variant is the predominant form of $K_{ir}3$ channels in the brain (Liao *et al.*, 1996). Lack of $K_{ir}3.2$ subunit leads to reduced $K_{ir}3.1$ subunit expression (Liao *et al.*, 1996; Signorini *et al.*, 1997) and to the loss of slow inhibitory postsynaptic responses in hippocampal PCs (Luscher *et al.*, 1997). Mice without the $K_{ir}3.2$ subunit also have high susceptibility for epilepsy (Signorini *et al.*, 1997). A major G-protein-coupled receptor activating $K_{ir}3$ channels is the metabotropic $GABA_B$ receptor ($GABA_B$Rs; (Luscher *et al.*, 1997)). Recent studies have suggested the

existence of a signalling complex that contains $GABA_BRs$, G proteins and $K_{ir}3$ channels (David *et al.*, 2006; Fowler *et al.*, 2007). These studies further emphasize the role of $K_{ir}3$ channels in mediating slow inhibition onto the postsynaptic cell.

Whole-cell patch-clamp and cell-attached recordings have shown the dendritic localization of $K_{ir}3$ channels in neocortical neurons and in hippocampal CA1 PCs (Takigawa & Alzheimer, 1999; Chen & Johnston, 2005). Moreover, in hippocampal CA1 PCs the level of spontaneous channel activity was significantly higher in apical dendrites than in somata (Takigawa & Alzheimer, 1999; Chen & Johnston, 2005). This increase may come from increased open probability of the channels or increased channel numbers. Indeed, light microscopic immunohistochemistry revealed a gradual increase in the strength of immunoreactivity for the $K_{ir}3.1$, $K_{ir}3.2$ and $K_{ir}3.3$ subunits in distal SR and SLM (Ponce *et al.*, 1996; Koyrakh *et al.*, 2005; Kulik *et al.*, 2006; Fernandez-Alacid *et al.*, 2011). However, the strength of the immunoreaction cannot be taken as direct evidence for an increased channel number in the distal apical dendrites of CA1 PCs. The increased immunoreactivity might have pre- or postsynaptic origin, thus it is possible that axon terminals or oblique dendrites and spines have higher $K_{ir}3$ channel density, which masks the lower but increasing density of $K_{ir}3$ channels in the apical dendrites. Electron microscopic immunogold studies have revealed that these subunits are mainly concentrated to dendritic shafts and spines in dendritic layers of the CA1 area, and occasionally gold particles were observed in axon terminals (Koyrakh *et al.*, 2005; Kulik *et al.*, 2006; Fernandez-Alacid *et al.*, 2011). In spite of detailed subcellular localization studies, the relative densities of $K_{ir}3$ channels in different axo-somato-dendritic compartments at increasing distances from the soma are still unknown.

1.3. The role of GABAergic inhibition in controlling neuronal excitability

Cortical information processing reflects the interplay of synaptic excitation and inhibition. The combination of these two synaptic conductances has a great impact on the membrane potential and input resistance of principal cells, and plays a fundamental role in regulating neuronal output. However, a special interest was attributed to inhibition because of its key role in shaping cortical activity. Perisomatic inhibition mediated by basket cells expressing either the molecular marker parvalbumin (PV) or

cholecystokinin (Somogyi & Klausberger, 2005) has a special role in controlling the output of principal cells. These cells were shown to control sodium-dependent APs (Miles *et al.*, 1996) and spike timing in CA1 PCs (Pouille & Scanziani, 2001) by limiting the temporal summation of EPSPs within a narrow time window (less than 2 milliseconds), thus making PCs coincidence detectors (Konig *et al.*, 1996). In addition to this, several studies described the role of perisomatic inhibition in network oscillations (Cobb *et al.*, 1995; Losonczy *et al.*, 2010; Royer *et al.*, 2012).

Cortical INs exert their activation by releasing the major inhibitory neurotransmitter molecule GABA, which activates ionotropic $GABA_AR$s and metabotropic $GABA_BR$s. The $GABA_BR$ is G_i/G_o protein-coupled, and thus in addition to association with membrane channels (i.e. $K_{ir}3$, Ca_v), it has effects on adenylate cyclase activity. As a result, activation of $GABA_BR$s has a slow modulatory effect on distinct neuronal compartments (Bettler *et al.*, 2004; Chalifoux & Carter, 2011). In contrast, ionotropic $GABA_AR$s, permeable to Cl^- and HCO^{3-}, mediate fast, phasic inhibition, when concentrated in synapses (Farrant & Nusser, 2005). However, activation of $GABA_AR$s outside the synapse can also affect neuronal excitability, but these ionic currents are regarded as tonic currents (Farrant & Nusser, 2005). $GABA_AR$s are the subject of the second part of my dissertation, therefore in the following chapters I will present a detailed description of the receptor superfamily.

1.3.1. Molecular and functional diversity of $GABA_A$ receptors

$GABA_AR$s are the major inhibitory receptors in the central nervous system (CNS) and belong to the ligand-gated ion channel superfamily. $GABA_AR$s are pentamers, each subunit is composed of four transmembrane α-helices that form an intrinsic anion selective channel (Fig. 5). With the complete sequence of the human genome and few other vertebrate species, it is now clear that there are 19 genes for $GABA_AR$s (Simon *et al.*, 2004). These include: six α, three β, three γ, one δ, one ε, one π and one θ $GABA_AR$s subunits, and three ρ subunits, which have been called $GABA_C$ receptors (Zhang *et al.*, 2001). Many $GABA_AR$ subtypes contain the α-, β- and γ-subunits with the likely stoichiometry of two α, two β and one γ (Olsen & Sieghart, 2008), which are arranged pseudo-symmetrically around the ion channel in the sequence

DOI:10.14753/SE.2015.1809

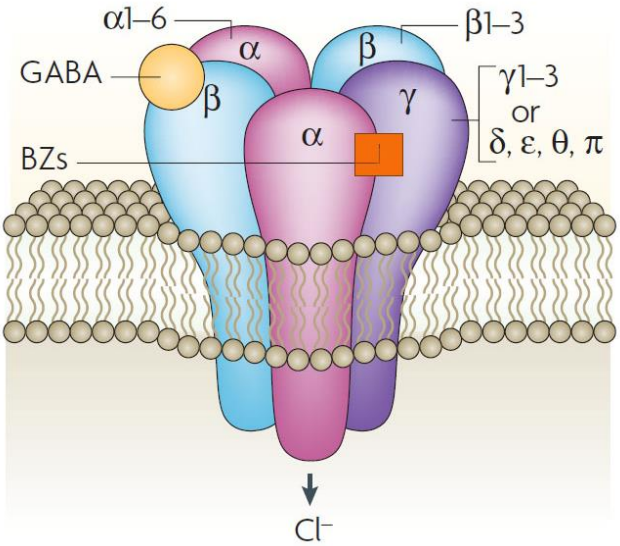

FIGURE 5. Structure of $GABA_ARs$. Five subunits from seven subunit subfamilies (α, β, γ, δ, ε, θ and π) assemble to form a heteropentameric Cl^--permeable channel. Usually two α subunits, two β subunits and one γ subunit forms the ion channel; the γ subunit can be replaced by δ, ε, θ or π subunits. Binding of the neurotransmitter GABA occurs at the interface between the α and β subunits, and the benzodiazepine (BZs) binding occurs at the interface between the α and γ subunits. (Jacob *et al.*, 2008)

of γ–β–α–β–α, anti-clockwise when viewed from the synaptic cleft (Baumann *et al.*, 2002). It is thought, that the majority of $GABA_ARs$ contain a single type of α- and β-subunit variant. The α1β2γ2 heteropentamer constitutes the largest population of $GABA_ARs$ in the CNS, followed by the α2β3γ2 and α3β3γ2 isoforms (Benke *et al.*, 1991a; Benke *et al.*, 1991b; Somogyi *et al.*, 1996). Receptors that incorporate the α4-α5-or α6-subunits, or the β1-, γ1-, γ3-, δ-, ε- and θ-subunits, are less numerous. GABA binding occurs at the β–α subunit interface and the γ–α subunit interface creates the benzodiazepine binding site. A second site for benzodiazepine binding has recently been shown to occur at the β–α interface (Sigel & Luscher, 2011).

The combinatorial co-assembly of these various subunit proteins underlies the structural heterogeneity of $GABA_ARs$ which is the key determinant of their pharmacological and functional diversity. The pharmacology of $GABA_ARs$ will be influenced by the γ and the α subunits, without major contribution of the β subunit. Receptors containing the γ2 subunit exhibit higher benzodiazepine sensitivity than the ones containing the γ1 subunit (Sieghart, 1995; Khom *et al.*, 2006). Receptors containing the γ3 subunit are modulated by benzodiazepine ligands, but with altered selectivity (Sieghart, 1995; Hevers & Luddens, 1998). The type of α subunit gives

another layer of complexity to the receptor pharmacology; distinct α subunit-containing receptors show different sensitivity to the benzodiazepine site ligands (Olsen & Sieghart, 2008). The type of subunit does not only determine receptor pharmacology, but the kinetic properties of $GABA_AR$-mediated inhibitory postsynaptic currents (IPSCs) are also influenced (Eyre *et al.*, 2012). Furthermore, the subunit composition greatly determines the cell surface distribution and dynamic regulation of $GABA_ARs$ (Farrant & Nusser, 2005). With the development of subunit-specific antibodies it became evident that different brain regions and cell-types show unique expression patterns for most of the $GABA_ARs$, whereas the γ2 subunit is expressed in almost every brain region and cell type (Wisden *et al.*, 1992; Fritschy & Mohler, 1995; Pirker *et al.*, 2000).

1.3.2. The role of the γ2 subunit in clustering $GABA_A$ receptors at inhibitory postsynaptic specializations

Studies using light microscopic immunofluorescence and electron microscopic immunogold methods allowed the precise subcellular localization of $GABA_AR$ α1, α2, α3, α6, β2/3 and γ2 subunits within the postsynaptic specializations of GABAergic synapses in many brain regions, including the cerebellum, globus pallidus, hippocampus and neocortex (Fritschy & Mohler, 1995; Nusser *et al.*, 1995; Somogyi *et al.*, 1996; Nusser *et al.*, 1998; Panzanelli *et al.*, 2011). Some of these subunits were also found in extrasynaptic plasma membranes (Farrant & Nusser, 2005; Kasugai *et al.*, 2010); cell surface receptors are highly mobile, they can distribute dynamically between synaptic and extrasynaptic locations (Jacob *et al.*, 2005; Triller & Choquet, 2005; Bogdanov *et al.*, 2006).

Receptors incorporating the γ2 subunit cluster at GABAergic synapses and they mediate fast inhibitory synaptic currents, regarded as phasic inhibition (Fig.6.A.) (Farrant & Nusser, 2005). This is particularly important, as the rapid synchronous activation of postsynaptic $GABA_ARs$ exerts a spatially and temporally localized inhibitory conductance to the postsynaptic neuron. In a subset of cells, the δ subunit is incorporated into the heteropentamer receptor channel in the place of the γ2 subunit, but these receptors were found exclusively in the extrasynaptic plasma membrane, where

they respond to the ambient concentration of GABA and exert a slow tonic inhibition onto the postsynaptic cell (Fig. 6.B.) (Farrant & Nusser, 2005). The δ subunit forms receptors specifically with the α6 and β2/3 subunits in cerebellar granule cells (GCs), and with the α4 and α1 subunits in thalamus and dentate gyrus (DG) GCs (Olsen & Sieghart, 2008), and in a subset of DG INs, respectively (Glykys *et al.*, 2007).

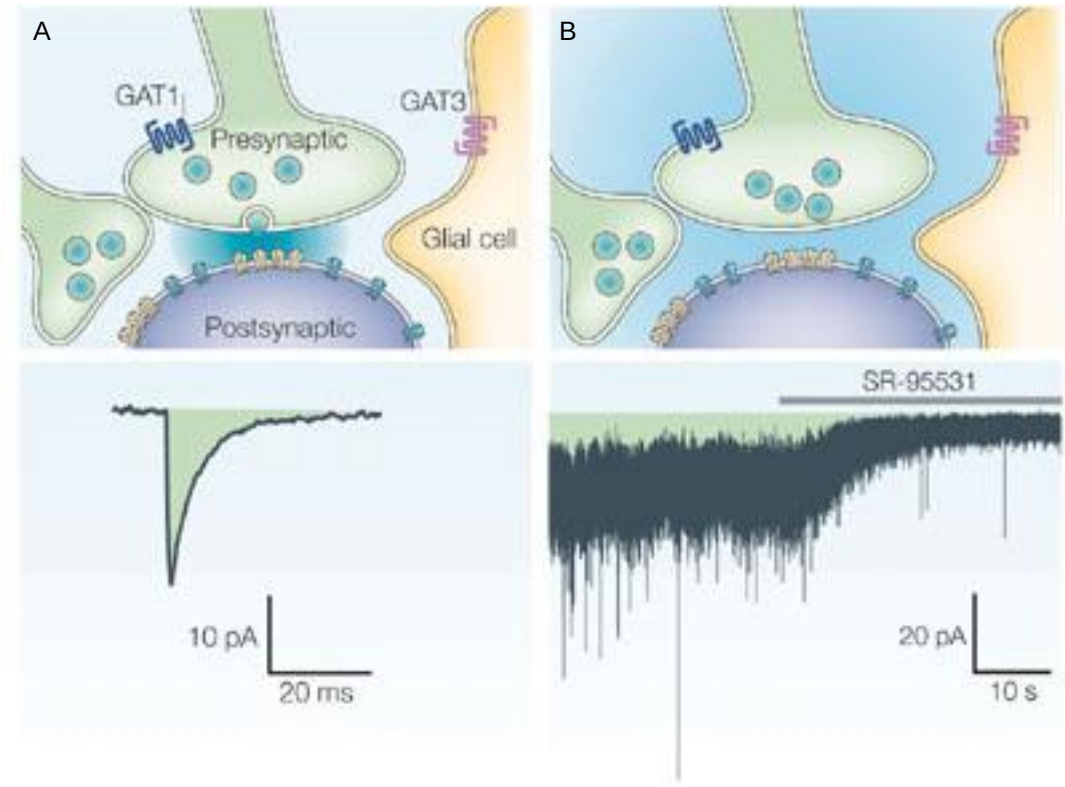

FIGURE 6. $GABA_AR$ localization and modes of activation. (A) $GABA_ARs$ clustered in the membrane beneath the release site (yellow) will be activated by the release of a single vesicle from the presynaptic nerve terminal. The blue shading indicates the spread of released GABA. Below the image averaged waveform of miniature inhibitory postsynaptic currents (mIPSCs) is shown. (B) Low concentration of ambient GABA (blue shading) activates $GABA_ARs$ localized in the extrasynaptic plasma membrane. The trace shows the tonic current that results from stochastic opening of these $GABA_ARs$, with superimposed phasic currents. The $GABA_AR$ antagonist, SR-95531 blocks the phasic current and the tonic current, causing an outward shift in the holding current. *Modified from* (Farrant & Nusser, 2005).

The PSD of GABAergic synapses contains a large repertoire of proteins which were shown to have a role in the targeting and stabilization of $GABA_ARs$ at the synapse. Gephyrin is the most important scaffolding protein for the stabilization of $GABA_ARs$ at both GABAergic and glycinergic synapses (Fritschy *et al.*, 2008; Tyagarajan &

Fritschy, 2014). In addition to this, the role of neuroligin-2 (NL-2) and collybistin was also described (Luscher *et al.*, 2011); NL-2 can interact with gephyrin to specifically activate collybistin, and subsequently guide membrane tethering of the inhibitory postsynaptic scaffold, together with the recruitment of $GABA_A$Rs to these sites (Poulopoulos *et al.*, 2009). However, some studies (Essrich *et al.*, 1998; Schweizer *et al.*, 2003) indicate the crucial role of γ2 subunits, as its deletion resulted in profound reduction in the clustering of both $GABA_A$Rs and gephyrin.

The uniqueness of the γ2 subunit is further emphasized by the fact that genetic deletion of the γ2, but not the α and β subunits, led to early postnatal lethality (Gunther *et al.*, 1995; Homanics *et al.*, 1997; Sur *et al.*, 2001; Vicini *et al.*, 2001). This rendered more difficult the study of γ2 subunit function in the CNS; therefore early studies were performed either in new-born animals (Gunther *et al.*, 1995), cell cultures (Essrich *et al.*, 1998; Brunig *et al.*, 2002; Alldred *et al.*, 2005) or upon developmentally-timed, Cre-recombinase-mediated deletion (Schweizer *et al.*, 2003). Although the study by Gunther et al. (Gunther *et al.*, 1995) reported no change in the mRNA expression and regional and subcellular distribution of major $GABA_A$R subunits, other gene deletion studies (Essrich *et al.*, 1998; Brunig *et al.*, 2002; Schweizer *et al.*, 2003; Alldred *et al.*, 2005; Sumegi *et al.*, 2012; Rovo *et al.*, 2014) have unequivocally found that clustering of the α1, α2 and β2/3 subunits in cells obtained from $\gamma2^{-/-}$ mice were disrupted. Interestingly, Essrich et al. (Essrich *et al.*, 1998) reported that some of the cultured neurons from $\gamma2^{-/-}$ mice exhibited $GABA_A$R-mediated IPSCs, despite the complete removal of the γ2 subunit. A previous study from our laboratory (Sumegi *et al.*, 2012) also detected $GABA_A$R-mediated IPSCs in $\gamma2^{-/-}$ cultured neurons, demonstrating that $GABA_A$Rs could still generate synaptic-like currents without the γ2 subunit. However, it should be noted that the presence of synaptic-like currents does not necessarily mean that the underlying $GABA_A$Rs are concentrated within the GABAergic postsynaptic specializations.

1.4. Structural organization of the studied brain areas

The cerebral cortex is the thin outer layer of the cerebral hemispheres that is responsible for much of the planning and execution of actions in everyday life.

DOI:10.14753/SE.2015.1809

Phylogenetically, the most recent part of the cortex is the neocortex, and the more ancient part of the cortex is the archicortex, which includes the hippocampus. In order to understand how such complex structures operate, one has to break down to its elementary structures (i.e. cells) and study the molecular organization of individual nerve cells, moreover the properties of individual synapses which together greatly influence the function of nerve cells. To address the aims of my dissertation, I studied the rodent hippocampus (Chapter 4.1. and 4.2.) and somatosensory cortex (Chapter 4.3).

The neocortex has six layers, which are numbered with Roman numerals from superficial to deep. Layer I is the molecular layer, which contains the dendrites of the cells located in the deeper layers, and very few neurons; layer II the external granular layer, is composed of small spherical cells; layer III the external pyramidal layer, contains many cell types; layer IV the internal granular layer; layer V is the internal pyramidal layer; and layer VI the multiform, or fusiform layer. The number of layers and the structural organization vary throughout the cortex; for example, the primary visual cortex has an extremely prominent layer IV that typically is further subdivided into at least three sublayer, in contrast, the primary motor cortex has no layer IV (Shepherd, 2004).

There are two basic types of neurons: projection neurons with spiny dendrites, which are excitatory (i.e. stellate cells and PCs), and local INs with smooth dendrites, which are inhibitory (Fig. 7.). Stellate and PCs are confined to layers II/III, IV, V and VI, whereas INs can be found throughout the cortical layers, where contact distinct subcellular compartments of principal cells, and comprise the most diverse cell population of the cortex. On one hand, their heterogeneity arises from their morphological diversity, which is attributable to their axonal arborisations that selectively target different compartments of PCs; e.g. basket cells inhibit the somatic and proximal dendritic region of principal cells, axo-axonic or Chandelier cells target the AIS, and Martinotti cells synapse on the apical dendritic region of PCs. On the other hand, the electrophysiological properties confer another layer of diversity; based on firing pattern, INs are classified as fast-spiking, non-adapting non-fast spiking, adapting, irregular spiking, intrinsic bursting and accelerating (Ascoli *et al.*, 2008). Finally, the protein expression is also characteristic to certain IN subtypes (Somogyi &

DOI:10.14753/SE.2015.1809

Klausberger, 2005; Klausberger & Somogyi, 2008; Eyre *et al.*, 2009; DeFelipe *et al.*, 2013).

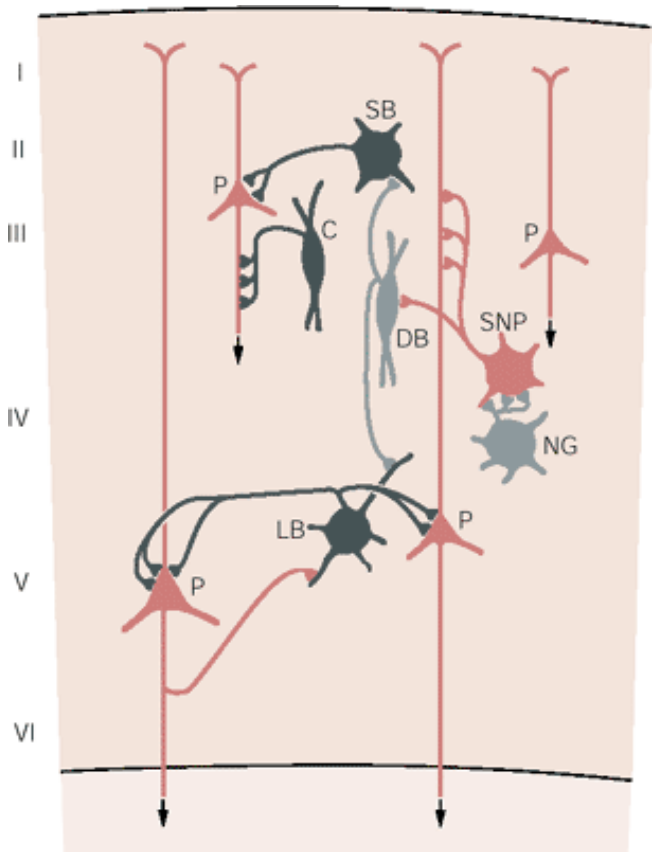

FIGURE 7. Synaptic organization of the neocortex. Principal cells (red) of the neocortex, including pyramidal cells (P) and spiny non-pyramidal cells (SNP) are localized to different layers and send long range excitatory connections to subcortical and cortical areas. Different types of GABAergic interneurons (grey) have different connections with principal cells. Chandelier cells (C) terminate exclusively on the axon initial segment of pyramidal cells; the large and small basket cells (LB, SB) innervate the perisomatic region; double bouquet cells (DB) innervate other interneurons; the neurogliaform cells (NG) can also inhibit other nearby cortical neurons by releasing the neurotransmitter GABA into the extracellular space. *Adapted from* (Kandel, 2000)

The neocortex receives input from the thalamus (layer IV), from other cortical regions on both sides of the brain (layer I to III) and from a variety of other sources, including the locus coeruleus (axons containing noradrenalin, mostly in layer VI), the ventral tegmental area and substantia nigra (dopaminergic pathway in all layers, except layer IV), the raphe (serotoninergic fibres in all layers), and the basal forebrain (cholinergic fibres in all layers; (Shepherd, 2004)). Layers V and VI, primarily connect the neocortex with subcortical regions, whereas layer II/III PCs give rise to corticocortical projections.

DOI:10.14753/SE.2015.1809

The hippocampus is probably the most widely studied and most thoroughly characterized region of the brain, which is attributable to its relative simple anatomical structure and its critical role in learning and memory, revealed in the 1950s (Scoville & Milner, 1957). The hippocampal formation includes the DG, hippocampus (*Cornu Ammonis,* CA), and subiculum. The hippocampus was further divided into subregions, termed CA1, CA2 and CA3 region. The hippocampal formation has also laminar organization; however, in contrast to the neocortex has a single cell layer, containing the principal cells. There are two types of principal cells in the hippocampus: the GCs in the DG, which lie in the granule cell layer, and the PCs in CA1 to CA3 regions, found in the pyramidal cell layer (PCL). Layers below and above the principal cell layer contain the local INs, which based on axonal target area, differently influence the activity of principal cells (Somogyi & Klausberger, 2005; Klausberger & Somogyi, 2008).

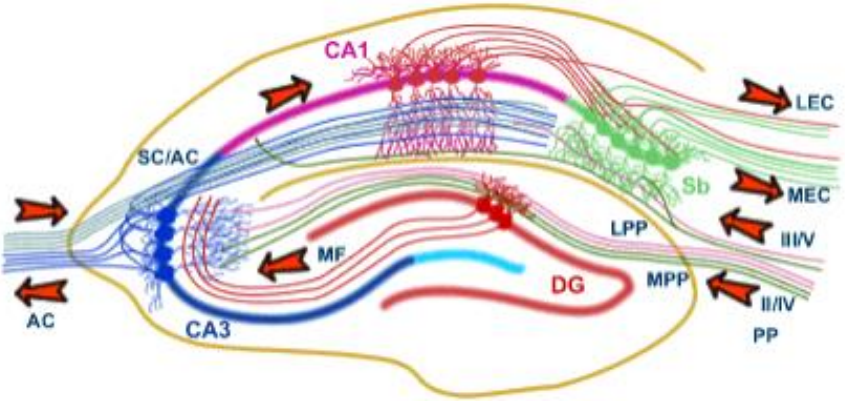

FIGURE 8. The thri-synaptic circuit of the hippocampus. The main input of the hippocampus originates from the entorhinal cortex (EC) that forms connections on granule cells of the dentate gyrus (DG) and pyramidal neurons of the hippocampus (CA3 to CA1) via the perforant path (PP). CA3 pyramidal neurons also receive input from the DG via the mossy fibers (MF). They send axons to the CA1 pyramidal cells via the Schaffer collaterals (SC) and to the contralateral CA1 region via the associational commissural pathway (AC). CA1 neurons send axons to the pyramidal cells of the subiculum (Sb), which send axons back to the EC. *Adapted from University of Bristol, Centre for Synaptic Plasticity (http://www.bristol.ac.uk/synaptic/pathways)*

The DG is the first stage of the hippocampal tri-synaptic circuit (Fig. 8.). Its main input is the perforant path, which originates from the superficial layers of the entorhinal cortex. In addition, the DG receives GABAergic and cholinergic input from the medial septum and the diagonal band of Broca. The principal neurons of the DG are the GCs,

which give rise to unmyelinated axons called the mossy fibres that project to the CA3 region.

The CA3 region receives input from the mossy fibres of DG GCs and the perforant path from the entorhinal cortex. The mossy fibre pathway terminates on the proximal dendrites of PCs, in the stratum lucidum, while the perforant path terminates on the distal dendrites of CA3 PCs, in the stratum lacunosum-moleculare (SLM). PCs of the CA3 region project towards the CA2 and CA1 areas (where form the Schaffer collaterals). CA3 PCs also send recurrent connections to other CA3 cells in the septal or dorsal direction. In addition, the CA3 region sends output fibres to the lateral septum. CA2 is a small region between CA3 and CA1. It receives perforant path input but does not receive mossy fibre connections, and its PCs are more similar to those in CA3 than those in the CA1 region.

The CA1 region forms the most significant output of the hippocampal circuit to the subiculum and to the layer V of the entorhinal cortex. It receives input from the superficial entorhinal cortex along the perforant pathway, which terminates in the SLM on the distal dendrites of CA1 PCs. Schaffer collaterals synapse on the proximal dendrites, in the stratum radiatum (SR). Unlike CA3, the CA1 region contains very few recurrent connections, which enter the stratum oriens (SO) and the PCL.

The subiculum receives its primary input from the CA1 region and from layer III of entorhinal cortex. Sends output to layer V of entorhinal cortex, but it also projects into many other areas, including the nucleus accumbens, the anterior thalamic nuclei, the medial mammillary nucleus, the lateral septum, and the presubiculum.

1.5. SDS-digested freeze-fracture replica labelling electron microscopy to study the two-dimensional distribution of membrane proteins

Most of our knowledge on the distribution of ion channels comes from light microscopic immunofluorescence and immunoperoxidase reactions (Fritschy & Mohler, 1995; Ponce *et al.*, 1996; Pirker *et al.*, 2000; Trimmer & Rhodes, 2004; Koyrakh *et al.*, 2005; Panzanelli *et al.*, 2011). Although these methods have high sensitivity, it does not allow the determination of exact ion channel densities, and it has been difficult to study sub-synaptic structures because the small size of the synapse is close to the diffraction-limited resolution of light microscopy. Nowadays with the development of new super-resolution techniques (stimulation emission depletion (STED); stochastic optical

reconstruction microscopy; photoactivation localization microscopy (PALM); reviewed by Maglione and Sigrist (Maglione & Sigrist, 2013)) it become possible to study the protein architecture of small subcellular structures such as synapses (Kittel *et al.*, 2006; Dani *et al.*, 2010). However, unlike electron microscopy, they do not provide intrinsic contrast of membranes, which is particularly powerful for identifying structures such as the synaptic cleft or vesicles or when the plasma membrane distribution of a given ion channel is investigated in distinct axo-somato-dendritic compartments. Electron microscopic immunoperoxidase studies of potassium channel subunits K_v4.2 (Alonso & Widmer, 1997) and K_v3.1b (Sekirnjak *et al.*, 1997) revealed the first plasma membrane labelling. However, due to the diffusible nature of the reaction end-product of the peroxidase enzyme reaction, this method is not suitable for quantification. In contrast, pre-embedding and post-embedding immunogold methods are more suitable for high-resolution localization and quantification of molecules (Nusser, 1999). However, gold particles representing membrane protein epitopes are distributed on either side of the membrane, therefore specific control must be done to confirm that the antibody recognizes the desired target. A limitation of the post-embedding immunogold method is imposed by resins, which restrict antibody diffusion; therefore only those antigen molecules are detected which are exposed at the section surface (Amiry-Moghaddam & Ottersen, 2013). Limitations of these electron microscopic techniques were overcome, by a new electron microscopic immunogold technique, the sodium dodecylsulphate-digested freeze-fracture replica labelling (SDS-FRL; (Fujimoto, 1995)).

Freeze-fracture electron microscopy has been established as a major technique in ultrastructure research since the 1950s (Steere, 1957). The technique provided great advances in our understanding of the two-dimensional structural organisation of cellular membranes and organelles. However, it was as late as in the 1990s, when it became possible to identify the chemical nature of the structural components of cell membranes revealed by freeze-fracture electron microscopy. By combining the freeze-fracture technique with immunogold cytochemistry (what has been called SDS-FRL), Fujimoto was the first to describe immunogold labelling of intercellular junction proteins (Fujimoto, 1995). This was followed by many other descriptions as well as quantitative analysis of the molecular components of the neuronal plasma membrane, including gap junction proteins, plasma membrane receptors, ion channels and proteins related to the

release machinery (Nagy *et al.*, 2004; Hagiwara *et al.*, 2005; Tanaka *et al.*, 2005; Masugi-Tokita & Shigemoto, 2007; Tarusawa *et al.*, 2009; Kasugai *et al.*, 2010; Kaufmann *et al.*, 2010; Indriati *et al.*, 2013).

The critical feature of the SDS-FRL technique is the fracture plane, which often follows a plane through the central hydrophobic core of the frozen membranes, splitting them into half-membrane leaflets (Fig. 9.A). The result is a three-dimensional view of the plasma membrane, with en face views of the membrane interior. The fractured membrane halves correspond to a phospholipid monolayer with associated proteins: the membrane half located adjacent to the protoplasm is called protoplasmic-face (P-face), while the membrane half adjacent to the extracellular space is called exoplasmic-face (E-face; Fig. 9.B). Details of the plasma membrane are made visible in the electron microscope by making a thin carbon-platinum-carbon replica of the fracture plane. The platinum is evaporated onto the specimen at an angle, so that it is deposited in varying thicknesses according to the topography of the fractured surface. As a result, high-resolution details of membrane structure are revealed, so that the integral membrane proteins (regarded as intramembrane particles (IMPs)) become visible. The tissue from the replica is removed by digestion with sodium dodecylsulphate (SDS). Although SDS dissolves unfractured portions of the membrane, it would not digest the split membrane halves, as their apolar domains are positioned against, and stabilized by, their carbon/

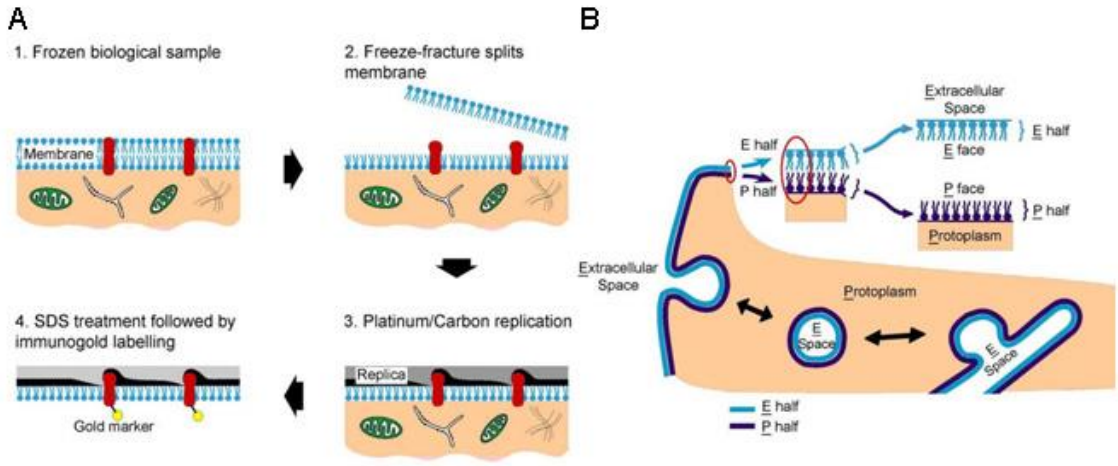

FIGURE 9. SDS-digested freeze-fracture replica-labelling. (A) The key steps in SDS-FRL: 1. Tissue is frozen. 2. The freeze-fracture process splits the lipid bilayer exposing the fracture face. 3. The specimen is evaporated by carbon/platinum/carbon. 4. The replica is treated with SDS to remove the tissue, followed by immunogold labelling. (B) Schematic illustrations of the two membrane halves after freeze-fracturing. *Modified from* (Robenek & Severs, 2008).

DOI:10.14753/SE.2015.1809

platinum/carbon casts (Fujimoto, 1995), therefore it is possible to label both the inner (P-face) and the outer (E-face) leaflets of the cellular membranes. Depending on the epitope of a given primary antibody against the studied membrane protein, the immunogold labelling will be visualized either on the P-face or the E-face. The key steps of performing SDS-FRL are illustrated in Fig. 9., and will be described in details in Chapter 3.5. The major advantage of the technique is its high sensitivity (Tanaka *et al.*, 2005) and the possibility of multiple labelling. Therefore, to address the aims of my dissertation I adopted the SDS-FRL technique.

DOI:10.14753/SE.2015.1809

2. AIMS OF THE DISSERTATION

In the first part of the dissertation my general aims were to investigate the cell surface distribution of two different potassium channels in rat CA1 PCs by using the highly selective high-resolution SDS-FRL method. In the second part of the dissertation I used the Cre-dependent virus-mediated γ2 subunit deletion strategy in combination with light microscopic immunofluorescent and electron microscopic SDS-FRL techniques to challenge the longstanding view on the role of γ2 subunits in clustering $GABA_A$Rs at inhibitory postsynaptic specializations.

My specific aims for the first part are:

1. What is the precise subcellular distribution pattern of the two potassium channel subunit (K_v4.2, K_{ir}3.2) on distinct axo-somato-dendritic compartments in CA1 PCs?
2. Does the K_v4.2 channel density follow the six-fold increase in I_A density along the proximo-distal axis of PCs?
3. Is the increased K_{ir}3 channel activity in the distal dendrites of CA1 PCs mirrored by an increased channel density?

My specific aims for the second part are:

1. Is the γ2 subunit necessary for clustering $GABA_A$Rs at inhibitory postsynaptic specializations in the sensorimotor cortex of $GABA_AR\gamma2^{77I}$lox mice?
2. What is the precise subcellular location of $GABA_A$Rs underlying the miniature IPSCs (mIPSCs) in cortical layer 2/3 cells lacking the γ2 subunit?
3. What is the subunit composition and densities of synaptic $GABA_A$Rs in neurons lacking the γ2 subunit?

Contributions:

The study on the role of the γ2 subunit (Chapter 4.3) was done in collaboration with my colleague Dr. Mark D. Eyre. He performed all whole-cell patch-clamp recordings that I am not going to present in this dissertation, while I carried out all light microscopic immunofluorescent and electron microscopic immunogold labellings of distinct $GABA_A$R subunits. In addition, the tonic $GABA_A$R-mediated current recordings presented in Chapter 4.3.3 were performed by Mark Eyre.

DOI:10.14753/SE.2015.1809

3. MATERIALS AND METHODS

All experimental procedures were carried out in accordance with the ethical guidelines of the Institute of Experimental Medicine of the Hungarian Academy of Sciences, which is in line with the European Union regulation of animal experimentations.

3.1. Virus injection

Male and female mice in which the γ2 gene is flanked by two loxP sites, and the 77th amino acid is mutated from phenylalanine to isoleucine ($GABA_AR\gamma2^{77I}$lox mice; (Wulff *et al.*, 2007) between 22 and 40 days postnatal (P) were anaesthetized with a mixture of ketamine:piplophen:xylazine (62.5:6.25:12.5 μg (g body weight)$^{-1}$) and 0.6 μl adeno-associated virus expressing a Cre-GFP fusion protein with a nuclear localization signal motif under a human synapsin promoter (AAV2/9 .hSynapsin. hGHintron. GFP-Cre. WPRE. SV40 (p1848), University of Pennsylvania Vector Core, Philadelphia, USA) was stereotaxically injected into the somatosensory cortex at 0.1 μl min^{-1} flow rate. The Cre-lox system is a tool for generating tissue-specific knockout mice and reporter mouse strains (Nagy, 2000). The Cre-recombinase of the P1 bacteriophage belongs to the integrase family of site-specific recombinases. It catalyses the recombination between two of its recognition sites, called loxP (Hamilton & Abremski, 1984). When the target gene (in my dissertation the γ2 gene) is flanked by two loxP sites oriented in the same direction, upon Cre-recombinase activation (here introduced virally into a small portion of the somatosensory cortex), the target gene will be deleted.

After the surgery the animals were allowed to recover either 2 weeks or 6 weeks. Slices for electrophysiological recordings were prepared 2 weeks after injection.

3.2. Tissue preparation for fluorescent immunohistochemistry and SDS-FRL

Adult male Wistar rats (P25–P52; n = 17), male wild-type (n = 3) and Kv4.2$^{-/-}$ mice (P68–P217; kindly provided by Prof. Daniel Johnston; n = 3) as well as male and

female $GABA_AR\gamma2^{77I}lox$ mice (P36–P80; n = 22) were deeply anesthetized with ketamine (0.5ml/100g). The animals were transcardially perfused with ice cold saline solution for one minute than followed by a fixative. For light microscopic immunofluorescent reactions animals were perfused with a fixative containing either 2 % or 4 % paraformaldehyde (PFA) and 15v/v % picric acid (PA) made up in 0.1 M phosphate buffer (PB) for 15–20 minutes, or with 2 % PFA in 0.1M Na-acetate for 15 minutes. Some animals were perfused with ice cold oxygenated artificial cerebrospinal fluid (ACSF) for 4 minutes followed by 50 minutes postfixation in 4 % PFA and 15v/v % PA in 0.1 M BP (Notter *et al.*, 2014). Afterwards 60 or 70 μm coronal forebrain sections were cut with a vibratome (VT1000S; Leica Microsystems, Wetzlar, Germany). For SDS-FRL animals were perfused with a fixative containing 2 % PFA and 15v/v % PA in 0.1 M PB for 15–16 minutes. Coronal sections of 80 μm thickness were cut, and then small tissue blocks from the dorsal hippocampus and from injected somatosensory cortex were trimmed. Tissue blocks from the injected cortical area were cut out based on the endogenous GFP signal in a way that a small non-injected area surrounded the injection zone. Sections were then cryoprotected overnight in 30 % glycerol.

3.3. Acute slice preparation for tonic $GABA_A$ receptor-mediated current recordings

Injected mice (n = 12) were deeply anaesthetized with Isoflurane (Abbott Laboratories Kft., Budapest, Hungary). After decapitation, the brain was removed and placed into ice-cold ACSF containing (in mM): 230 sucrose, 2.5 KCl, 25 glucose, 1.25 NaH_2PO_4, 24 $NaHCO_3$, 4 $MgCl_2$, and 0.5 $CaCl_2$. Coronal slices from the cerebral cortex were cut at 250 μm thickness with a vibratome (VT1000S; Leica Microsystems) and were stored in ACSF containing (in mM): 126 NaCl, 2.5 KCl, 25 glucose, 1.25 NaH_2PO_4, 24 $NaHCO_3$, 2 $MgCl_2$ and 2 $CaCl_2$. All extracellular solutions were bubbled continuously with 95% O_2 and 5% CO_2, resulting in a pH of 7.4. After a 30 minute recovery period at 33 °C, slices were further incubated at room temperature until they were transferred to the recording chamber.

3.4. Fluorescent immunohistochemistry

Following several washings in 0.1 M PB and Tris-buffered saline (TBS), free-floating sections were blocked in 10 % normal goat serum (NGS), followed by an overnight incubation in the primary antibody solution made up in TBS containing 2 % NGS and 0.1 % Triton X-100. The used primary antibodies are listed in Table 1. Next, sections were incubated in a mixture of secondary antibody solutions made up in TBS containing 2 % NGS with or without 0.1 % Triton X-100 for 2 hours. The following secondary antibodies were used: A488-conjugated goat anti-rabbit (1:500; Life Technologies, Carlsbad, CA, USA) and goat anti-guinea pig IgGs (1:500; Life Technologies), Cy3-conjugated goat anti-rabbit (1:1000; Jackson ImmunoResearch Europe Ltd, Newmarket, UK) and donkey anti-guinea pig IgGs (1:1000, Jackson) and Cy5-conjugated goat anti-mouse IgGs (1:500, Jackson). Finally, the sections were washed and mounted on glass slides in Vectashield (Vector Laboratories, Burlingame, CA, USA). Images from the CA1 region and from injected or non-injected cortices were acquired using a confocal laser scanning microscope (FV1000; Olympus, Tokyo, Japan) with 10X (NA = 0.4), 20X (NA = 0.75) or 60X (NA = 1.35) objectives.

3.5. SDS-FRL

Small tissue blocks from the CA1 region and injected cortex were frozen in a high-pressure freezing machine (HPM 100, Leica Microsystems, Vienna, Austria) and fractured at -135 ºC in a freeze-fracture machine (BAF060, Leica Microsystems). The fractured tissue surfaces were coated with thin layers of carbon (5 nm), platinum (2 nm) and carbon (20 nm). Tissue debris from the replicas were digested in a solution containing 2.5 % SDS and 20 % sucrose in TBS (pH = 8.3) at 80 ºC overnight. Following several washes in TBS containing 0.05 % bovine serum albumin (BSA), replicas were blocked in TBS containing 0.1 %–5 % BSA for 1 hour, then incubated overnight in blocking solution containing the primary antibodies listed in Table 1. Replicas were then incubated for 2 hours in TBS containing either 1 % or 5 % BSA and the following secondary antibodies: goat anti-rabbit IgGs coupled to 10 nm gold particles (1:100; British Biocell International, Cardiff, UK), goat anti-mouse IgGs

DOI:10.14753/SE.2015.1809

Table 1. Primary antibodies used in the immunoreactions and reference to their specificity. Numbers in the top right index of dilutions indicate the type of immunoreactions: 1 – fluorescent immunohistochemistry; 2 – SDS-FRL.

Primary antibody	Source, Cat. number	Antigen	Species	Dilution	Specificity, characterization, reference
Kv4.2	Alomone Labs, Jerusalem, Israel; APC-023	aa 454–469	Rabbit	1:500[1]	this study
				1:5000[2]	this study
PSD-95	Millipore, MA, USA; MAB1598	rat-PSD-95	Mouse	1:3000[2]	
$GABA_AR\beta3$	NeuroMab, Davis, CA, USA; 75-149	aa 370–433	Mouse	1:800[2]	labelling pattern as published with other β3 antibodies
SNAP-25	SySy, Goettingen, Germany; 111 001	aa. 20–40	Mouse	1:5000[2]	(von Kriegstein & Schmitz, 2003)
Kir3.1	Frontier Inst., Hokkaido, Japan; GIRK1-Rb-Af530-1	aa 469–501	Rabbit	1:500[1]	(Aguado *et al.*, 2008)
Kir3.2	Alomone Labs; APC-006	aa 374–414	Rabbit	1:200[1]	(Koyrakh *et al.*, 2005; Kulik *et al.*, 2006)
				1:600[2]	
Kir3.3	Frontier Inst.; GIRK3-Rb-Af750-1	aa 358–389	Rabbit	1:500[1]	(Aguado *et al.*, 2008)
pan-Neurofascin	NeuroMab; 75-027	aa 1066–1174	Mouse	1:150[2]	(Schafer *et al.*, 2004)
Cre	Millipore; MAB3120	aa 77–343	Mouse	1:5000[1]	
$GABA_AR\gamma2$	gift from Prof. JM Fritschy		Guinea Pig	1:1000[1]	(Gunther *et al.*, 1995)
$GABA_AR\alpha1$	gift from Prof. JM Fritschy		Rabbit	1:1000[1]	(Benke *et al.*, 1991a)
				1:1000[2]	
$GABA_AR\beta3$	SySy; 224 404	aa 344–429	Guinea Pig	1:500[1]	labelling pattern as published with other β3 antibodies
				1:600[2]	
$GABA_AR\gamma2$	SySy; 224 004	aa 39–67	Guinea Pig	1:500[2]	labelling pattern as published with other γ2 antibodies
$GABA_AR\gamma2$	SySy; 224 003	aa 39–67	Rabbit	1:600[2]	labelling pattern as published with other γ2 antibodies
Neuroligin-2	SySy; 129 203	aa 732–749	Rabbit	1:1000[2]	(Briatore *et al.*, 2010))
$GABA_AR\delta$	gift from Prof. W Sieghart	aa 1–44	Rabbit	1:500[1]	(Jones *et al.*, 1997; Tretter *et al.*, 2001; Peng *et al.*, 2002)
Parvalbumin	Swant, Marly, Switzerland; 235		Mouse	1:1000[1]	(Celio *et al.*, 1988)
$GABA_AR\alpha1$	gift from Prof. JM Fritschy		Guinea Pig	1:1000[1]	(Kralic *et al.*, 2006)
Gephyrin	SySy; 147 021	aa 268–270	Mouse	1:500[1]	
Kv3.1b	NeuroMab; 75-041	aa 437–585	Mouse	1:500[1]	
$GABA_AR\alpha4$	gift from Prof. W Sieghart	aa 1–14	Rabbit	1:500[1]	(Bencsits *et al.*, 1999)
Kv2.1	Upstate, Lake Placid, NY, USA; 05-411	aa 509–853	Mouse	1:1000[1]	
$GABA_AR\alpha5$	gift from Prof. JM Fritschy		Guinea Pig	1:2000[1]	(Fritschy *et al.*, 1997)

coupled to 5 or 15 nm gold particles (1:100 or 1:50; British Biocell) and goat anti-guinea pig IgGs coupled to 5 nm gold particles (1:50; British Biocell). In double-labelling reactions, a mixture of the two primary antibodies was applied, followed by a mixture of the two secondary antibodies. For $GABA_AR$ labelling in cortex, the antibodies were applied sequentially as follows: on the first day, the primary antibody raised in guinea-pig was applied overnight at room temperature; on the second day, goat-anti guinea-pig IgGs coupled to 5 nm gold particles diluted in 5 % BSA was applied to label the first primary antibody, and this was followed by the application of the second primary antibody (raised in rabbit); on the third day, goat-anti rabbit IgGs coupled to 10 nm gold particles was applied to label the second primary antibody. Finally, replicas were rinsed in TBS and distilled water before they were picked up on copper parallel bar grids. Specimens were analysed with a transmission electron microscope (JEM-1011, JEOL Ltd., Tokyo, Japan).

3.6. Quantitative analysis of immunogold labelling for the $K_v4.2$ and $K_{ir}3.2$ subunits in the rat CA1 region

Quantitative analysis of immunogold labelling for the $K_v4.2$ and the $K_{ir}3.2$ subunits was performed on CA1 PC somata, AISs, 11 different dendritic compartments and axon terminals from SR and SLM of the CA1 area (n = 5 rats for each subunit). The subcellular compartments were imaged with a Cantega G2 camera at 10000-12000X magnifications and were grouped based on their calculated distance from the SP. The distance (d) of an individual process (P) from the SP was calculated from the position of the SP and from the stage coordinate of the process (X; Y) using the following equation:

$$d_{P(X;\,Y)} = |(y2 - y1)\cdot X + (x1 - x2)\cdot Y + x2\cdot y1 - x1\cdot y2| / \sqrt{(y2 - y1)^2 + (x1 - x2)^2}$$

Position of the SP was determined by an imaginary line connecting two end points of the SP with coordinates (x1; y1) and (x2; y2), respectively. According to this, layers were categorized as follows: 0-120 μm: proximal SR; 120-240 μm: middle SR; 240-360 μm: distal SR and above 360 μm: SLM. Main apical dendrites, oblique dendrites and dendritic spines were grouped according to these criteria. CA1 PC main apical dendrites were identified based on their large diameter and the presence of spines. Oblique

dendrites were identified based on their small diameter and the presence of at least one emerging spine from the dendritic shaft. Spines were identified based on either their ultrastructure (e.g. small diameter structure emerging from a dendrite) or from the presence of a PSD on isolated spine heads (identified by labelling the PSD-95; n = 2 rats for the $K_v4.2$). In these double-labelling reactions the mean density of immunogold particles labelling for the $K_v4.2$ subunit in dendritic spines was not significantly different ($p > 0.05$, Student's *t*-test) than that found in single-labelling reactions, therefore the data were pooled together. Axon terminals were identified either based on the presence of gold particles labelling SNAP-25 (n = 3 rats for $K_v4.2$); or based on the presence of an active zone facing a PSD on the opposing E-face of a spine or dendrite (n = 3 rats for $K_{ir}3.2$). For the $K_{ir}3.2$ subunit AISs were also imaged from SP and stratum oriens (SO). To unequivocally identify the AISs pan-Neurofascin was used as a molecular marker. The $GABA_AR$ β3 subunit was used to identify GABAergic synapses on PC somata and dendrites. Antibodies against the $K_v4.2$ and $K_{ir}3.2$ subunits recognized intracellular epitopes on their target proteins and consequently were visualized by gold particles on the P-face. Nonspecific background labelling was measured on E-face structures surrounding the measured P-faces, as described previously (Lorincz & Nusser, 2010) and was subtracted from the mean gold particle densities of different subcellular compartments. Gold particle counting and area measurements were performed with iTEM software (Olympus Soft Imaging Solutions, Münster, Germany). Gold particle densities are presented as mean ± standard deviation (SD) between animals. Statistical comparisons were performed with STATISTICA software (Scientific Computing, Rockaway, NJ, USA) and significance was taken as $p < 0.05$.

3.7. Quantification of immunogold particles labelling $GABA_A$ receptors in somata of cortical neurons from injected $GABA_AR\gamma2^{77I}$lox mice

For quantifying the immunogold particles labelling different $GABA_AR$ subunits, the 'mirror replica' technique was used (Hagiwara *et al.*, 2005). I made double-replica pairs, where one face of the replica was labelled for NL-2, a protein known to be present in GABAergic synapses (Varoqueaux *et al.*, 2004). This labelling was visualized on the

P-face in agreement with the cytoplasmic location of the epitope recognised by the NL-2 antibody. In a set of experiments the guinea-pig anti- $GABA_AR$ β3 antibody was co-labelled with NL-2. The complementary face of the replica (in this case, the E-face) was labelled for either the rabbit anti-$GABA_AR$ γ2 alone, or the guinea pig anti-$GABA_AR$ γ2 and rabbit anti-$GABA_AR$ α1 were co-localized. First, somata of layer 2/3 cells were randomly chosen at low magnifications, and images were taken at 15000X–25000X magnification for all NL-2-containing synapses and for the surrounding extrasynaptic regions on a given soma. Then, the complementary face of the replica was scanned to locate the same soma based on nearby morphological landmarks, and the mirror half of the same synapses were imaged. The synaptic area in each image was delineated based on the IMP cluster and the NL-2 labelling on the P-face using the closed polygon tool of the ITEM software (Olympus Soft Imaging Solutions). The E-face image was then superimposed on the P-face image in Photoshop CS3, and the synaptic area was projected onto the E-face image. Gold particles inside this polygon shaped synaptic area and up to 30 nm away from its edges were counted for NL-2, γ2, α1 and β3 subunits on both faces of a replica. I considered only those synapses in which a minimum of four gold particles labelling the NL-2 were present. Only intact and completely fractured synapses were quantified. The replica was tilted whenever the synaptic area was not flat. I only analysed synapses that were larger than 0.008 μm^2. This value derives from preliminary quantifications conducted two weeks post injection (not shown in the dissertation), and represents the smallest synaptic area found in putative γ2 subunit-lacking cells. Extrasynaptic gold particles were counted on the same imaged somatic surfaces, and gold particle numbers and densities were calculated. Although, I was looking for cortical PC somata, I could not exclude the possibility that some IN somata were also sampled, as based on purely morphological characteristics one cannot differentiate between PCs and INs with this technique. The nonspecific background labelling was calculated on either the E-face or the P-face depending on the location of the epitope of a given antibody and subsequently subtracted from the mean gold particle densities. Gold particle densities are presented as mean ± standard deviation (SD) between cells. Statistical comparisons were performed with STATISTICA software (Scientific Computing, Rockaway, NJ, USA) and significance was taken as $p < 0.05$.

3.8. Testing the specificity of the immunoreactions

Specificity of the fluorescent immunoreactions for $K_v4.2$ subunit was tested by using $K_v4.2^{-/-}$ mice. To confirm the specificity of SDS-digested replica immunogold labelling for $K_v4.2$ subunit, the above described immunogold reactions were repeated in three $K_v4.2^{+/+}$ and three $K_v4.2^{-/-}$ mice, with the exception that here the layer categorization was as follows: 0-100 μm: proximal SR, 100-200 μm: middle SR, 200-300 μm: distal SR and above 300 μm: SLM. In $K_v4.2^{-/-}$ mice the immunogold particle density for the $K_v4.2$ subunit measured on P-face was similar to the gold particle density measured on the E-face in replicas obtained from wild-type mice and rats, validating my approach of estimating the level of nonspecific labelling on the E-face.

In the present study, I used the same anti-$K_{ir}3.2$ antibody as the one used by Kulik et al. (Kulik *et al.*, 2006) and Koyrakh et al. (Koyrakh *et al.*, 2005) and obtained a very similar labelling pattern; the specificity of the reactions was verified in $K_{ir}3.2^{-/-}$ mice by Kulik et al. (Kulik *et al.*, 2006) and Koyrakh et al. (Koyrakh *et al.*, 2005). The specificity of immunolabelling for the $K_{ir}3.1$ and $K_{ir}3.3$ subunits with these antibodies was proven in the cerebellum by Aguado et al. (Aguado *et al.*, 2008) using $K_{ir}3.1^{-/-}$ and $K_{ir}3.3^{-/-}$ mice, respectively and the specificity of the $K_{ir}3.3$ labelling in the hippocampus is presented in the web site of the company. My immunolabelling both in the cerebellum and the hippocampus is identical to the ones shown in the website and in Aguado et al. (Aguado *et al.*, 2008).

My immunoreactions for the $GABA_AR$ α1, α4, α5, β3, γ2 and δ subunits with the primary antibodies listed in Table 3.1., were very similar to previously published labelling patterns (Pirker *et al.*, 2000). The specificity of the listed antibodies, except those obtained from Synaptic System (guinea pig β3, rabbit and guinea pig γ2), have been described earlier (for details see Table 1.).

3.9. Electrophysiological recordings of tonic $GABA_A$ receptor-mediated currents

Electrophysiological recordings of tonic currents were conducted by my collaborator, Dr. Mark D. Eyre. Somatic whole-cell voltage-clamp recordings (-70 mV) were performed at 26.5 ± 1.0 °C using IR-DIC on an Olympus BX50WI microscope

with a 40X water immersion objective. Recordings were carried out using a mixed K-gluconate- and KCl-based intracellular solution (containing in mM: 65 K-gluconate, 70 KCl, 2.5 NaCl, 1.5 $MgCl_2$, 0.025 EGTA, 10 HEPES, 2 Mg-ATP, 0.4 Mg-GTP, 10 creatinine phosphate, and 8 biocytin; pH = 7.33; 270–290 mOsm). Kynurenic acid (3 mM, Sigma-Aldrich Kft., Budapest, Hungary) was used to inhibit ionotropic glutamate receptors. After initial stabilization and a baseline recording period of 6 minutes, 1 μM THIP (Gaboxadol, Sigma-Aldrich) was washed in for 18 minutes, then followed by 20 μM SR95531 (Sigma-Aldrich). Cells were identified by their somatic diameter and shape, dendrite configuration and their location in cortical layer 2/3 using IR-DIC optics. Additionally, sequence of hyper- and depolarizing current injections was used to determine firing parameters. To define the change in holding current (i.e. tonic current) of each cell, 100 ms-long segments of holding current recordings, resampled every second, were binned into 1 minute intervals, and differences between the minute immediately preceding drug application and the second minute post-drug-wash in were calculated. Spontaneous IPSCs were recorded from INs and further analysed off-line with EVAN 1.5 (Nusser *et al.*, 2001). Recordings were performed with MultiClamp 700A and 700B amplifiers (Axon Instruments, Foster City, CA). Cells with an access resistance of > 20 MΩ or > 20 % change from baseline were excluded from the analysis. Patch pipettes were pulled (Zeitz Universal Puller; Zeitz-Instrumente Vertriebs, Munich, Germany) from thick-walled borosilicate glass capillaries with an inner filament (1.5 mm outer diameter, 0.86 mm inner diameter; Sutter Instruments, Novato, CA). After recordings, slices were fixed in 0.1 M PB containing 2 % PFA and 15v/v % PA for 24 hours prior to *post-hoc* visualization of the biocytin-filled cells.

3.10. *Post-hoc* visualization of biocytin-filled cells

Slices were washed several times in 0.1 M PB, embedded in agar and resectioned at 60 μm thickness with a vibratome. Sections were then washed in TBS, blocked in TBS containing 10 % NGS for 1 hour, and then incubated in a solution of mouse anti-Cre (1:5000, Millipore, Darmstadt, Germany) and rabbit anti-GFP (1:1000, Millipore) primary antibodies diluted in TBS containing 2 % NGS and 0.1 % triton X-100 overnight at room temperature. Sections were then washed three times in TBS,

DOI:10.14753/SE.2015.1809

incubated in TBS containing Alexa-488-conjugated goat anti-rabbit (1:500, Life Technologies) and Cy5-conjugated goat anti-mouse (1:500, Jackson) secondary antisera, Cy3-conjugated streptavidin (1:500, Jackson), 2 % NGS and 0.1 % Triton X-100 for 2 hours, followed by washing and mounting on glass slides in Vectashield (Vector Labs). Images were acquired using a confocal laser scanning microscope (FV1000, Olympus) with a 20X objective.

DOI:10.14753/SE.2015.1809

4. RESULTS

4.1 Subcellular distribution of the K_v4.2 subunit in the hippocampal CA1 area

4.1.1 Distribution of K_v4.2 subunit immunoreactivity in the CA1 region and specificity of the immunoreaction

Light microscopic immunofluorescent reactions for the K_v4.2 subunit revealed a rather uniform labelling pattern throughout the SO and SR of the CA1 area of rat dorsal hippocampus with a slightly reduced fluorescent intensity in the SLM (Fig. 10.A), in line with previous reports (Maletic-Savatic *et al.*, 1995; Varga, 2000; Rhodes *et al.*, 2004). Next, to validate the specificity of the immunofluorescent reactions $K_v4.2^{-/-}$ mice were used. The labelling pattern in control mice (Fig. 10.B) was very similar to that obtained in rats. The complete lack of labelling in the $K_v4.2^{-/-}$ mice (Fig. 10.C) demonstrates that the immunolabelling at the light microscopic level is due to specific antibody-antigen interactions. To quantitatively compare the K_v4.2 subunit content of

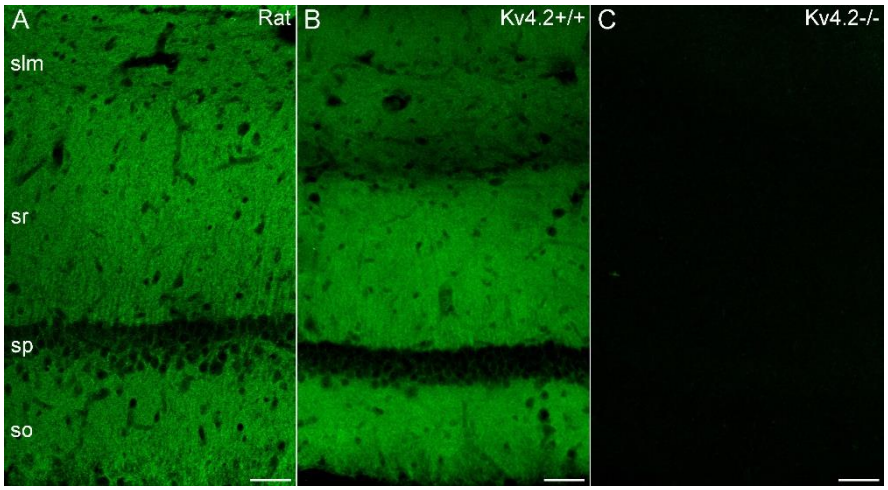

FIGURE 10. Distribution of the K_v4.2 subunit immunoreactivity in the hippocampal CA1 region and specificity of immunoreaction. (A) Immunofluorescent reaction for the K_v4.2 subunit shows a strong homogenous neuropil labelling in strata oriens and radiatum of rat CA1 region with a slight decrease in the stratum lacunosum-moleculare. (B) Similar labelling pattern was observed in the mouse tissue. (C) The immunofluorescent signal was absent in the $K_v4.2^{-/-}$ mice, demonstrating the specificity of the immunoreaction. so: stratum oriens; sp: stratum pyramidale; sr: stratum radiatum; slm: stratum lacunosum-moleculare. Scale bars: 50 μm.

distinct somato-dendritic compartments, I carried out immunogold labelling using the electron microscopic SDS-FRL method. The gold particle densities in main apical dendrites, oblique dendrites and dendritic spines in the proximal, middle and distal parts of the SR, dendritic shafts and spines in the SLM in addition to the somata of CA1 PCs have been systematically investigated.

4.1.2. High-resolution immunogold localization of the K_v4.2 subunit along the CA1 PC somato-dendritic axis

Electron microscopic analysis of the replicas revealed many gold particles labelling the K_v4.2 subunit on P-faces of somatic and dendritic plasma membranes, consistent with the intracellular location of the epitope (aa 454-469) recognized by the rabbit anti-K_v4.2 antibody. Gold particles were apparently randomly distributed and showed a rather similar distribution pattern in the plasma membranes of somata and main apical dendrites of CA1 PC (Fig. 11.). Quantification of the immunogold reactions demonstrated a moderate distance-dependent increase (Fig. 13.) in gold particle density (background subtracted mean ± SD, where SD is the SD between animals) along the proximo-distal axis of the main apical dendrites within the SR (proximal SR: 7.1 ± 3.7 gold/μm^2, middle: 11.2 ± 3.6 gold/μm^2 and distal: 10.7 ± 2.8 gold/μm^2; n=5 rats) with a slight decrease in dendrites of the SLM (8.2 ± 2.8 gold/μm^2). The density of K_v4.2 subunit in the proximal apical dendrites was very similar to that found in the somata (6.2 ± 1.2 gold/μm^2; Fig. 11.A–D and Fig. 13.). The average relative increase from the proximal to distal dendrites within the SR was 69 ± 50 % in five rats.

To investigate whether a much higher density of the K_v4.2 subunit in oblique dendrites or dendritic spines could mask the slight increase found in main apical dendrites and therefore result in a uniform staining of the SR as observed with light microscopy, I quantified gold particle densities in oblique dendrites and dendritic spines in the above mentioned three subdivisions of the SR (Fig. 12.). Gold particle densities in oblique dendrites (proximal SR: 10.3 ± 4.7 gold/μm^2, middle: 11.4 ± 4.2 gold/μm^2, distal: 12.5 ± 4.9 gold/μm^2; n=5 rats) and in dendritic spines (proximal SR: 10.2 ± 6.0 gold/μm^2, middle: 14.3 ± 3.2 gold/μm^2, distal: 12.8 ± 3.1 gold/μm^2, SLM: 10.4 ± 5.0 gold/μm^2; n=5 rats) showed an almost identical increasing-decreasing pattern to that

DOI:10.14753/SE.2015.1809

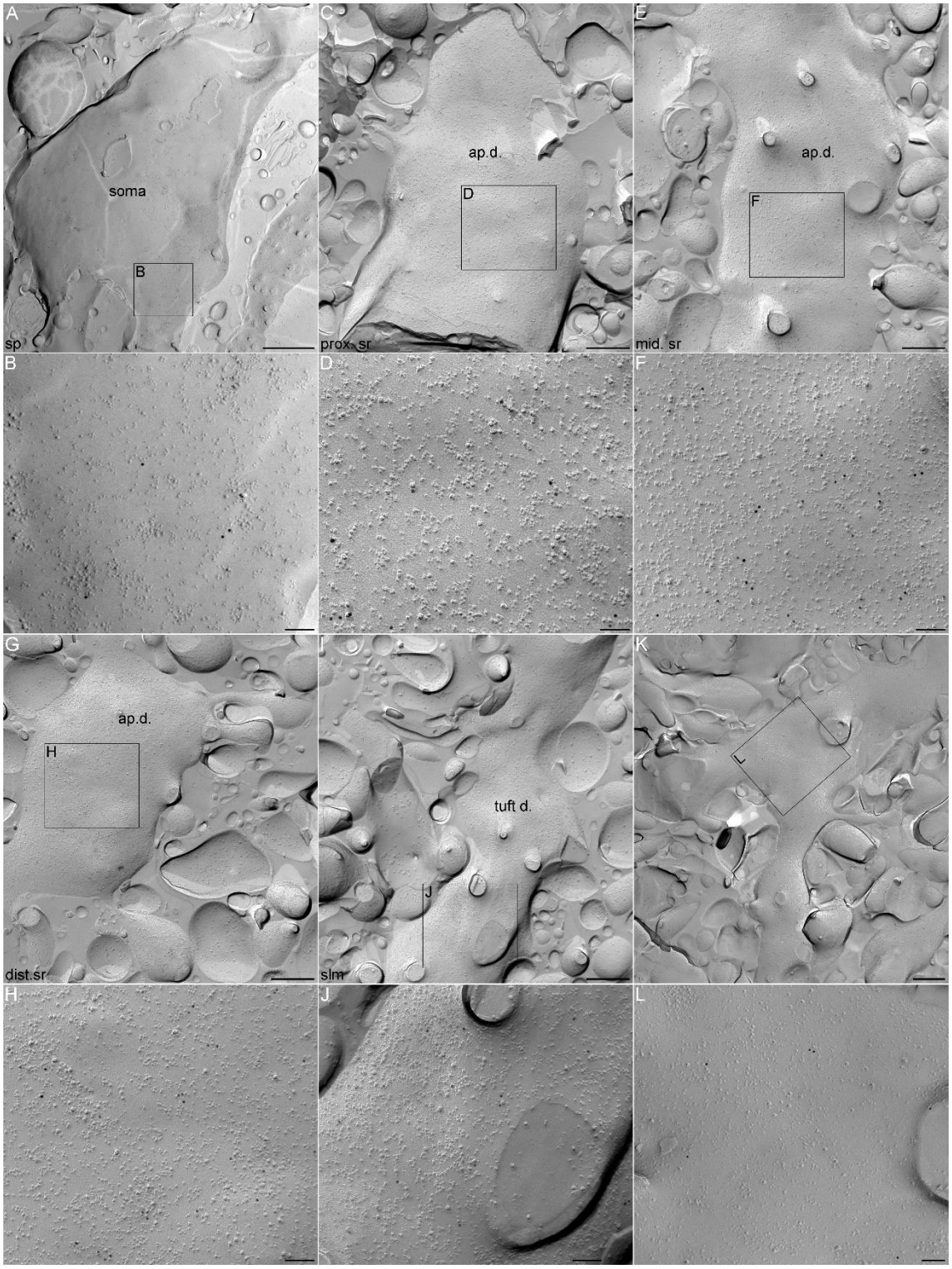

FUGURE 11. High-resolution immunogold localization of the K_v4.2 subunit on CA1 PC soma and apical dendrite. (A, C, E, G, I) Low-magnification P-face images of a PC soma (A) and apical dendrites from proximal (C), middle (E) and distal part of stratum radiatum (G) and tuft dendrite from lacunosum-moleculare (I) show a rather homogenous distribution of gold particles labelling for the Kv4.2 subunit. (B, D, F, H, J) High-magnification images of the boxed region in *(continued on the next page)*

(A, C, E, G, I). (K) Gold particles are homogenously distributed around a branchpoint. (L) High-magnification view of the boxed region in (K). sp: stratum pyramidale; prox. sr: proximal stratum radiatum; mid. sr: middle stratum radiatum; dist. sr: distal stratum radiatum, slm: stratum lacunosum-moleculare, ap.d.: apical dendrite, tuft d.: tuft dendrite. Scale bars: 1 μm (A); 500 nm (C, E, G, I, K); 100 nm (B, D, F, H, J, L).

found for the main apical trunks (Fig. 13.). In each subregion of the SR, the average densities in oblique dendrites and spines were only 26 ± 16 % higher than those found in the main apical trunks, demonstrating the lack of large quantitative differences in the densities of $K_v4.2$ subunit among these distinct dendritic compartments. The densities of gold particles in all examined compartments, but the somatic membranes, were above the nonspecific background labelling (0.7 ± 0.7 gold/μm^2; One-way ANOVA with Dunnett's *post hoc* test, $p < 0.05$). Despite the increasing-decreasing tendency in the density of gold particles along the dendritic regions, statistical comparisons of the background subtracted densities revealed no significant difference among these dendritic compartments ($p = 0.08$, One-way ANOVA; Fig. 13.).

Previous studies suggested that A-type potassium channels potentially located around dendritic branch points have a critical role in gating the propagation of dendritic spikes towards the soma or into other dendrites (Cai *et al.*, 2004; Losonczy *et al.*, 2008). Therefore, I specifically investigated immunolabelling for the $K_v4.2$ subunit around

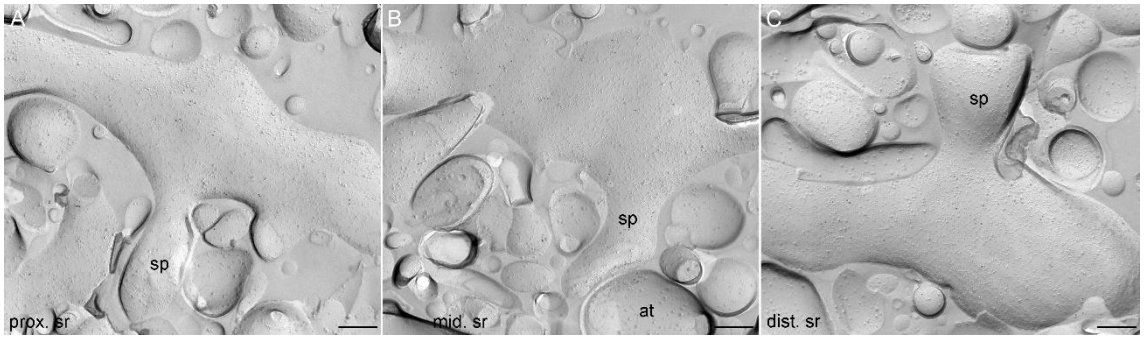

FIGURE 12. Immunogold labelling for the $K_v4.2$ subunit in oblique dendrites of the stratum radiatum. (A) Immunogold particles labelling the $K_v4.2$ subunit are homogenously distributed along the P-face of a spiny oblique dendrite in the proximal stratum radiatum. (B) Slightly more immunogold particles can be seen in an oblique dendrite from the middle stratum radiatum. Note a spine emerging from the dendrite that contains relative high density of immunogold particles. (C). A spiny oblique dendrite in the distal stratum radiatum contains many more immunogold particles labelling the $K_v4.2$ subunit. prox. sr: proximal stratum radiatum; mid. sr: middle stratum radiatum; dist. sr: distal stratum radiatum; sp: spine, at: axon terminal. Scale bars: 250 nm (A–C).

branch points, but could not detect any clustering or increase in particle density (Fig. 11.K and L).

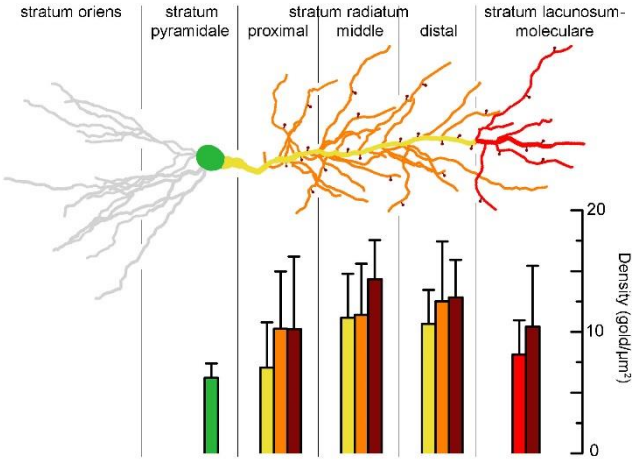

FIGURE 13. Densities of immunogold particles labelling for the K_v4.2 subunit in distinct somato-dendritic compartments of CA1 PCs. Bar graphs illustrate the background subtracted densities (mean ± SD, in gold/µm^2) of immunogold particles in the somato-dendritic compartments. Bars are colour coded to different subcellular compartments as indicated in the schematic drawing of a CA1 PC. Note the moderate increase in density within the stratum radiatum and the subsequent decrease in the stratum lacunosum-moleculare.

4.1.3. Specificity of K_v4.2 subunit immunogold labelling in CA1 PCs using SDS-FRL

To validate the specificity of immunogold labelling on SDS-FRL, the reactions were repeated in control and $K_v4.2^{-/-}$ mice (Fig. 14.A, B). In control mice, the strength of the reaction was similar ($p = 0.21$, unpaired Student's *t*-test) to that obtained in five rats as assessed from the gold particle densities (background subtracted) in the main apical dendrites from middle SR (8.1 ± 2.6 gold/µm^2, n = 3 control mice; Fig. 14.A) and showed a similar labelling pattern within the SR and SLM to that found in rats. In contrast, in $K_v4.2^{-/-}$ mice, the mean density of gold particles on P-face structures (soma: 0.8 ± 0.5 gold/µm^2; apical dendrite: 1.1 ± 1.2 gold/µm^2; oblique dendrite: 1.4 ± 1.6 gold/µm^2; SLM: 1.1 ± 0.9 gold/µm^2 and dendritic spine: 1.6 ± 1.6 gold/µm^2; without background subtraction; n=3 mice; Fig. 14.B) was not significantly different from that obtained in the E-face structures around them (0.4 ± 0.1 gold/µm^2; n = 3; $p = 0.94$, One-way ANOVA). The low insignificant labelling in $K_v4.2^{-/-}$ tissue was consistent in all analysed somato-dendritic compartments throughout the depth of the SR and SLM,

demonstrating the specificity of immunogold labelling in all somato-dendritic compartments.

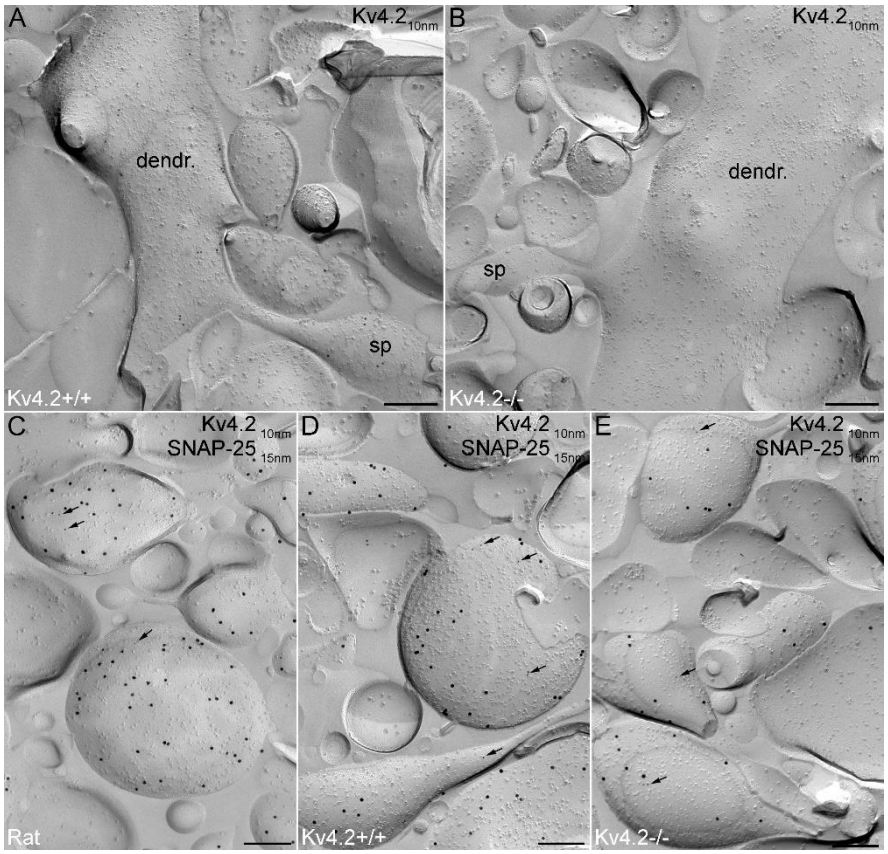

FIGURE 14. Specificity test for K_v4.2 subunit labelling on the axo-somato-dendritic surface of CA1 PCs using SDS-FRL. (A) Electron micrograph illustrating the P-face of a spiny dendrite of control mouse immunolabelled for the K_v4.2 subunit. Note that immunogold labelling for the Kv4.2 subunit in mouse is similar to that seen in rat. (B) Immunogold labelling is missing on the P-face of a spiny dendrite from the $K_v4.2^{-/-}$ mouse. (C) Axon terminals identified by immunolabelling for the SNAP-25 (15 nm gold) contain low number of immunogold particles (arrows) for the Kv4.2 subunit (10 nm gold) in rat. (D and E) Immunogold particles for the Kv4.2 subunit were present in axon terminals from both $K_v4.2^{+/+}$ (D) and $K_v4.2^{-/-}$ mice (E) at approximately the same density. dendr., dendrite; sp, spine. Scale bars: 250 nm (A–E).

4.1.4. SNAP-25 containing axon terminals have a low density of immunogold particles for the K_v4.2 subunit, which persists in $K_v4.2^{-/-}$ mice

Surprisingly, I observed that gold particles for the K_v4.2 subunit were not only confined to somato-dendritic plasma membranes, but were present in presumed presynaptic axon terminals at low densities. To unequivocally identify these weakly labelled structures, I performed double-labelling experiments for K_v4.2 and SNAP-25, a

member of the SNARE complex that is located exclusively in axons (Hagiwara *et al.*, 2005). In these double-labelling reactions, the strength of the $K_v4.2$ labelling in apical dendrites from the middle SR (10.5 ± 4.6 gold/μm^2; background subtracted; n = 3 rats) was very similar to that found in single-labelling reactions (p = 0.83; unpaired Student's *t*-test). The SNAP-25 positive structures contained on average 2.4 ± 0.6 gold particles/μm^2 (without background subtraction; n = 3 rats; Fig. 14.C). Although this density is only one-fourths of that found on the somato-dendritic compartments, it is still significantly ($p < 0.01$, unpaired Student's *t*-test) higher than the background labelling (0.5 ± 0.4 gold/μm^2). The presence of significant immunolabelling in axon terminals is surprising, because the $K_v4.2$ subunit believed to form somato-dendritic ion channels. To confirm the specificity of immunogold labelling on axon terminals, I repeated these experiments in control and $K_v4.2^{-/-}$ mice. The labelling intensity in control mice (2.6 ± 1.6 gold/μm^2; without background subtraction; n = 3 mice; Fig. 14.D) was very similar (p = 0.83; unpaired Student's *t*-test) to that found in rats, but the density of gold particles labelling the $K_v4.2$ subunit was almost identical in the axon terminals of control and $K_v4.2^{-/-}$ mice (2.2 ± 0.4 gold/μm^2; n = 3 mice; p = 0.69, unpaired Student's *t*-test; Fig. 14.E). This value was significantly ($p < 0.01$, unpaired Student's *t*-test) higher than the background labelling on the surrounding E-face structures (0.6 ± 0.2 gold/μm^2). Taken together, these results reveal that the immunogold labelling in the somato-dendritic compartments is due to specific antibody-$K_v4.2$ subunit interactions, however, the same antibody under identical experimental conditions provides a weak, nonspecific labelling in axon terminals.

4.1.5. The $K_v4.2$ subunit is excluded from the postsynaptic membrane specializations in the CA1 area

Finally, I investigated whether the $K_v4.2$ subunit is concentrated in GABAergic or glutamatergic synapses as suggested to occur in the supraoptic nucleus (Alonso & Widmer, 1997), developing cerebellum (Shibasaki *et al.*, 2004), visual cortex (Burkhalter *et al.*, 2006) and subiculum (Jinno *et al.*, 2005). The SDS-FRL technique allows the visualization of neurotransmitter receptors and their associated proteins in both GABAergic (Kasugai *et al.*, 2010; Lorincz & Nusser, 2010) and glutamatergic

DOI:10.14753/SE.2015.1809

synapses (Kulik *et al.*, 2006; Masugi-Tokita & Shigemoto, 2007). Therefore, the K_V4.2 subunit was co-localized with PSD-95, which clearly marks the PSD of excitatory synapses on the P-face of the replica (Kulik *et al.*, 2006) and with the $GABA_AR$ β3 subunit (Kasugai *et al.*, 2010; Lorincz & Nusser, 2010), which labels inhibitory synapses also on the P-face.

I could not find any evidence for the enrichment of K_V4.2 subunits in GABAergic or glutamatergic synapses, only few scattered gold particles were found around the periphery of some excitatory synapses (Fig. 15.A). Immunogold particles labelling the K_V4.2 subunits infrequently clustered on somatic and dendritic membranes, but they never co-localized with the $GABA_AR$ β3 subunit (Fig. 15.B). These results provide evidence for the lack of synaptic accumulation of the K_V4.2 subunit in CA1 PCs.

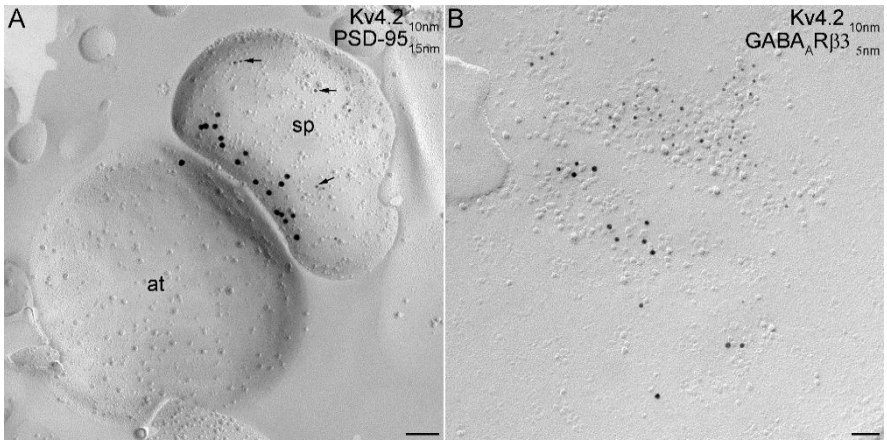

FIGURE 15. The K_V4.2 subunit is excluded from postsynaptic membrane specializations. (A) Electron micrograph illustrating an excitatory synapse, revealed by the presence of the postsynaptic density marker PSD-95 (15 nm gold). Arrowheads point to gold particles labelling the K_V4.2 subunit (10 nm gold) around the postsynaptic density. (B) High-magnification image of an inhibitory synapse identified by the enrichment of gold particles (5 nm gold) labelling the $GABA_AR$ β3 subunit. Note the clustering of gold particles labelling the K_V4.2 subunit in the vicinity of the inhibitory synapse. Scale bars: 100 nm (A); 50 nm (B).

DOI:10.14753/SE.2015.1809

4.2. Subcellular distribution of the $K_{ir}3.2$ subunit in the hippocampal CA1 area

4.2.1 Immunofluorescent labelling for three $K_{ir}3$ subunits in the hippocampal CA1 region

Using fluorescent immunohistochemistry I investigated the regional distribution of $K_{ir}3.1$, $K_{ir}3.2$ and $K_{ir}3.3$ subunits in the CA1 area of rat hippocampus (Fig. 16.). Light microscopic fluorescent immunohistochemistry for the $K_{ir}3.1$ subunit (Fig. 16.A) revealed weak immunostaining of the SO, stratum pyramidale (SP) and the proximal part of the SR. Stronger immunolabelling could be observed in the distal part of SR, with the strongest immunoreactivity in the SLM. Similar non-uniform labelling pattern could be observed for the $K_{ir}3.2$ subunit in the CA1 region (Fig. 16.B) however, the immunosignal was stronger than seen for the $K_{ir}3.1$ subunit. Immunolabelling for the $K_{ir}3.3$ subunit was very weak (Fig. 16.C) throughout the neuropil of all dendritic layers in the CA1 region, with a slight increase towards the distal part of the SR and SLM. These observations are in line with previous reports on the $K_{ir}3.1$-3 subunit distributions

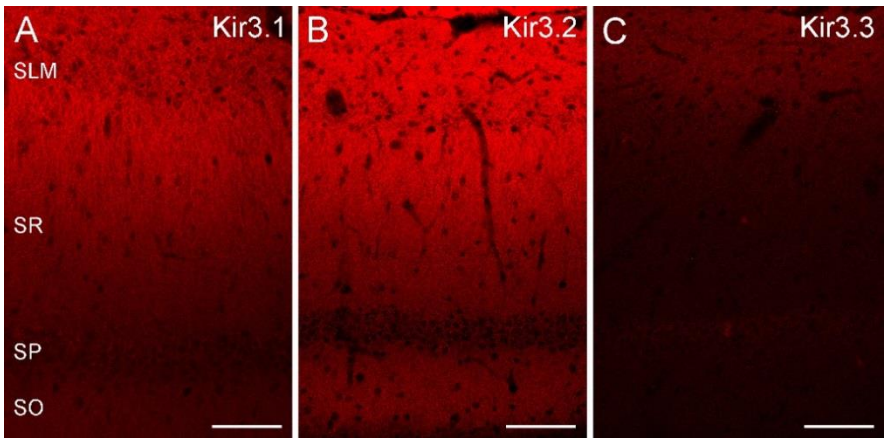

FIGURE 16. Distribution of three $K_{ir}3$ subunits in the CA1 region of rat hippocampus. (A) Immunofluorescent reaction for the $K_{ir}3.1$ subunit shows a modest labelling in stratum oriens and in the proximal part of radiatum with a gradual increase towards the distal part of the strata radiatum and lacunosum-moleculare. (B) Similar labelling pattern is observed for the $K_{ir}3.2$ subunit, with the most intense immunolabelling in the distal part of the strata radiatum and lacunosum-moleculare. (C) Immunoreactivity for the $K_{ir}3.3$ subunit is weak in the CA1 area, but the intensity of the signal increases toward the distal strata radiatum and lacunosum-moleculare. so: stratum oriens; sp: stratum pyramidale; sr: stratum radiatum; slm: stratum lacunosum-moleculare. Scale bars: 100 μm (A–C).

in the CA1 region (Ponce *et al.*, 1996; Koyrakh *et al.*, 2005; Kulik *et al.*, 2006; Fernandez-Alacid *et al.*, 2011).

Of these three $K_{ir}3$ subunits, the $K_{ir}3.2$ subunit is unique in that it can form functional heterotetrameric as well as homotetrameric complexes (Dascal, 1997), furthermore it is involved in the cell surface targeting of other $K_{ir}3$ subunits (Ma *et al.*, 2002). Therefore, I decided to perform a quantitative electron microscopic analysis of this subunit and investigated whether and how its density on the apical dendrites of CA1 PCs changes with distance from the soma.

4.2.2. Distance-dependent increase in the density of $K_{ir}3.2$ subunits in CA1 PC apical dendrites

To reveal the presence of $K_{ir}3.2$ subunits in somata, main apical dendrites, small diameter oblique dendrites, dendritic spines and AISs of CA1 PCs, as well as to quantify its density in the plasma membrane, I performed SDS-FRL. High-resolution electron microscopic analysis revealed very few gold particles labelling the $K_{ir}3.2$ subunit on the P-face membranes (epitope 374–414 is cytoplasmic) of PC somata and proximal apical dendrites (Fig. 17.A–C). In contrast to this, many more gold particles can be observed in apical dendrites from the distal part of the SR, and in dendritic tufts from the SLM (Fig. 17.D–G). Next, I investigated the presence of gold particles labelling for the $K_{ir}3.2$ subunit in the small diameter oblique dendrites as well as dendritic spines from the SR and SLM. Electron microscopic examination of spiny oblique dendrites revealed only few immunogold particles for $K_{ir}3.2$ subunits in the proximal and middle SR (Fig. 18.A and B), whereas more gold particles could be seen in spiny oblique dendrites from the distal SR (Fig. 18.C).

Following the quantitative analysis of the immunogold reactions, I found that the background subtracted densities of gold particles (mean ± SD, where SD is the SD between animals) in PC somata (0.4 ± 0.2 gold/μm^2; n = 5 rats), proximal, middle and distal apical dendrites in the SR (0.5 ± 0.1 gold/μm^2, 2.0 ± 0.6 gold/μm^2, 3.5 ± 1.3 gold/μm^2) and dendritic tufts in SLM (5.1 ± 2.1 gold/μm^2) showed a quasi linear increase as a function of distance from the soma (Fig. 19.A). Similar distance dependent

DOI:10.14753/SE.2015.1809

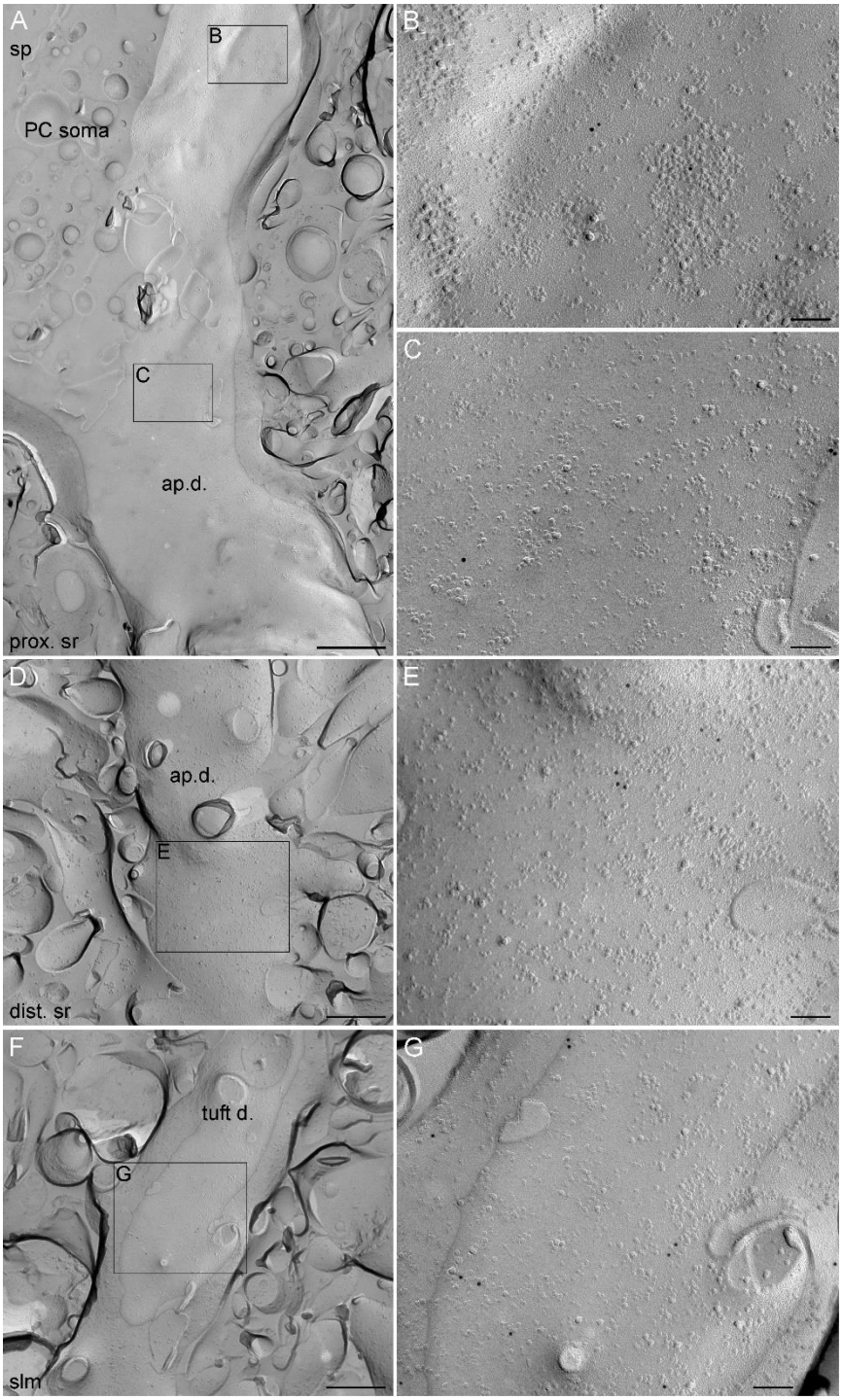

FIGURE 17. Somatodendritic localization of the K_{ir}3.2 subunit in rat CA1 PCs by using SDS-FRL. (A) Low-magnification image of the P-face of a PC soma and proximal apical dendrite. (B and C) High-magnification images of the boxed areas shown in (A). (D and F) Low-magnification images of a spiny apical dendrite from distal stratum radiatum and a tuft dendrite from stratum lacunosum-moleculare labelled for the K_{ir}3.2. (E and G) High magnification images of the boxed areas shown in (D and F). sp: stratum pyramidale; prox. sr: proximal stratum radiatum; dist. sr: distal stratum radiatum, slm: stratum lacunosum-moleculare; ap.d.: apical dendrite; tuft d.: tudt dendrite. Scale bars: 1 μm (A), 500 nm (D, F), 100 nm (B, C, E, G).

DOI:10.14753/SE.2015.1809

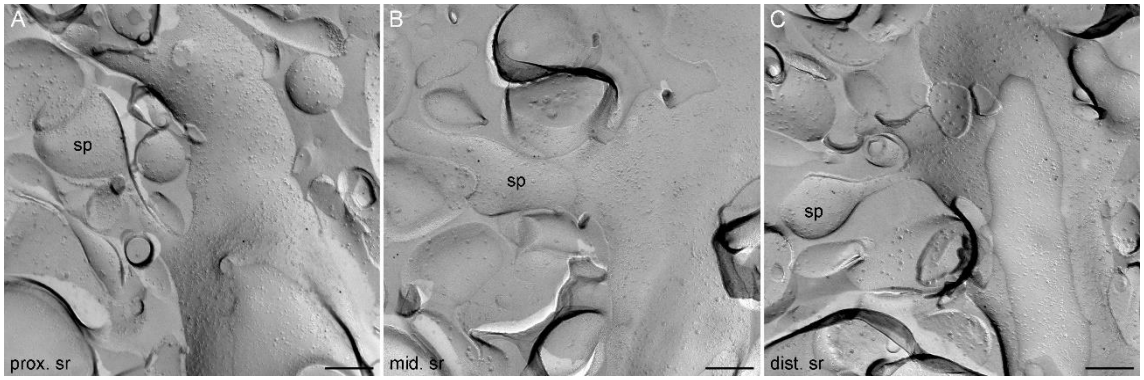

FIGURE 18. Distribution of gold particles labelling the K_v4.2 subunit in oblique dendrites from the stratum radiatum. (A–C) Low amount of immunogold particles are homogenously distributed along the P-face of a spiny oblique dendrites in the proximal and middle stratum radiatum (A and B) with slightly more gold particles in a spiny oblique dendrite from the distal radiatum (C). prox. sr: proximal stratum radiatum; mid. sr: middle stratum radiatum; dist. sr: distal stratum radiatum; sp: spine. Scale bars: 250 nm (A–C).

increase in the densities of gold particles was found in oblique dendrites (proximal SR: 1.5 ± 0.5 gold/μm^2; middle SR: 2.5 ± 0.6; distal SR: 3.9 ± 1.9 gold/μm^2) and in dendritic spines (proximal SR: 1.4 ± 1.2 gold/μm^2; middle SR: 2.0 ± 1.6 gold/μm^2; distal SR 3.1± 2.2 gold/μm^2; SLM: 3.9 ± 2.4 gold/μm^2). Of these, oblique dendrites from the middle SR, main apical dendrites, oblique dendrites and spines from the distal part of the SR, and dendritic tufts and spines from the SLM showed significantly higher density of gold particles than the nonspecific background labelling (0.7 ± 0.2 gold/μm^2; One-way ANOVA with Dunnett's *post hoc* test, $p < 0.05$). Statistical comparisons of the background subtracted densities revealed significantly higher gold particle density in the distal SR and SLM for all subcellular compartments than in PC somata (One-way ANOVA with Dunnett's *post hoc* test, $p < 0.05$; Fig. 19.A).

Finally, I investigated the gold particle density for the K_{ir}3.2 subunit on the AISs of CA1 PCs. To identify the AISs I carried out double-labelling experiments with the AIS marker pan-Neurofascin and the K_{ir}3.2 subunit. In these reactions, the density (background subtracted) of gold particles labelling the K_{ir}3.2 subunit in dendritic tufts in the SLM (13.5 ± 1.0 gold/μm^2) was even stronger than in single labelling reactions (5.1 ± 2.1 gold/μm^2) with a similarly low background (0.5 ± 0.1 gold/μm^2 n = 3 rat). However, the density of gold particles in the AISs was not significantly different from the nonspecific background labelling (One way ANOVA, $p < 0.001$ with Dunnett's post-hoc test, $p = 0.95$; n = 3 rats; Fig. 19.B).

DOI:10.14753/SE.2015.1809

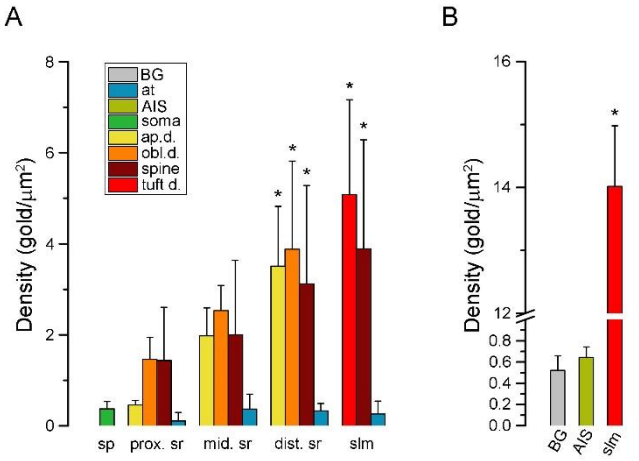

FIGURE 19. Densities of $K_{ir}3.2$ subunits in distinct subcellular compartments of rat CA1 PCs. (A) Bar graphs demonstrate the background subtracted densities (mean ± SD) of gold particles in different subcellular compartments of CA1 PCs. * denotes values that are significantly different from the somatic labelling (One-way ANOVA with Dunnett's *post-hoc* test, $p < 0.05$; n = 5 rats and n = 3 rats for axon terminals). (B) Gold particle density in the AIS was not significantly different ($p = 0.95$) from the background labelling. * denotes density value that is significantly different from the background (One-way ANOVA with Dunnett's post-hoc test, $p < 0.001$).

4.2.3 The $K_{ir}3.2$ subunit is excluded from the presynaptic axon terminals in the CA1 region

As a final step, I investigated whether the $K_{ir}3.2$ subunit is present in the presynaptic nerve terminals from the CA1 region, as was previously described for $K_{ir}3.2$ subunits in cortical and hippocampal axon terminals (Kulik *et al.*, 2006; Ladera *et al.*, 2008) or for the $K_{ir}3.1$ subunits in thalamocortical nerve terminals as well as in axon terminals from the SR and SLM in the hippocampus (Ponce *et al.*, 1996; Koyrakh *et al.*, 2005), and for all three $K_{ir}3$ subunits in parallel fibres from the cerebellum (Fernandez-Alacid *et al.*, 2009). The axon terminals were identified as P-face membrane profiles containing an active zone facing a PSD on the opposing E-face of a spine or dendritic shaft from SR and SLM of the CA1 region. The density (without background subtraction) of gold particles labelling for the $K_{ir}3.2$ subunit on the axon terminals was as follows: proximal SR: 0.4 ± 0.4 gold/µm^2; middle SR: 1.0 ± 0.6 gold/µm^2; distal SR: 1.0 ± 0.1 gold/µm^2; SLM: 0.8 ± 0.3 gold/µm^2 (n = 3 rats). Density values were not significantly different from the background labelling (0.7 ± 0.2 gold/µm^2; One-way ANOVA with Dunnett's *post-hoc* test, $p > 0.05$; Fig. 19.A), demonstrating that in my

DOI:10.14753/SE.2015.1809

experimental conditions with the sensitivity of this method, presynaptic $K_{ir}3.2$ channels remained undetectable with this antibody.

4.3. Clustering of $GABA_A$ receptors without the γ2 subunit in cortical perisomatic synapses

Electrophysiological experiments conducted by my colleague Dr. Mark D. Eyre revealed the presence of inhibitory synaptic currents in cortical PC perisomatic synapses in the absence of the $GABA_AR$ γ2 subunit in $GABA_AR\gamma2^{77I}$lox mice. Using Cre-GFP fusion protein-expressing adeno-associated viruses injected into the somatosensory cortex of $GABA_AR\gamma2^{77I}$lox mice, he has shown that two weeks after injection, spontaneously occurring fast-rising mIPSCs were detected but had slower decay kinetics in Cre-recombinase positive (Cre^+) PCs compared to Cre-recombinase negative (Cre^-) PCs (Kerti-Szigeti *et al.*, 2014). Although this suggests that synaptic-like currents can be generated without the γ2 subunit, I have to emphasize that these currents cannot be taken as evidence that the underlying receptors are indeed concentrated within the postsynaptic specializations of GABAergic synapses. It is possible that slow current components arise from the activation of receptors in the perisynaptic region (Chen & Diamond, 2002). Alternatively, the fast-rising synaptic currents can originate from spillover, as has been described in the cerebellum for mossy fibre to granule cell synapses (DiGregorio *et al.*, 2002). But where are then the $GABA_ARs$ in the plasma membrane of Cre^+ cells? Is the γ2 subunit necessary for clustering $GABA_ARs$ to the postsynaptic specializations?

To reveal the precise subcellular location, densities, and subunit composition of synaptic $GABA_ARs$ in neurons lacking the γ2 subunit, I performed light microscopic immunofluorescent and electron microscopic SDS-FRL studies in $GABA_AR\gamma2^{77I}$lox mice.

DOI:10.14753/SE.2015.1809

4.3.1. Immunofluorescent labelling for distinct $GABA_A$ receptor subunits within the virus injection zone

First, I investigated the effect of Cre-recombinase expression two weeks post injection in the cortex of virus-injected $GABA_AR\gamma2^{77I}lox$ mice using immunofluorescent labelling against Cre and various $GABA_AR$ subunits. Strong immunolabelling for Cre was observed in a localized region in the injected hemisphere,

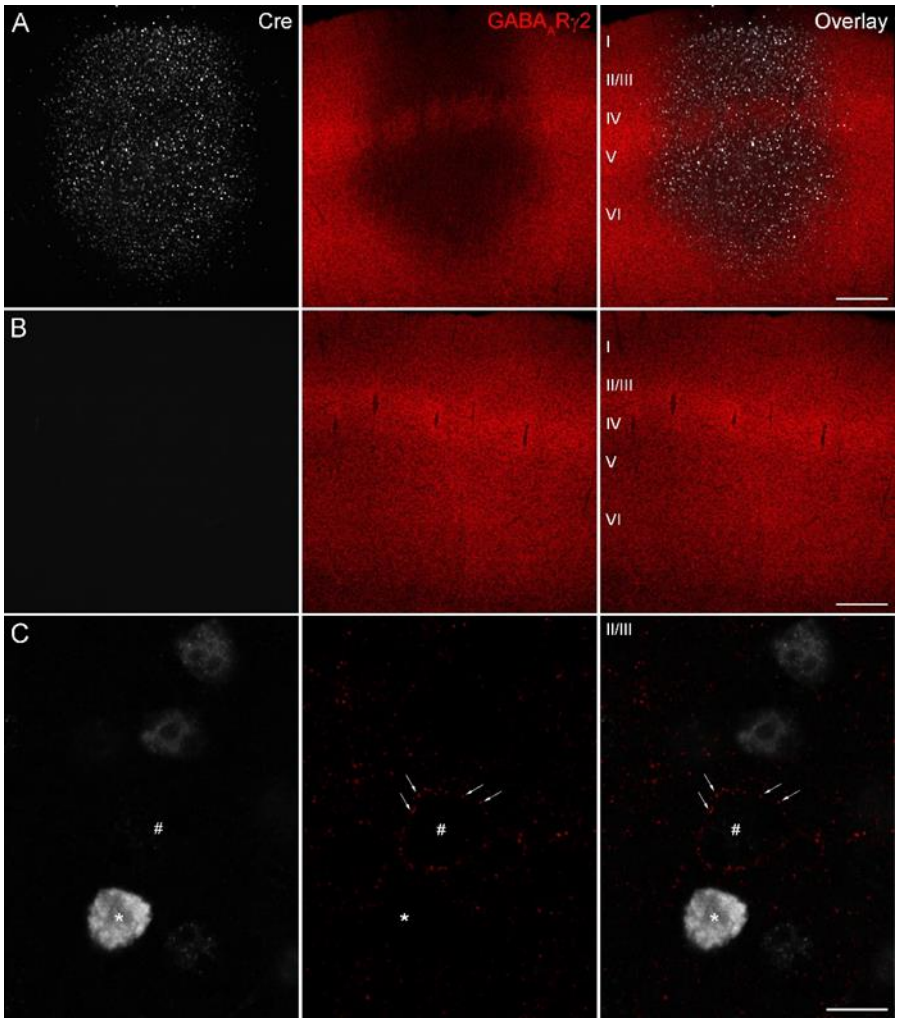

FIGURE 20. *In vivo* AAV virus expression of Cre-recombinase disrupts the expression of the $GABA_AR$ γ2 subunit in neocortical neurons of $GABA_AR\gamma2^{77I}lox$ mice. (A) Cre immunoreactivity (white) delineates the injection zone. Immunoreactivity for the γ2 subunit is greatly reduced (red) within it. (B) Contralateral cortex shows the lack of Cre immunolabelling and strong γ2 immunoreactivity (red). (C) High-magnification images of a Cre-immunopositive (*) and an immunonegative (#) cell within the injection zone. Arrows point to strong γ2 immunoreactive clusters surrounding the Cre-immunonegative cell. Roman numerals indicate cortical layers. Scale bars: 200 μm (A and B), 10 μm (C).

which overlapped with a strong reduction of the immunoreactivity for $GABA_AR$ γ2 subunit (Fig. 20.A). Contrary to this, the contralateral hemisphere showed no change in the γ2 subunit labelling intensity (Fig. 20.B). Upon examination of the virus injection zone at high magnification, I could find Cre immunoreactive neuronal nuclei that had greatly reduced immunosignal for the γ2 subunit in their surrounding somatic plasma membrane (Fig. 20.C, *) compared to strong punctate γ2 labelling (Fig. 20.C, #, arrows) in Cre^- cells.

In contrast, immunoreactivity for both the $GABA_AR$ α1 and β3 subunits appeared unchanged within the Cre immunoreactive injection zone at low magnifications (Fig. 21.A). When examined at high magnification, immunofluorescent labelling for both the α1 and β3 subunits was punctate and of similar intensities for both Cre^+ and Cre^- layer 2/3 putative PCs (Fig. 21.B, * and #, respectively). Putative

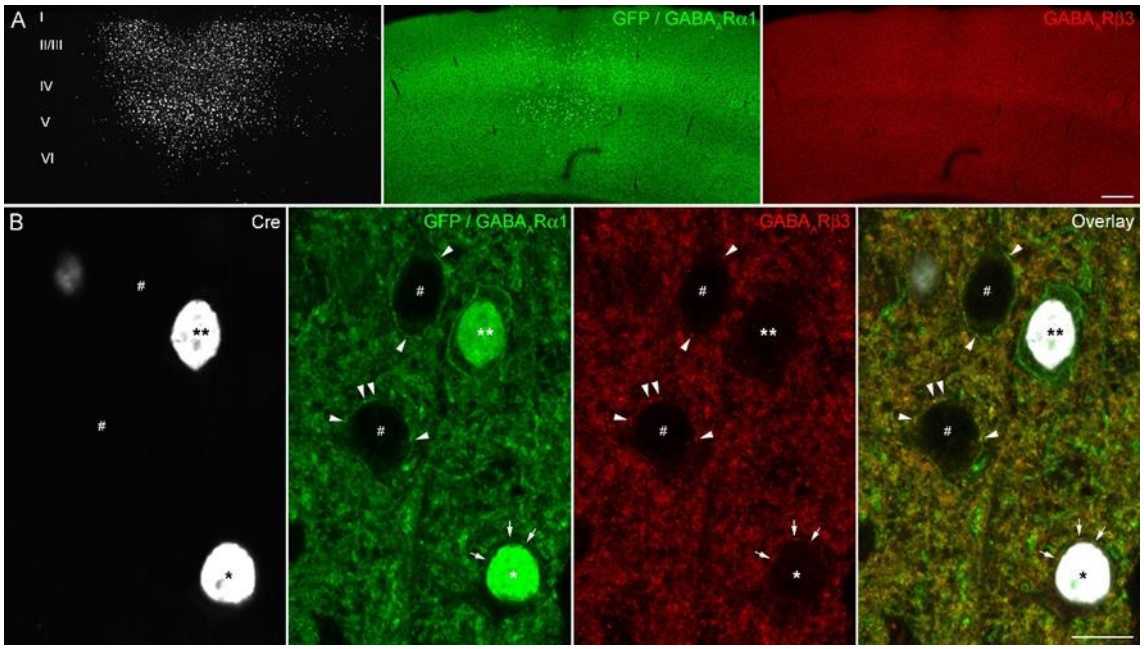

FIGURE 21. Immunofluorescent labelling for the $GABA_AR$ α1 and β3 subunits is unchanged within the virus injection zone. (A) Cre immunoreactivity (white) delineates the injection zone where immunoreactivity for the α1 (green) and the β3 (red) subunits are unchanged. (B) High-magnification view of cells immunonegative (#) and immunopositive (*, **) for Cre (white). In both Cre-immunonegative and immunopositive cells, $GABA_AR$ labelling for α1 (green) and the β3 (red) subunits is often punctate (arrowheads and arrows respectively), indicating the labelling of synaptic receptors. The lack of β3 clusters around a cell indicated by **, suggests that this is a putative IN that very strongly expresses the α1 subunit but not the β3 subunit. Note the endogenous GFP (green) is also visible in the nuclei of Cre-expressing cells. Roman numerals indicate cortical layers. Scale bars: 200 μm (A), 10 μm (B).

GABAergic INs immunoreactive for Cre were also found within the injection zone; their perisomatic plasma membranes remained strongly α1 immunopositive, although as expected for this cell type, they were immunonegative for the β3 subunit (Fig. 21.B, **).

The lack of change in punctate immunofluorescent labelling for α1 and β3 subunits despite the absence of the γ2 subunit in Cre^+ cells suggest the possible synaptic clustering of $GABA_A$Rs. Therefore it is conceivable that the remaining α and β subunits form αβ subunit-only heteropentamer receptor channels, which can form functional $GABA_A$Rs in expression systems, as was suggested to occur in neurons *in situ* (Mortensen & Smart, 2006). However, application of 10 μM of $ZnCl_2$, which at this concentration should inhibit the αβ subunit-only receptors ((Draguhn *et al.*, 1990; Smart *et al.*, 1991); pharmacological experiments performed by Mark Eyre, for details see in (Kerti-Szigeti *et al.*, 2014)) failed to block mIPSCs in Cre^+ cells, indicating that αβ subunit-only receptors are unlikely to be responsible for the remaining mIPSCs following the γ2 subunit deletion. This raises the possibility that a different $GABA_A$R subunit took the place of the γ2 subunit in the pentameric channel. Potentially the δ, ε, γ1 and γ3 subunits could associate with the remaining αβ subunits.

4.3.2. Increased $GABA_A$ receptor δ subunit expression in cortical PV-containing interneurons following γ2 subunit deletion

To test whether the γ2 subunit was replaced with the δ subunit, I performed fluorescent immunolabelling for the δ subunit in the cortex of virus-injected $GABA_A R\gamma2^{77I}$lox mice. Surprisingly, I could see increased immunofluorescent signal for the δ subunit within the injection zone delineated by immunoreactivity for the Cre-recombinase (Fig. 22.A). At high magnification it was evident that a subset of Cre-expressing cortical INs showed strong immunolabelling for the δ subunit in their plasma membrane. The labelling pattern of neurogliaform cells with this antibody in the injected cortex, as well as the neuropil labelling in the molecular layer of the DG, was very similar to that described previously (Peng *et al.*, 2002; Olah *et al.*, 2009); the specificity of those immunoreactions have been tested using $\delta^{-/-}$ mice (Peng *et al.*, 2002; Olah *et al.*, 2009). To identify these INs, I performed fluorescent immunolabelling for

DOI:10.14753/SE.2015.1809

PV. Cre$^+$, PV-containing INs (PV INs) showed strong labelling for the δ subunit in their somato-dendritic membrane (Fig. 22.B). In contrast, PV INs outside the injection area showed a rather cytoplasmic staining for the δ subunit (Fig. 22.C). These results indicate that in the absence of the γ2 subunit, Cre$^+$, PV-containing, putative fast-spiking

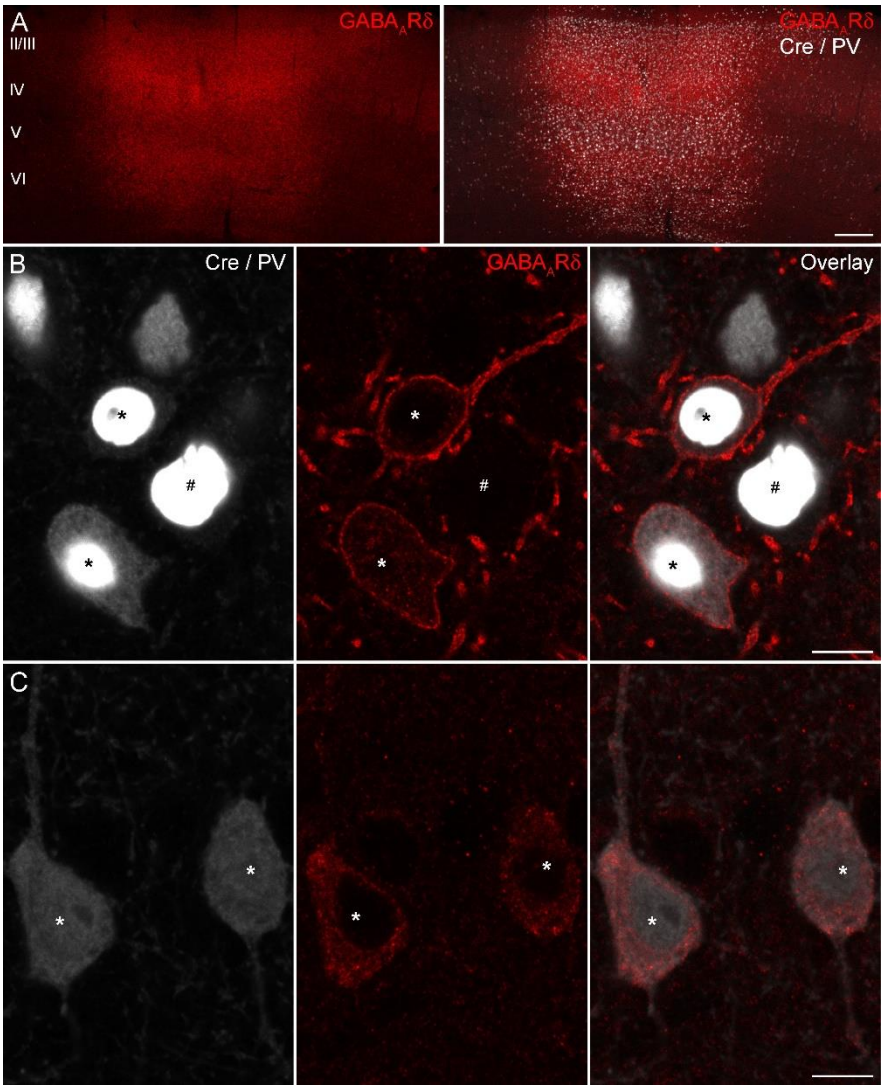

FIGURE 22. Increased fluorescent labelling for the GABA$_A$R δ subunit in Cre$^+$ PV-containing INs within the virus injection zone. (A) Increased immunoreactivity for the δ subunit (red) in the cortex overlaps with the injection zone delineated by Cre immunoreactivity (white on the overlay image). (B) High-magnification image depicted from the injection zone shows two Cre-expressing PV-containing INs (white, same secondary antibody; *) which contain strong plasma membrane labelling for the δ subunit (red). # shows a Cre-expressing cell which is immunonegative for both PV and the δ subunit. (C) * indicate two PV immunoreactive INs (white) in the vicinity of the injection zone which show cytoplasmic staining for the δ subunit (red). Roman numerals indicate cortical layers. Scale bars: 200 µm (A), 10 µm (B, C).

interneurons (FSINs) upregulate the δ subunit in their plasma membrane.

Unfortunately immunohistochemical labelling for the ε, γ1 and γ3 subunits in $GABA_AR\gamma2^{77I}$lox mice was unobtainable due to the lack of suitable specific antibody labelling against these subunits. Therefore the potential presence of either of these subunits in the plasma membrane of Cre^+ cells cannot be excluded.

Early works have shown that the δ subunit specifically co-assembles with α4 and α6 subunits (Jones *et al.*, 1997; Sur *et al.*, 1999), and more recently in DG INs partnership with the α1 subunits was described (Glykys *et al.*, 2007). To gain insight into the subunit composition of $GABA_ARs$ in these Cre^+ δ subunit-expressing putative FSINs, I performed immunofluorescent labelling for the α1 and α4 subunits. Immunoreactivity for the α1 subunit (Fig. 23.A and B), but not for the α4 subunit (Fig. 23.C), was present in the plasma membrane of Cre^+ δ subunit-expressing INs. Comparing the immunoreactivity for α1 subunit in these Cre^+ and Cre^- δ subunit-expressing putative FSINs, revealed no apparent change in fluorescent intensity (Fig. 23.A and B).

To reveal if the δ subunit can replace the γ2 subunit in GABAergic postsynaptic specializations, triple-labelling for the α1 and δ subunits, and gephyrin (which can be used as a marker of inhibitory synapses) was made. Interestingly, gephyrin clusters were absent from the somatic plasma membrane of δ subunit-containing Cre^+ INs within the injection zone (Fig. 23.A). In contrast, gephyrin clusters were present in the somata of Cre^- δ subunit-containing INs, where they co-localized with the α1 subunits but not with the δ subunit (Fig. 23.B).

One should be careful when interpreting this data, as the loss of gephyrin clusters does not necessarily mean the lack of GABAergic synapses, because other postsynaptic scaffolding molecules, such as the NL-2, can be involved in clustering $GABA_ARs$ at the synapse (Poulopoulos *et al.*, 2009). In addition to this, Mark Eyre could record spontaneous IPSCs from both Cre^+ and Cre^- putative FSINs of virus-injected $GABA_AR\gamma2^{77I}$lox mice (Fig. 24.A and B) at two weeks post injection. The frequency, amplitude and 10-90 % rise time of spontaneous IPSCs were not significantly different between Cre^+ and Cre^- FSINs ($p > 0.05$, paired Student's *t*-test), whereas the decay time constant was significantly slower ($p < 0.001$, paired Student's *t*-test) in Cre^+ FSINs compared to Cre^- cells (Fig. 24.C). Taken together, this suggests that

DOI:10.14753/SE.2015.1809

synaptic-like currents are maintained in Cre^+ putative FSINs following γ2 subunit deletion, but with altered kinetics.

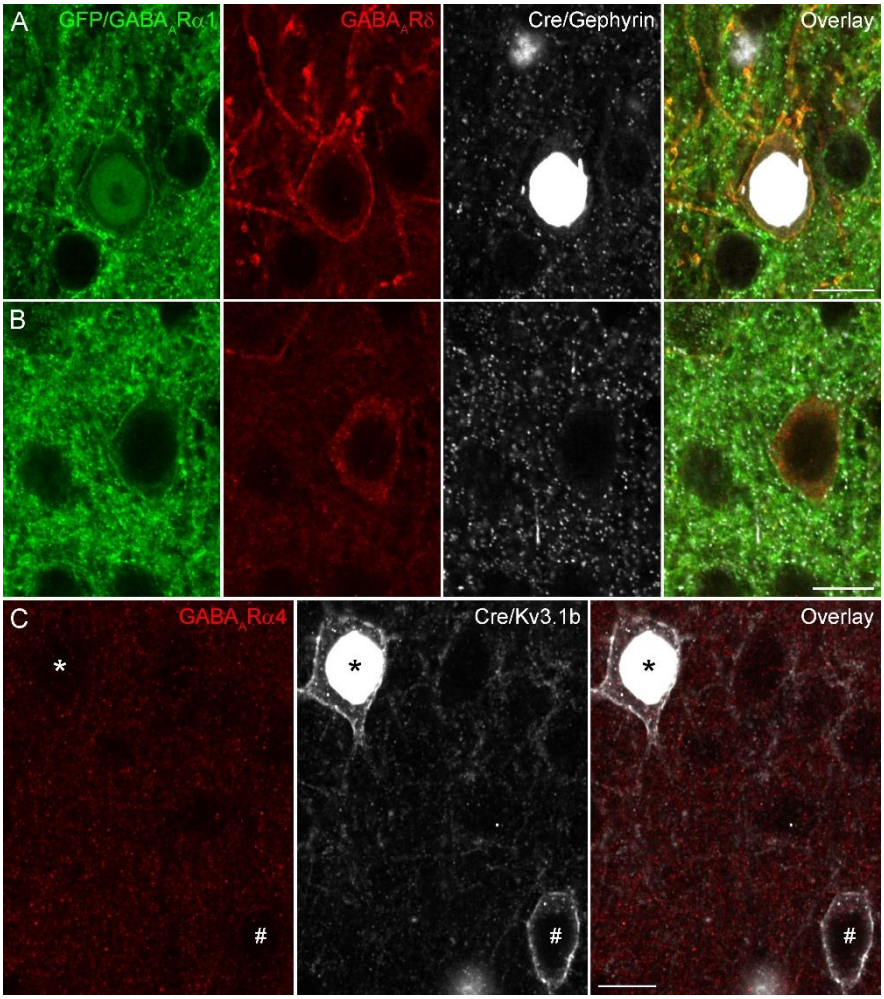

FIGURE 23. The δ subunit co-localizes with the $GABA_AR$ α1 subunit in Cre-expressing neurons. (A) Triple immunofluorescent labelling for the α1 subunit (green), the δ subunit (red), Cre and gephyrin (white, same secondary antibody) are shown. Note the co-localization of the α1 and δ subunits, which appears as yellow clusters in the plasma membrane of the cell (overlay image). The gephyrin clusters (white) are missing from the plasma membrane of a Cre^+ cell. The endogenous GFP (green) is also present in the nucleus of the cell. (B) A Cre-immunonegative cell from the vicinity of the injection zone shows punctate α1 (green) staining in its plasma membrane, which often co-localizes with gephyrin (white). (C) The $GABA_AR$ α4 subunit (red) is not expressed in either Cre^+ or Cre^- (white; * and #, respectively) putative FSINs, identified by Kv3.1b labelling. Scale bars: 10 μm (A–C).

Although from these experiments one cannot conclude that the δ subunit is absent from the GABAergic synapses of Cre^+ putative FSINs, it is worth noting that THDOC and DS2 (both acting on δ subunit-containing receptors) did not have any

effect on the amplitude and decay time constant of mIPSCs recorded from Cre^+ PCs and INs (experiments performed by Mark Eyre, for details see in (Kerti-Szigeti *et al.*, 2014)). Because the δ subunit was not found in the synapse (Nusser *et al.*, 1998; Wei *et al.*, 2003) and electrophysiological experiments showed its role in tonic inhibition (Nusser & Mody, 2002; Stell *et al.*, 2003), the most likely explanation is that δ subunits present in the somato-dendritic compartments of Cre^+ putative FSINs are localized to the extrasynaptic membrane.

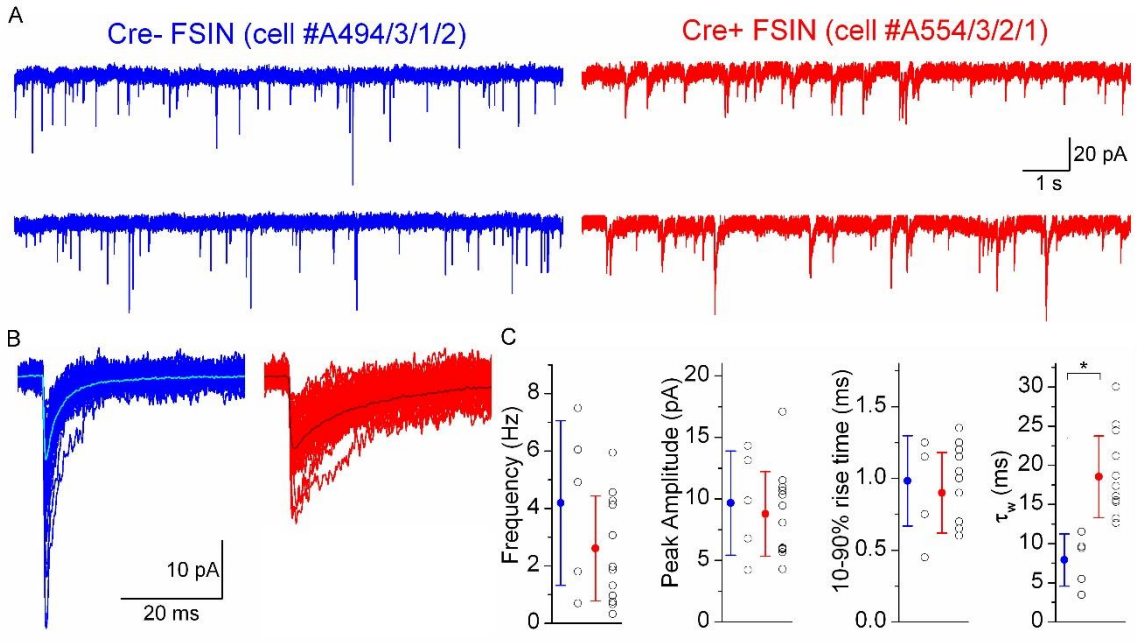

FIGURE 24. Neocortical FSINs lacking the $GABA_AR$ γ2 subunit display spontaneous IPSCs with altered decay kinetics. (A) Continuous whole-cell voltage-clamp recordings of spontaneous IPSCs from layer 2/3 Cre^- (left; blue) and Cre^+ (right; red) FSINs. (B) Average and individual spontaneous IPSC traces color-coded by experimental category are shown for the two example cells in (A). (C) Summary of peak amplitude, 10-90% rise time and weighted decay time constant (τ_w) of spontaneous IPSCs recorded in distinct experimental conditions. The mean τ_w of spontaneous IPSCs recorded from Cre^+ cells is significantly slower than in Cre^- cells (*; $p < 0.001$, paired Student's *t*-test).

4.3.3. Fast-spiking interneurons show a larger outward shift in the holding current following SR95531 application

To assess whether the increased δ immunoreactivity in Cre^+ FSINs is mirrored by an increased tonic inhibition, Mark Eyre performed *in vitro* somatic whole-cell voltage-clamp recordings from the somatosensory cortex of injected $GABA_AR\gamma2^{77I}$lox

DOI:10.14753/SE.2015.1809

mice. To obtain an objective measure of the mean tonic current, he used a method based on measuring the change in holding current following the application of SR95531, a $GABA_AR$ antagonist (Nusser & Mody, 2002). He specifically looked at FSINs within the injection zone identified by their high-frequency firing patterns to long depolarizing current injections (Fig. 25.A).

First, to increase tonic currents in these cells, he applied 1 µM THIP, which is a selective positive allosteric modulator of δ subunit-containing $GABA_ARs$ (Brown *et al.*, 2002), then washed in SR95531. Application of 20 µM SR95531 resulted in the

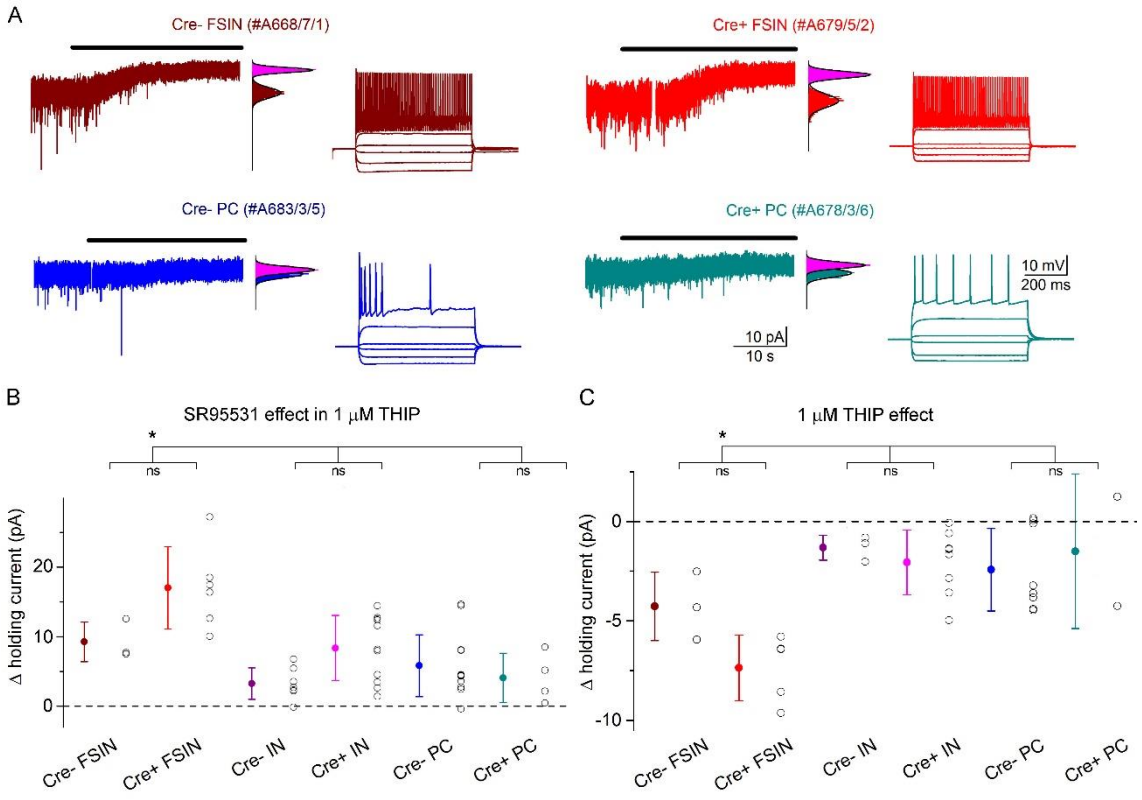

FIGURE 25. FSINs show a larger outward shift in the holding current following SR95531 application. (A) Left, Whole-cell voltage-clamp recordings of layer 2/3 cells color-coded by cell category. Top black horizontal lines indicate the perfusion of 20 µM SR95531. Right to the traces fits to the all-points histogram from segments before (color-coded by cell category) and after (magenta) SR95531 application are shown. The firing responses of the recorded neurons to hyper- and depolarizing current injections are also shown. (B and C) Summary of changes in the holding current for individual cells and group averages for each cell category upon application of SR95531 in the presence of 1 µm THIP (B) and upon 1 µm THIP application alone (C) * $p < 0.001$, Factorial ANOVA, *post-hoc* comparisons with Tukey's Unequal n HSD test; ns: non-significant.

complete disappearance of spontaneous IPSCs in both Cre^+ and Cre^- cells, and in Cre^+ FSINs produced a larger outward shift in the holding current than in Cre^- FSINs (Fig. 25.A, B). The shift in the holding current was almost 2 fold larger in Cre^+ FSINs (17.0 ± 5.9 pA) compared to Cre^- FSINs (9.3 ± 2.9 pA), but was not significantly different ($p = 0.26$; Factorial ANOVA, *post-hoc* comparisons with Tukey's Unequal n HSD test; n = 9 cells; Fig. 25.B). There was no significant difference between the change in the holding current in Cre^- vs. Cre^+ non-fast-spiking INs or PCs ($p = 0.26$ and $p = 0.99$, respectively; Factorial ANOVA, *post-hoc* comparisons with Tukey's Unequal n HSD test; n= 18 cells and 17 cells, respectively). However, the effect of SR95531 on holding current was significantly larger in FSINs than in other cell types ($p < 0.001$; Factorial ANOVA, *post-hoc* comparisons across cell-types with Tukey's Unequal n HSD test; Fig.25.B). When Mark applied the THIP alone, this resulted in a greater potentiation of the tonic current in Cre^+ FSINs (-7.4 ± 1.6 pA) compared to Cre^- FSINs (-4.3 ± 1.7 pA), but the effect was not significantly different ($p = 0.36$; Factorial ANOVA, *post-hoc* comparisons with Tukey's Unequal n HSD test; n = 8 cells; Fig. 25.C). However, when the THIP effect was compared across cell-types, the potentiation was significantly larger in FSINs than in other cell types ($p < 0.001$; Factorial ANOVA, *post-hoc* comparisons across cell-types with Tukey's Unequal n HSD test; Fig. 25.C). Taken together these results suggest a slight increase in the tonic currents in Cre-expressing putative FSINs, which is probably mediated by the δ subunit-containing receptors.

4.3.4. Immunofluorescent labelling for $GABA_A$ receptor α5 subunit is unchanged within the virus injection zone

The $GABA_AR$ α5 subunits, which probably form α5β3γ2 receptors (Farrant & Nusser, 2005), are localized to the extrasynaptic plasma membrane in hippocampal CA1 PCs (Pirker *et al.*, 2000; Sieghart & Sperk, 2002; Prenosil *et al.*, 2006), where they mediate tonic inhibition (Caraiscos *et al.*, 2004; Glykys & Mody, 2006). To reveal whether, the removal of the γ2 subunit from cortical PCs resulted in alterations in the expression of α5 subunits, I performed fluorescent immunohistochemistry. Immunoreactivity for the α5 subunit was unchanged within the injection zone (Fig. 26.A and B). At higher magnification, neuropil labelling in the injected cortex was very

similar to the non-injected hemisphere (Fig. 26.C and D). Here, I used double-labelling with the Kv2.1, which labels the plasma membrane of nerve cells (Kirizs *et al.*, 2014), and I specifically examined only those cells which looked like PCs. Immunoreactivity for the α5 subunit was similar in the plasma membrane of Cre^+ and Cre^- putative PCs (Fig. 26.C and D).

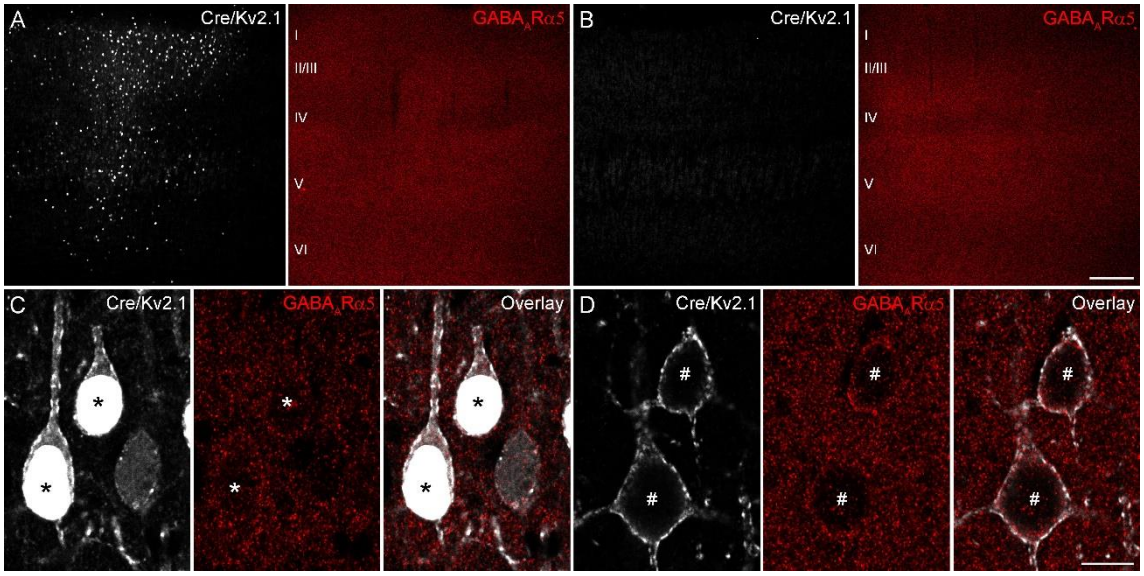

FIGURE 26. Immunoreactivity for the $GABA_AR$ α5 subunit is unchanged within the injection zone. (A) Cre immunoractivity (white) delineates the injection zone where immunolabelling for the α5 subunit is unchanged. (B) Contralateral hemisphere shows the lack of Cre immunostaining (white) and identical α5 immunoractivity (red) to that in the injection zone (A). (C and D) High magnification views of Cre-positive putative PCs (white), and immunoreactivity for the α5 subunit (red) from the injected (C) and contralateral (D) hemisphere. Note the similar α5 subunit labelling in the plasma membrane of putative PCs, delineated by immunolabelling for the Kv2.1 (white; same secondary antibody as the one used for visualizing the Cre recombinase). Roman numerals indicate cortical layers. Scale bars: 200 μm (A and B), 10 μm (C and D).

4.3.5. Freeze-fracture replica immunogold labelling demonstrates the synaptic location of $GABA_A$ receptor α1 and β3 subunits in perisomatic synapses of cortical Cre^+ cells

To provide direct evidence for the synaptic enrichment of $GABA_ARs$ in γ2 subunit-lacking cells, I carried out SDS-FRL of different $GABA_AR$ subunits (Figs. 27., 28.). Unfortunately, SDS treatment removes the majority of cytoplasmic and nuclear proteins from the replica; as a result the detection of Cre-recombinase by SDS-FRL is

very limited. However, based on the immunofluorescent data, the lack of the γ2 subunit in a given neuron seems to be a good indicator of the presence of Cre-recombinase in the nucleus. Therefore, I quantitatively assessed the γ2 content of a given cell to categorize it as either γ2-negative ($\gamma2^-$) or γ2-positive (γ2+), representing putative Cre^+ or Cre^- cells, respectively.

Paired recording experiments conducted by Mark Eyre established that unitary IPSCs could originate from perisomatic synapses for details see in (Kerti-Szigeti *et al.*, 2014), justifying my strategy of concentrating on somatic synapses with the SDS-FRL method. Most of the antibodies against different $GABA_A$Rs subunits available in our laboratory label on the E-face of the replica, where the typical clusters of IMPs characteristic for the PSD of GABAergic synapses on P-faces is absent (Kasugai *et al.*, 2010), making it difficult to delineate the border of a synapse. In order to identify inhibitory synapses, I used the GABAergic synapse-specific marker NL-2 (Varoqueaux *et al.*, 2004). Our NL-2 antibody recognizes intracellular epitopes and therefore labels on the P-face of the replica. This necessitated the use of 'mirror replica' technique (Hagiwara *et al.*, 2005); where the E-face of the replica was labelled for distinct $GABA_A$Rs and the complementary P-face was labelled either for NL-2 alone or in a subset of experiments together with the $GABA_A$R β3 subunit. In the P-face, the aggregation of IMPs and the gold particles labelling the NL-2, allowed the identification and delineation of GABAergic synapses. This synaptic area was then projected to the E-face and gold particles within the area and up to 30 nm from its edge were quantified.

Physiological data performed by Mark Eyre demonstrated that alteration in the decay kinetics of mIPSCs was stabilized from two weeks post-injection onwards (Kerti-Szigeti *et al.*, 2014). However, the possibility that some γ2 subunit proteins still remained in GABAergic synapses two weeks post-injection, making it difficult to differentiate between $\gamma2^+$ and $\gamma2^-$ cells, directed me to perform SDS-FRL on samples six weeks post-injection. This provides a more rigorous test of the potential synaptic clustering of the α and β subunits in the complete absence of the γ2 subunit.

First, I randomly selected somata within the layer 2/3 of virus injection zone originating from $GABA_A R\gamma2^{77I}$ mice, where I could find clusters of gold particles labelling for NL-2 (Figs. 27.A, E and 28.A, E). This indicated that perisomatic GABAergic synapses must be present following the γ2 subunit removal from the cortex.

DOI:10.14753/SE.2015.1809

Next, on the complementary face of the replica I quantitatively assessed the γ2 subunit content of the same cells in order to categorize them as either $\gamma2^+$ or $\gamma2^-$, respectively. Based on quantitative measurements of the synaptic γ2 subunit density, the cells fell indeed into two populations: a subset of cells contained mean synaptic γ2 density close to 0 (10.9 ± 13.9 gold/μm^2 with the guinea pig anti-γ2 antibody, Fig. 29.B and 2.0 ± 6.3 gold/μm^2 with the rabbit anti-γ2 antibody, Fig. 29.F; data from two $GABA_AR\gamma2^{77I}$ mice were pooled and mean density values were corrected for background, the values are expressed as mean ± SD, where the SD is the SD between cells; this applies to all data presented below), whereas the rest of the cells contained high density of gold particles

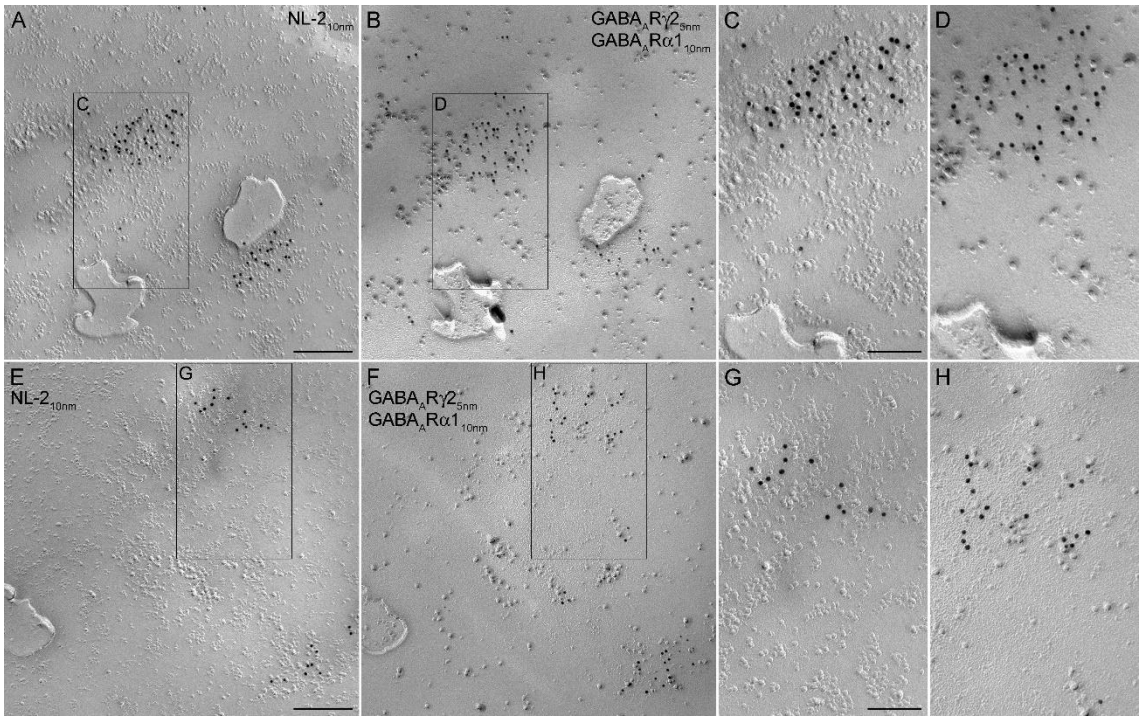

FIGURE 27. Immunogold labelling for the $GABA_AR$ γ2 and α1 subunits in GABAergic perisomatic synapses six weeks after virus injection. (A) P-face image of a layer 2/3 soma within the injection zone, showing immunogold labelling for NL-2 (10 nm gold). The clusters of gold particles delineate GABAergic synapses. (B) Complementary E-face image shows strong immunogold labelling for the α1 (10 nm gold) and γ2 (5 nm gold) subunits. (C and D) High-magnification images of the boxed areas outlined in (A and B). (E and F) Complementary P- (E) and E-face (F) image of another soma from the same replica as that presented in (A–D), showing two NL-2-containing synapses on the P-face. Note the presence of strong immunogold labelling for α1 subunit, but the lack of labelling for the γ2 subunit on the corresponding E-face. (G and H) High-magnification images of the boxed areas outlined in (E and F). Scale bars: 200 nm (A, B, E, F), 100 nm (C, D, G, H).

(176.0 ± 63.4 gold/μm^2 with the guinea pig antibody, Fig. 29.B and 1021.7 ± 154.4 gold/μm^2 with the rabbit antibody, Fig. 29.F). These results provide evidence that the absence or presence of the γ2 subunit can be used to categorize cells within the injection zone as putative Cre$^+$ or Cre$^-$, respectively. After the cells were categorized as either γ2$^+$ or γ2$^-$, I quantitatively assessed the density of synaptic NL-2, α1, and β3 subunits and compared the synaptic area in the two cell category (Fig. 29.A–H).

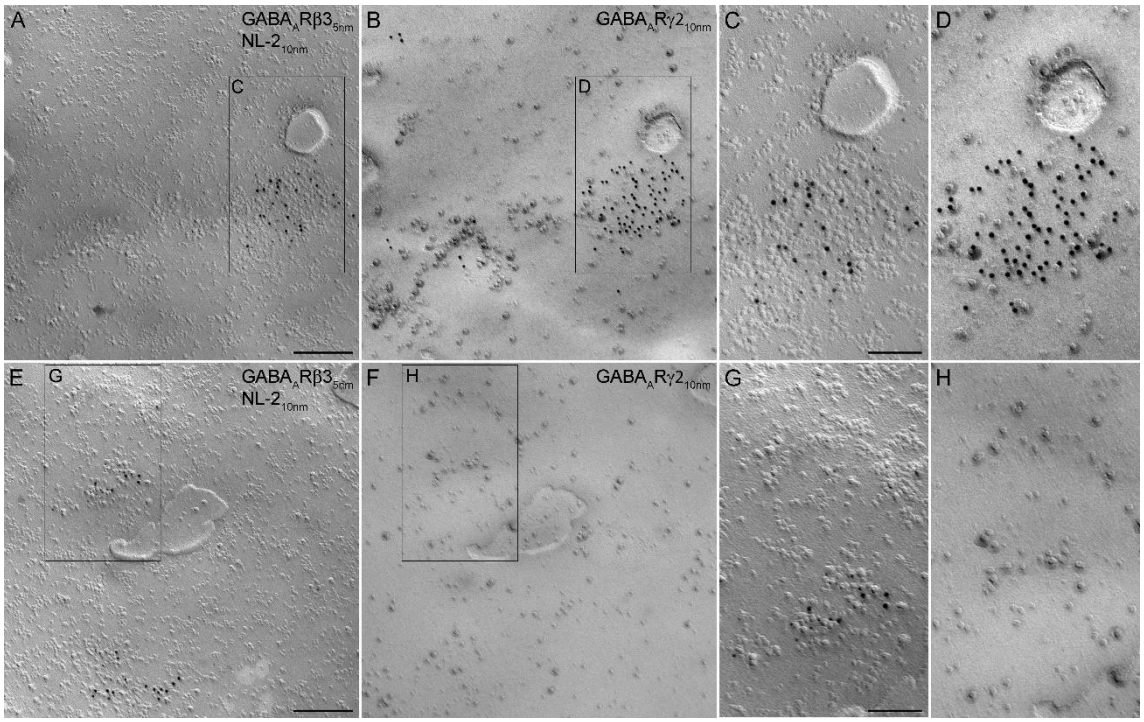

FIGURE 28. Immunogold labelling for the GABA$_A$R γ2 and β3 subunits in GABAergic perisomatic synapses six weeks after virus injection. (A and B) Mirror replica image of a layer 2/3 soma within the injection zone double-labelled on the P-face (A) for NL-2 (10 nm gold) and β3 subunit (5 nm gold) and on the E-face (B) for γ2 subunit (10 nm gold). (C and D) High-magnification images of the boxed areas outlined in (A and B). (E and F) Complementary P- and E-face images of another soma from the same replica as shown in (A–D), with synapses immunolabelled for NL-2 and the β3 subunit (E), but devoid of labelling for the γ2 subunit (F). (G and H) High-magnification images of the boxed areas outlined in (E and F). Scale bars: 200 nm (A, B, E, F), 100 nm (C, D, G, H).

First I looked at the synaptic density of NL-2 in γ2$^-$ and γ2$^+$ cells and found no significant difference, irrespective whether NL-2 was labelled on its own ($p = 0.52$; One-way ANOVA; Figs. 27. and 29.A) or it was double-labelled ($p = 0.47$; One-way ANOVA) with the β3 subunit (Figs. 28. and 29.E). Immunogold particles for the

DOI:10.14753/SE.2015.1809

$GABA_AR$ α1 (Fig. 27.) subunit were present in NL-2 positive synapses originating from both $\gamma2^+$ and $\gamma2^-$ cells. Despite the slightly reduced mean synaptic α1 density (Fig. 29.C) in the $\gamma2^-$ cells, there was no significant difference between the two cell population ($p = 0.07$; One-way ANOVA). Similarly, β3 subunits were also concentrated in NL-2-containing synapses (Fig. 28.) originating from both $\gamma2^+$ and $\gamma2^-$ cells. Although quantitative measurements revealed a slightly reduced mean synaptic β3 density (Fig. 29.G) in the $\gamma2^-$ cells, this was not significantly different from that found in $\gamma2^+$ cells

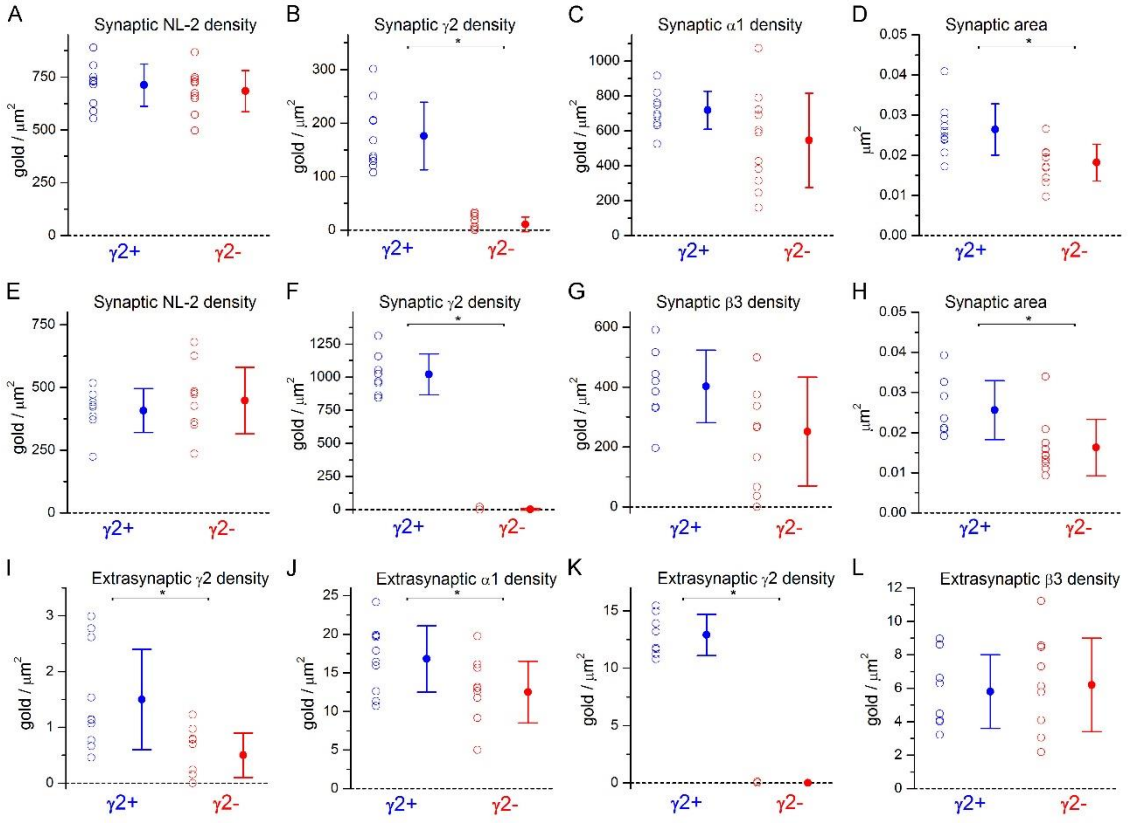

FIGURE 29. Quantitative measurements conducted 6 weeks post injection in cortical layer 2/3 neurons within the injection zone. (A–C, E–G) The background-subtracted density values of synaptic immunogold labelling for NL-2 (A, E), γ2 ((B), guinea pig antibody; (F), rabbit antibody), α1 (C) and β3 (G) subunits are shown for individual $\gamma2^+$ and $\gamma2^-$ (red) cells with the respective population means. * $p < 0.00001$ (B) and * $p < 0.0001$ (F); One-way ANOVA. (D, H) The mean area of $\gamma2^-$ perisomatic synapses (red) is significantly smaller than that of $\gamma2^+$ synapses (blue; * $p < 0.001$; One-way ANOVA; applies for both). (I–L) The background-subtracted density values for extrasynaptic immunogold labelling for γ2 ((I), guinea pig antibody; (K), rabbit antibody), α1 (J) and β3 (L) subunits are shown for individual $\gamma2^+$ and $\gamma2^-$ (red) cells with the respective population means. * $p < 0.05$; One-way ANOVA, applies for all. Data from two $GABA_AR\gamma2^{77I}$ mice were pooled.

(p=0.06; One-way ANOVA). In one cell, all synapses were β3 negative, indicating that the somatic plasma membrane likely belonged to a β3 immunonegative GABAergic IN. Taken together, these results provide direct evidence for the synaptic enrichment of $GABA_A$Rs without the γ2 subunit.

An interesting finding of this investigation was that the area of GABAergic somatic synapses estimated from the NL-2 labelling, was significantly ($p < 0.03$; Tukey's *post-hoc* test) smaller in $\gamma2^-$ cells (0.018 ± 0.008 μm^2; n = 113 synapses on 21 cells from two mice, pooled across α1 and β3 subunit experiments) compared to $\gamma2^+$ cells (0.025 ± 0.014 μm^2; n = 239 synapses on 18 cells from two mice, pooled across α1 and β3 subunit experiments; Fig. 29.D and Fig. 29.H). This indicates that the total number of synaptic NL-2, α1 and β3 subunits is somewhat reduced in Cre^+ cells.

In addition to the quantitative analysis of synaptic α1 and β3 subunits, I assessed the extrasynaptic labelling for these two subunits by counting gold particles outside the synaptic areas delineated on the P- or E-face membranes of the quantified cells. Similarly to the synaptic γ2 density, the extrasynaptic gold particle density for the γ2 subunit (Fig. 29.I and K) was almost 0 in the $\gamma2^-$ cells (0.5 ± 0.4 gold/μm^2 in $\gamma2^-$ cells vs. 1.5 ± 0.9 gold/μm^2 in $\gamma2^+$ cells with the guinea pig antibody; 0.0 ± 0.0 gold/μm^2 in $\gamma2^-$ cells vs. 12.9 ± 1.8 gold/μm^2 in $\gamma2^+$ cells with the rabbit antibody). Extrasynaptic gold particle density for the α1 subunit was significantly reduced in the $\gamma2^-$ cells compared to $\gamma2^+$ cells ($p = 0.03$; One-way ANOVA; Fig. 29.J), while the extrasynaptic β3 density did not changed ($p = 0.75$; One-way ANOVA; Fig. 29.L). From the mean gold density values for α1 subunit a ratio of synaptic to extrasynaptic density was calculated, which was 46 vs. 47 in the $\gamma2^+$ vs. $\gamma2^-$ cells, respectively. The ratio of synaptic to extrasynaptic β3 density was 72 vs. 40 in the $\gamma2^+$ vs. $\gamma2^-$ cells, respectively. The unchanged ratio of synaptic to extrasynaptic α1 subunit densities in the two cell category indicates that the total cell-surface number of α1 subunits is somewhat reduced in Cre^+ cells. The almost two fold reduction in the synaptic to extrasynaptic β3 subunit density ratio could be the result of a somewhat larger reduction in the synaptic β3 subunit density in $\gamma2^-$ cells or a slight increase in the extrasynaptic receptor pool. However, these alterations support the dynamic interaction between synaptic and extrasynaptic receptors, as has been suggested to occur by single-particle tracking studies (Jacob *et al.*, 2005; Bogdanov *et al.*, 2006).

DOI:10.14753/SE.2015.1809

5. DISCUSSION

In the present dissertation, by using the high-resolution SDS-FRL technique, I revealed the unique somato-dendritic distribution and densities of two molecularly and functionally distinct potassium channel subunits in CA1 PCs (i.e. $K_v4.2$ and $K_{ir}3.2$). Furthermore, I provided evidence for the synaptic clustering of $GABA_AR$ α1 and β3 subunits in the absence of γ2 subunit in cortical layer 2/3 cells of $GABA_AR\gamma2^{77I}$lox mice.

During the last decade a great effort was made on describing the cell type- and compartment-specific distribution of voltage- and ligand-gated ion channels. These studies mostly consisted of electrophysiological (i.e. patch-clamp) and light microscopic and electron microscopic studies using subunit-specific antibodies. The combination of these methods allowed the function of a particular ion channel to be linked with the underlying structure. Although patch-pipette recordings allow the sub-cellular identification of ion channels at relatively large cellular compartments, like soma, dendrite and AIS, the small diameter oblique dendrites and axon terminals remain inaccessible to these techniques. In contrast, electron microscopic immunolocalization techniques allow the study of subcellular compartments at nanometer resolution. Moreover, using the SDS-FRL technique it became possible to visualize and quantify transmembrane proteins over large plasma membrane areas without the need for reconstruction of the studied subcellular compartment, which was previously necessary for conventional serial section electron microscopic techniques. The combination of the techniques mentioned above, give insight into the subcellular distribution, as well as function of different ion channels, and promote our understanding on the computational properties of nerve cells.

5.1. Novel distribution pattern of the $K_v4.2$ subunit along the somato-dendritic axis of CA1 PCs

In the first part of the dissertation, I revealed a previously unseen distribution pattern of the $K_v4.2$ subunit on the surface of CA1 PCs, where its density shows a moderate increase from proximal to distal dendrites in the SR, then a slight decrease in

the SLM (Kerti *et al.*, 2012). The approximately 70 % increase in the density within the SR is much less than the reported six-fold increase in I_A in the distal apical dendritic trunk (Hoffman *et al.*, 1997)**.** Although the density of the $K_v4.2$ subunit is slightly higher in small-diameter oblique dendrites and dendritic spines than in the corresponding main apical trunk, the approximately 25 % difference is unlikely to underlie a fundamentally distinct role of I_A in main vs. oblique dendrites. What could be the reason for the discrepancy between I_A and $K_v4.2$ subunit, when dendritic I_A is exclusively mediated by this subunit in CA1 PCs?

A possible explanation could be that the $K_v4.2$ subunits are in distinct functional states along the apical dendrites of PCs; i.e. channels in the distal dendrites conduct K^+ within a hyperpolarized voltage range compared to that of their somatic/proximal dendritic counterparts (Hoffman *et al.*, 1997). Thus we can assume that interactions with some auxiliary proteins and certain posttranslational modifications might regulate the function of these channels. Indeed, in hippocampal CA1 neurons the ternary complex of K_v4, dipeptidyl peptidase-like type II proteins (DPP6, DPP10) and voltage-gated potassium channel-interacting proteins (KChIPs) is thought to underlie the native I_A (Kim & Hoffman, 2008; Maffie & Rudy, 2008). Immunoreactivity for KChIP2 and KChIP4 (the two auxiliary proteins expressed by CA1 PCs), and DPP6 show increasing-decreasing labelling patterns in the SR and SLM of the CA1 area, similar to that of the $K_v4.2$ subunit (Rhodes *et al.*, 2004; Clark *et al.*, 2008). The formation of specific ternary $K_v4.2$–DPPX–KChIP complexes results in currents with different kinetic properties of activation and inactivation; moreover, the two families of auxiliary proteins enhance the cell surface expression of $K_v4.2$ channels (Kim & Hoffman, 2008). A recent study demonstrated elegantly the critical role of DPP6 in generating the I_A gradient along the proximo-distal axis of CA1 PCs (Sun *et al.*, 2011).

Kv4.2 channels, as many other ion channels, are substrates for phosphorylation which can modulate its cell surface expression. It has been shown that $K_v4.2$ channels in hippocampal CA1 PC dendrites are regulated by protein kinase C (PKC), protein kinase A (PKA), Ca^{2+}/calmodulin-dependent protein kinase II (CaMKII) and mitogen-activated protein kinase (Hoffman & Johnston, 1998; Yuan *et al.*, 2002). Phosphorylation by PKC and PKA results in a 15 mV depolarizing shift in the activation curve of I_A in CA1 PC dendrites (Hoffman & Johnston, 1998). As a result,

DOI:10.14753/SE.2015.1809

the same depolarization activates less I_A following PKA/PKC phosphorylation of the channels. Therefore, a distance-dependent decrease in the phosphorylation state of the $K_v4.2$ subunit along the proximo-distal dendrites of CA1 PCs could reconcile the differences in the activation curve of I_A in distal and proximal dendrites. However, it does not explain the differences in the peak I_A density increase and $K_v4.2$ density in main apical trunks within the SR. It should be noted that phosphorylation by PKA also causes internalization of $K_v4.2$ channels from spine plasma membranes of PCs (Kim *et al.*, 2007; Hammond *et al.*, 2008) and that cycling rate is significantly higher in the distal dendrites than in the proximal ones (Nestor & Hoffman, 2012). Such regulation, however, results in changes in surface density of the channels, which is readily detectable with SDS-FRL.

My results, showing the specificity of immunogold signal on the somato-dendritic compartments and the lack of it in axon terminals, demonstrate that a given antibody could provide specific and nonspecific labelling in distinct subcellular compartments under identical experimental conditions. It is important to note that immunosignal obtained with light microscopic fluorescent techniques completely disappeared in $K_v4.2^{-/-}$ mice, demonstrating that all immunosignals in these light microscopic reactions were due to specific antibody–$K_v4.2$ protein interactions. If I had taken these light microscopic control experiments as evidence for the specificity of the immunogold signal in SDS-FRL, I would have erroneously concluded the presynaptic presence of the $K_v4.2$ subunit. This emphasizes that the specificity of an immunoreaction needs to be tested under each experimental condition, in each brain region, cell type and even subcellular compartment (Lorincz & Nusser, 2008); as a given antibody under the same immunoreaction can provide both specific and nonspecific labelling patterns in different subcellular compartments. This is not surprising, because the cross-reacting protein could have a subcellular compartment-specific distribution pattern within the examined brain region.

DOI:10.14753/SE.2015.1809

5.2. Increased immunogold particle density for the $K_{ir}3.2$ subunits in the distal apical dendrites of CA1 PCs

In contrast to the $K_v4.2$ subunit, the density of gold particles labelling the $K_{ir}3.2$ subunit showed a quasi linear increase from the soma towards the distal dendrites, with no significant difference between the main apical dendrites, oblique dendrites or dendritic spines at approximately the same distance from the soma. This is in good agreement with the work of Chen and Johnston (Chen & Johnston, 2005), who described an enhanced spontaneous activity of $K_{ir}3$ channels at resting membrane potential in the apical dendrites of CA1 PCs as compared to somata, which might be the result of increased channel number or increased open probability of the channels. The increased immunogold density in the distal part of the SR and SLM suggest that the larger spontaneous activity of $K_{ir}3$ channels is likely the result of an increased channel density in the distal apical dendrites. However, it should be noted that the function of $K_{ir}3$ channels may depend on the constitutive activity of metabotropic receptors or ambient concentration of their agonists (Makara & Magee, 2013). Immunoreactivity for $GABA_BRs$ (the most common activators of the $K_{ir}3$ channels) is not uniform within the CA1 area; the immunosignal is higher in SLM than in the SR (Kulik *et al.*, 2003; Lopez-Bendito *et al.*, 2004). In addition, an SDS-FRL immunogold study has shown the close proximity of $K_{ir}3.2$ and $GABA_{B1}Rs$ on CA1 PC dendrites and spines (Kulik *et al.*, 2006). It is known that, in dendrites, constitutively active $K_{ir}3$ channels contribute to the resting membrane potential and underlie slow inhibition onto the postsynaptic cell (Luscher *et al.*, 1997). Furthermore, they control synaptic integration and dendritic signalling of electrical events (Takigawa & Alzheimer, 2002), and according to a recent study they are involved in compartmentalized dendritic integration and AP output regulation in CA3 PC thin dendrites (Makara & Magee, 2013). It would be interesting to see whether such compartmentalized dendritic integration also takes place in CA1 PCs, which would require detailed electrophysiological and computational experiments.

Gold particles labelling the $K_{ir}3.2$ subunit have been found occasionally in presynaptic axon terminals in the CA1 area. However, quantitative results revealed that the density was not significantly different from the background labelling obtained on surrounding E-face membranes. Other studies (Drake *et al.*, 1997; Koyrakh *et al.*, 2005;

Kulik *et al.*, 2006) have also described few gold particles labelling the $K_{ir}3.1$ and $K_{ir}3.2$ subunits in the CA1 area; however their densities were not quantified.

5.3. Unique distribution pattern of distinct ion channel subunits in CA1 PCs

In my dissertation I show a detailed quantitative study of two distinct potassium channel subunit on the surface of CA1 PCs. Previously, our laboratory has examined the cell surface distribution of the HCN1 channel subunit and found an exclusive somato-dendritic distribution (Lorincz *et al.*, 2002). Similarly, both the $K_v4.2$ and the $K_{ir}3.2$ subunits were localized to the somato-dendritic surface of CA1 PCs. Electrophysiological recordings demonstrated a similar distance-dependent increase in both the I_H and I_A along the apical dendrites of CA1 PCs (Hoffman *et al.*, 1997; Magee, 1998). However, electron microscopic immunogold studies revealed that unlike HCN1, the $K_v4.2$ subunit does not follow the distance-dependent increase in the current density along the apical dendrites of CA1 PCs. Instead of having a monotonous increase, the density of the $K_v4.2$ subunit first slightly increases within the SR, then decreases in the SLM. Contrary to $K_v4.2$ subunit distribution, the density of $K_{ir}3.2$ subunits showed a quasi linear increase along the apical dendrites of CA1 PCs, which clearly matched with the increased channel activity described in the distal dendrites of the CA1 PCs (Chen & Johnston, 2005). All three channels were present in dendritic spines, but the density of HCN1 channels was two- to three-fold lower in dendritic spines than in shafts at the same distance from the soma, while the density of $K_v4.2$ and $K_{ir}3.2$ subunits in spines was not significantly different than that in the corresponding apical trunk. None of these channels were present in the axon terminals from the CA1 region.

The distribution patterns of these ion channels are very different from those of the $Na_v1.6$ subunit of the voltage-gated sodium channel family, and $K_v1.1$ and $K_v2.1$ subunits. Interestingly, the $Na_v1.6$ subunit shows a distance-dependent decrease from proximal to distal dendrites of CA1 PCs (Lorincz & Nusser, 2010), whereas the highest density was found in nodes of Ranvier and in AISs, and was absent from the spines. Similarly to $Na_v1.6$ subunits, the $K_v1.1$ and $K_v2.1$ subunits have been also localized to the AIS (Kirizs *et al.*, 2014). This study was done in collaboration with Tekla Kirizs, who performed immunolocalization of the $K_v1.1$ and $K_v2.1$ subunits, whereas I

performed immunolocalization of the $K_{ir}3$ subunits, which are presented in this dissertation. Here, I summarize the major findings of Tekla Kirizs, which improve our understanding of the subcellular distribution of voltage-gated ion channels in CA1 PCs. She found that the $K_v1.1$ subunit is restricted to axonal compartments, and the density of $K_v1.1$ in AISs was eight-fold higher than in axon terminals. In contrast, the $K_v2.1$ has an axo-somato-dendritic distribution, with almost similar densities (~10 gold/μm^2) in AISs, somata and proximal apical dendrites, but with no detectable labelling in oblique dendrites or spines. Although both subunits were present in the AISs, they occupied discrete, non-overlapping subdomains within the AISs of CA1 PCs (Kirizs *et al.*, 2014).

Taken together, these data suggest that in addition to the molecular and functional diversity of individual ion channels, their expression profile is also unique; different subunits have cell type- and subcellular compartment-specific distribution patterns (Nusser, 2012). Further investigations are needed to dissect if a subcellular compartment-specific plasticity of these channels can occur; more exactly, it would be interesting to investigate whether changes in activity in a neuronal network (i.e. enriched environment) would result in a spatial rearrangement of an ion channel at certain subcellular compartments of CA1 PCs.

5.4. Clustering of $GABA_A$ receptors in the absence of the γ2 subunit in neocortical layer 2/3 cells

In the second part of the dissertation I challenged the long-standing view on the role of $GABA_AR$ γ2 subunits in clustering $GABA_ARs$ at inhibitory postsynaptic specializations (Essrich *et al.*, 1998; Schweizer *et al.*, 2003). By using a temporally and spatially restricted Cre-recombinase-mediated deletion of the γ2 subunit gene, Mark Eyre has found that inhibitory synaptic currents remained in Cre^+, γ2 subunit-lacking cortical neurons. Using the high-resolution SDS-FRL technique, here I demonstrate that $GABA_AR$ α1 and β3 subunits are concentrated in perisomatic inhibitory synapses of γ2 subunit-lacking cortical neurons.

These data demonstrate that the γ2 subunit is not essential for fast inhibitory synaptic transmission and postsynaptic receptor clustering in neurons of the adult somatosensory cortex. This is in contrast with the work of Schweizer et al. (Schweizer

et al., 2003), who found that the γ2 subunit is required for maintenance of $GABA_A$Rs at mature synapses. This and other reports examining cultured cortical cells derived from $\gamma2^{0/0}$ animals (Essrich *et al.*, 1998; Sumegi *et al.*, 2012) have shown strong reductions in clustered immunofluorescent labelling for the γ2, α1, α2 subunits and gephyrin. A recent study using the same virally-mediated γ2 subunit deletion approach has shown that the spontaneous and evoked GABAergic synaptic currents disappeared in thalamocortical cells when the presynaptic, reticular thalamic neurons fired in tonic mode, which was mirrored by a reduced intensity in the immunofluorescent labelling for the α1 subunit (Rovo *et al.*, 2014). Contrary to these findings, my immunofluorescent reactions demonstrated a dramatic reduction of the γ2 subunit, but no change in the α1 and β3 subunit immunolabelling intensity within the injection zone. Moreover, the labelling for α1 and β3 subunits were clustered in the somatic plasma membrane of Cre^+ cells, indicative of synaptic receptor clustering (Fritschy *et al.*, 1998). To provide more precise evidence that these clusters indeed represent synaptic $GABA_A$Rs in the Cre^+ cells, I turned to SDS-FRL. High-resolution immunogold labelling for NL-2 demonstrated the presence of GABAergic synapses on the somata of $\gamma2^-$ cells, where the densities of the α1 and β3 subunits were comparable to those found in $\gamma2^+$ cells. Although the densities of the α1 and β3 subunits were not significantly different, their absolute number in the synapse was reduced in $\gamma2^-$ compared to $\gamma2^+$ cells due to smaller synaptic areas. I have to emphasize that although I detected the α1 and β3 subunits in somatic synapses of $\gamma2^-$ cells, this does not exclude the presence of other α and β subunits (i.e., α2 and β2) likely to be present at these synapses.

Data obtained by electrophysiological recordings and SDS-FRL suggest two possibilities, which might account for the presence mIPSCs and $GABA_A$R clustering in the Cre^+, $\gamma2^-$ cortical cells. (1) First, it is easy to conceive that the remaining αβ subunits co-assembled to form functional heteropentamers in the $\gamma2^-$ cells, as has been suggested to occur in expression systems and neurons *in situ* (Mortensen & Smart, 2006). However, when Mark Eyre recorded mIPSCs in the presence of 10 μM Zn^{2+}, which at low concentrations specifically inhibits the αβ subunit-only receptors (Draguhn *et al.*, 1990; Smart *et al.*, 1991), he found no change in the mIPSC frequency or peak amplitude (Kerti-Szigeti *et al.*, 2014). This argues against the presence of αβ subunit-only receptors in the synapses of $\gamma2^-$ cells. (2) A second possibility is that a different

$GABA_AR$ subunit replaced the missing γ2 subunit to maintain the heteropentameric assembly. The series of pharmacological experiments performed by Mark Eyre indicated that the subunit composition of the synaptic receptors is most likely αβγ3, rather than αβ-only, αβδ, αβε or αβγ1 (Kerti-Szigeti *et al.*, 2014). The potential presence of γ3 subunits in the receptor can account for the lack of Zn^{2+} effect on mIPSC frequency and peak amplitude, as αβγ3 receptors are less sensitive to Zn^{2+} than the αβ subunit-only receptors (Draguhn *et al.*, 1990; Herb *et al.*, 1992).

Our conclusion is in line with that of Baer et al. (Baer *et al.*, 1999) who demonstrated that the transgenic overexpression of the γ3 subunit could rescue the synaptic clustering of the α1 and α2 subunits and gephyrin in $\gamma2^{0/0}$ mice, similarly to the γ2 subunit when overexpressed in $\gamma2^{-/-}$ neurons (Alldred *et al.*, 2005). Although expressed in very restricted brain regions (Wilson-Shaw *et al.*, 1991; Herb *et al.*, 1992; Pirker *et al.*, 2000), the γ3 subunit is equal to the γ2 subunit in its ability to form functional heteropentamer receptor channels (Knoflach *et al.*, 1991). A low level of mRNA for the γ3 subunit has been detected in the mouse cortex (Wilson-Shaw *et al.*, 1991), but unfortunately I could not provide a direct immunohistochemical demonstration of the γ3 subunit in somatic synapses due to the lack of suitable, specific antibody labelling against the γ3 subunit.

An unexplainable finding of this study was the almost 2-fold reduction in the synaptic area on $\gamma2^-$ cells compared to their $\gamma2^+$ counterparts. Synaptic area was delineated based on the immunogold labelling for NL-2, a cell adhesion protein known to be present in inhibitory synapses (Varoqueaux *et al.*, 2004). However, besides NL-2, other molecules have been recognized as scaffolding proteins at GABAergic synapses, the most important being gephyrin (Fritschy *et al.*, 2012; Tyagarajan & Fritschy, 2014). It was shown that NL-2 can interact with gephyrin to activate collybistin, and subsequently recruit $GABA_ARs$ to the postsynaptic site (Poulopoulos *et al.*, 2009). Therefore, I hypothesize that the change in the synaptic area might be the consequence of a change in the molecular composition of the postsynaptic scaffold in the Cre^+, $\gamma2^-$ cells. Panzanelli et al. (Panzanelli *et al.*, 2011) reported the loss of gephyrin, but not NL-2 clusters, in the perisomatic synapses of CA1 PCs in mice lacking the $GABA_AR$ α2 subunit. In a subset of immunofluorescent reactions (Fig. 23.A) I indeed observed reduced gephyrin clustering in Cre^+ cells within the injection zone. This qualitative

observation is in line with previous results (Essrich *et al.*, 1998; Brunig *et al.*, 2002; Schweizer *et al.*, 2003) showing reduced gephyrin clustering in the absence of the γ2 subunit. I have to point out that direct electron microscopic demonstration of the change in gephyrin clustering in Cre^+ cells was not possible, because good quality immunogold labelling for the gephyrin on replica was not obtainable, as not all antibodies provide specific labelling on the replica.

In addition to the scaffolding proteins mentioned above (NL-2, collybistin, gephyrin), the dystrophin-glycoprotein complex has also been described in a subset of neurons in cortical areas, including the entire cerebral cortex, hippocampus, and cerebellum (Fritschy *et al.*, 2012), with selective somato-dendritic expression (Knuesel *et al.*, 1999; Panzanelli *et al.*, 2011). Therefore, further investigations are needed to reveal if the loss of γ2 subunits from the synapse would alter the distribution of the dystrophin-glycoprotein complex in cortical perisomatic synapses, leading to reduced inhibitory PSD size.

The upregulated $GABA_AR$ δ subunit in the somato-dendritic compartments of Cre^+ PV INs is somewhat intriguing. Using light microscopic immunofluorescent labelling for the δ subunit in $GABA_AR\gamma2^{77I}$lox mice, I observed an increased immunosignal within the injection zone, which was confined to Cre^+ PV INs. In contrast, PV INs outside the injection zone showed weak, cytoplasmic-like labelling for the δ subunit. The presence of the δ subunit has been described in a subset of DG INs, where they specifically co-assemble with the α1 subunit (Glykys *et al.*, 2007). However, based on qualitative observations, I could not detect any change in the immunofluorescent labelling for the α1 subunit in those Cre^+ cells where the δ subunit was upregulated. Unfortunately, high-resolution SDS-FRL demonstration of the upregulated δ subunit, as well as possible changes in the α1 subunit expression in the plasma membrane of Cre^+, PV-containing putative FSINs was not obtainable, due to the difficulty to find and label FSINs in a replica. The δ subunit-containing $GABA_ARs$ mediate tonic inhibition and are expressed extrasynaptically (Nusser *et al.*, 1998; Stell *et al.*, 2003; Wei *et al.*, 2003; Sun *et al.*, 2004). Electrophysiological recordings performed by Mark Eyre revealed that Cre^+ FSINs show a larger outward shift in the holding current following SR95531 application compared to other cell types. Cre^+ FSINs showed a trend toward larger tonic currents, which were potentiated by THIP,

although these changes were not statistically significant. Taken together, these results suggest that the δ subunit is most likely expressed in the extrasynaptic plasma membrane of Cre^{+}, PV-containing putative FSINs, where it contributes to tonic inhibition.

Interestingly, in $\delta^{-/-}$ mice, the expression of the γ2 subunit is increased in areas where the δ subunit is normally expressed, including cerebellar and DG GCs and thalamic relay cells (Tretter *et al.*, 2001; Peng *et al.*, 2002). This, however, indicates that in a subset of cortical cell types, where tonic inhibition specifically controls the input-output transformations of a given neuron (Brickley *et al.*, 1996; Hamann *et al.*, 2002; Semyanov *et al.*, 2003; Chadderton *et al.*, 2004), the γ2 and δ subunits are interchangeable. Tonic inhibition in hippocampal INs decreases their excitability and subsequently regulates the inhibitory drive to PCs (Semyanov *et al.*, 2003) as well as the frequency of gamma oscillations (Mann & Mody, 2010; Ferando & Mody, 2013). PV INs specifically target the soma and proximal dendritic region of PCs. Therefore, I speculate that Cre^{+} PV INs may upregulate the δ subunit in their plasma membrane to counterbalance possible alterations in the local cortical networks following the removal of the γ2 subunit from INs and PCs. Taken together, these data highlight the extraordinary plasticity of cortical neurons (PCs and INs) to maintain proper perisomatic GABAergic neurotransmission despite the lack of γ2 subunits, thus preserving the balanced excitation and inhibition in cortical microcircuits.

DOI:10.14753/SE.2015.1809

6. CONCLUSIONS

Conclusions for the first part of my dissertation are:

1. Distribution of immunogold particles for the $K_v4.2$ subunit shows homogenous distribution pattern along the proximo-distal axis of rat CA1 PCs.
2. The steep increase in I_A current density cannot be explained by a corresponding increase in channel number.
3. Probably other mechanisms are involved in the generation of I_A current density: such as interactions with auxiliary subunits (KChIPs and DPP6) and phosphorylation.
4. Distribution of immunogold particles for the $K_{ir}3.2$ subunit shows a quasi linear increase from the soma towards the distal dendrites of CA1 PCs.
5. There is no significant difference in $K_{ir}3.2$ density between the main apical dendrites, oblique dendrites or dendritic spines at approximately the same distance from the soma.

In the first part of my dissertation I revealed a previously unseen subcellular distribution pattern and density of two functionally different potassium channel (i.e. $K_v4.2$ and $K_{ir}3.2$) subunits in the rat CA1 PCs. My results suggest that potassium channels regulate neuronal excitability in a compartment-specific manner.

Conclusions for the second part of my dissertation are:

1. Both α and β subunits are concentrated in inhibitory synapses following virus-mediated γ2 subunit deletion.
2. The density of gold particles labelling the synaptic α1 and β3 subunits is unchanged in cells lacking the γ2 subunit.
3. Pharmacological experiments performed by my colleague Dr. Mark D. Eyre indicate that in Cre^+ cells the γ3 subunit replaced the γ2 subunit in the heteropentameric receptor channels.
4. The $GABA_A$ receptor δ subunit is upregulated in the somato-dendritic plasma membrane of Cre^+ PV INs.

Experiments conducted in the second part of my dissertation revealed that postsynaptic $GABA_A$ receptor clustering can still occur in mouse cortical layer 2/3 neurons following γ2 subunit deletion.

DOI:10.14753/SE.2015.1809

7. SUMMARY

Understanding the function of cortical pyramidal cells (PCs) begins with an appreciation of their plasma membrane's ion channel content. However, much of what we know about the ion channel repertoire of PCs comes from electrophysiological and light microscopic immunohistochemical studies. Among the ion channels, potassium channels have received special attention in the last decade, although the precise subcellular distribution and densities of most of these channels are still lacking.

In the first part of the dissertation I aimed to determine the precise subcellular distribution and densities of two potassium channel subunits (i.e. $K_v4.2$ and $K_{ir}3.2$) in the rat CA1 PCs, by using the high-resolution SDS-FRL technique.

I demonstrated that the distribution of immunogold particles for the $K_v4.2$ subunit has homogenous distribution pattern along the proximo-distal axis of CA1 PCs apical dendrites. Furthermore, I provided evidence that the $K_v4.2$ subunit is excluded from the postsynaptic membrane specializations of both excitatory and inhibitory synapses. The immunogold particle density for the $K_{ir}3.2$ subunit shows a quasi linear distance-dependent increase along the apical dendrites of CA1 PCs. Here, I revealed a unique subcellular and compartment-specific distribution pattern and density for two functionally distinct potassium channel in the rat hippocampal CA1 region.

In the second part of the dissertation I challenged the long-standing view on the role of $GABA_AR$ γ2 subunit in clustering $GABA_ARs$ at inhibitory postsynaptic specializations.

By using a virus-mediated γ2 subunit gene deletion strategy and SDS-FRL, I show that both the α1 and β3 subunits are concentrated in the inhibitory synapses of cortical layer 2/3 cells lacking the γ2 subunit, without change in their density. Pharmacological experiments performed by my colleague Dr. Mark D. Eyre indicate that in γ2 subunit-lacking cells the γ3 subunit replaced the γ2 subunit in the heteropentameric receptor channels. In addition, I found that parvalbumin-containing interneurons within the injection zone upregulate the δ subunit in their plasma membrane. My results demonstrate that the γ2 subunit is not essential for postsynaptic receptor clustering in nerve cells of the adult mouse somatosensory cortex.

DOI:10.14753/SE.2015.1809

8. ÖSSZEFOGLALÁS

Ahhoz, hogy megértsük a kérgi piramissejtek működését, először ismernünk kell a plazmamembránban elhelyezkedő ioncsatorna-összetételt. A legtöbb információnk a piramissejt ioncsatorna összetételéről elektrofiziológiai valamint fénymikroszkópos immunhisztokémiai kísérletekből származik. Az utóbbi évtizedben az ioncsatornák közül a feszültségfüggő kálium csatornák különös figyelmet kaptak molekuláris és funkcionális heterogenitásuk miatt, viszont számos alegység pontos szubcelluláris eloszlása és sűrűsége még ismeretlen.

A disszertációm első részében, az volt a célom, hogy a nagyfelbontású SDS-maratott fagyasztva-tört replika jelölés (SDS-FRL) módszerét használva, feltérképezzem két kálium csatorna alegység (a $K_v4.2$ és a $K_{ir}3.2$ alegységek) szubcelluláris eloszlását és sűrűséget patkány CA1 piramissejteken.

Kimutattam, hogy a $K_v4.2$ alegységet jelölő immunarany szemcsék eloszlása homogén eloszlást mutat a CA1 piramissejtek apikális dendritfája mentén. Továbbá, bebizonyítottam, hogy a $K_v4.2$ csatorna nincs jelen a serkentő és gátló szinapszisokban. A $K_{ir}3.2$ alegységet jelölő aranyszemcsék sűrűsége a távolság függvényében egyenletesen nő a piramissejtek apikális dendritfája mentén. Munkám során feltártam két funkcionálisan különböző kálium csatorna egyedi szubcelluláris és kompartment-függő eloszlását és sűrűségét a patkány hippokampusz CA1 régiójában.

A disszertáció második részében azt vizsgáltam, hogy valóban szükséges-e a γ2 alegység a $GABA_A$ receptorok szinaptikus bedúsulásához?

Lokális vírus-mediálta γ2 alegység gén-kiütést követően, kvantitatív elektron mikroszkópos fagyasztva-tört replika jelöléssel kimutattam, hogy a γ2 alegység-hiányos sejtek gátló szinapszisaiban az α1 és β3 alegységek változatlan sűrűséggel megtalálhatóak. Továbbá, a Dr. Mark D. Eyre kollégám által végzett farmakológiai kísérletek azt bizonyítják, hogy a γ2 alegységet a γ3 alegység helyettesíti a γ2 alegység-hiányos sejtekben. Munkám során arra is fény derült, hogy az injektált kérgi területen belül lévő parvalbumin-tartalmú interneuronok plazmamembránjában megnövekedett a δ alegység expressziója. Eredményeim azt mutatják, hogy a γ2 alegység nem elengedhetetlen a $GABA_A$ receptorok szinaptikus bedúsulásához egér szomatoszenzoros kéregben.

9. REFERENCES

Aguado, C., Colon, J., Ciruela, F., Schlaudraff, F., Cabanero, M.J., Perry, C., Watanabe, M., Liss, B., Wickman, K. & Lujan, R. (2008) Cell type-specific subunit composition of G protein-gated potassium channels in the cerebellum. J. Neurochem., 105, 497-511.

Alldred, M.J., Mulder-Rosi, J., Lingenfelter, S.E., Chen, G. & Luscher, B. (2005) Distinct gamma2 subunit domains mediate clustering and synaptic function of postsynaptic GABAA receptors and gephyrin. J. Neurosci., 25, 594-603.

Alonso, G. & Widmer, H. (1997) Clustering of KV4.2 potassium channels in postsynaptic membrane of rat supraoptic neurons: an ultrastructural study. Neuroscience, 77, 617-621.

Amiry-Moghaddam, M. & Ottersen, O.P. (2013) Immunogold cytochemistry in neuroscience. Nat. Neurosci., 16, 798-804.

Armstrong, C.M. & Hille, B. (1998) Voltage-gated ion channels and electrical excitability. Neuron, 20, 371-380.

Ascoli, G.A., Alonso-Nanclares, L., Anderson, S.A., Barrionuevo, G., Benavides-Piccione, R., Burkhalter, A., Buzsaki, G., Cauli, B., Defelipe, J., Fairen, A., Feldmeyer, D., Fishell, G., Fregnac, Y., Freund, T.F., Gardner, D., Gardner, E.P., Goldberg, J.H., Helmstaedter, M., Hestrin, S., Karube, F., Kisvarday, Z.F., Lambolez, B., Lewis, D.A., Marin, O., Markram, H., Munoz, A., Packer, A., Petersen, C.C., Rockland, K.S., Rossier, J., Rudy, B., Somogyi, P., Staiger, J.F., Tamas, G., Thomson, A.M., Toledo-Rodriguez, M., Wang, Y., West, D.C. & Yuste, R. (2008) Petilla terminology: nomenclature of features of GABAergic interneurons of the cerebral cortex. Nat. Rev. Neurosci., 9, 557-568.

Baer, K., Essrich, C., Benson, J.A., Benke, D., Bluethmann, H., Fritschy, J.M. & Luscher, B. (1999) Postsynaptic clustering of gamma-aminobutyric acid type A receptors by the gamma3 subunit in vivo. Proc. Natl. Acad. Sci. U. S. A., 96, 12860-12865.

Baumann, S.W., Baur, R. & Sigel, E. (2002) Forced subunit assembly in alpha1beta2gamma2 GABAA receptors. Insight into the absolute arrangement. J. Biol. Chem., 277, 46020-46025.

Bencsits, E., Ebert, V., Tretter, V. & Sieghart, W. (1999) A significant part of native gamma-aminobutyric AcidA receptors containing alpha4 subunits do not contain gamma or delta subunits. J. Biol. Chem., 274, 19613-19616.

Bender, K.J. & Trussell, L.O. (2012) The physiology of the axon initial segment. Annu. Rev. Neurosci., 35, 249-265.

Benke, D., Cicin-Sain, A., Mertens, S. & Mohler, H. (1991a) Immunochemical identification of the alpha 1- and alpha 3-subunits of the GABAA-receptor in rat brain. J. Recept. Res., 11, 407-424.

Benke, D., Mertens, S., Trzeciak, A., Gillessen, D. & Mohler, H. (1991b) GABAA receptors display association of gamma 2-subunit with alpha 1- and beta 2/3-subunits. J. Biol. Chem., 266, 4478-4483.

Bettler, B., Kaupmann, K., Mosbacher, J. & Gassmann, M. (2004) Molecular structure and physiological functions of GABA(B) receptors. Physiol. Rev., 84, 835-867.

Birnbaum, S.G., Varga, A.W., Yuan, L.L., Anderson, A.E., Sweatt, J.D. & Schrader, L.A. (2004) Structure and function of Kv4-family transient potassium channels. Physiol. Rev., 84, 803-833.

Bogdanov, Y., Michels, G., Armstrong-Gold, C., Haydon, P.G., Lindstrom, J., Pangalos, M. & Moss, S.J. (2006) Synaptic GABAA receptors are directly recruited from their extrasynaptic counterparts. EMBO J., 25, 4381-4389.

Briatore, F., Patrizi, A., Viltono, L., Sassoe-Pognetto, M. & Wulff, P. (2010) Quantitative organization of GABAergic synapses in the molecular layer of the mouse cerebellar cortex. PLoS One, 5, e12119.

Brickley, S.G., Cull-Candy, S.G. & Farrant, M. (1996) Development of a tonic form of synaptic inhibition in rat cerebellar granule cells resulting from persistent activation of GABAA receptors. J. Physiol., 497 (Pt 3), 753-759.

Brown, N., Kerby, J., Bonnert, T.P., Whiting, P.J. & Wafford, K.A. (2002) Pharmacological characterization of a novel cell line expressing human alpha(4)beta(3)delta GABA(A) receptors. Br. J. Pharmacol., 136, 965-974.

Brunig, I., Suter, A., Knuesel, I., Luscher, B. & Fritschy, J.M. (2002) GABAergic terminals are required for postsynaptic clustering of dystrophin but not of GABA(A) receptors and gephyrin. J. Neurosci., 22, 4805-4813.

Bucurenciu, I., Bischofberger, J. & Jonas, P. (2010) A small number of open Ca2+ channels trigger transmitter release at a central GABAergic synapse. Nat. Neurosci., 13, 19-21.

Burkhalter, A., Gonchar, Y., Mellor, R.L. & Nerbonne, J.M. (2006) Differential expression of I(A) channel subunits Kv4.2 and Kv4.3 in mouse visual cortical neurons and synapses. J. Neurosci., 26, 12274-12282.

Cai, X., Liang, C.W., Muralidharan, S., Kao, J.P., Tang, C.M. & Thompson, S.M. (2004) Unique roles of SK and Kv4.2 potassium channels in dendritic integration. Neuron, 44, 351-364.

Caraiscos, V.B., Elliott, E.M., You-Ten, K.E., Cheng, V.Y., Belelli, D., Newell, J.G., Jackson, M.F., Lambert, J.J., Rosahl, T.W., Wafford, K.A., MacDonald, J.F. & Orser, B.A. (2004) Tonic inhibition in mouse hippocampal CA1 pyramidal neurons is mediated by alpha5 subunit-containing gamma-aminobutyric acid type A receptors. Proc. Natl. Acad. Sci. U. S. A., 101, 3662-3667.

Cash, S. & Yuste, R. (1999) Linear summation of excitatory inputs by CA1 pyramidal neurons. Neuron, 22, 383-394.

Celio, M.R., Baier, W., Scharer, L., de Viragh, P.A. & Gerday, C. (1988) Monoclonal antibodies directed against the calcium binding protein parvalbumin. Cell Calcium, 9, 81-86.

Chadderton, P., Margrie, T.W. & Hausser, M. (2004) Integration of quanta in cerebellar granule cells during sensory processing. Nature, 428, 856-860.

Chalifoux, J.R. & Carter, A.G. (2011) GABAB receptor modulation of synaptic function. Curr. Opin. Neurobiol., 21, 339-344.

Chandy, K.G. (1991) Simplified gene nomenclature. Nature, 352, 26.

Chen, S. & Diamond, J.S. (2002) Synaptically released glutamate activates extrasynaptic NMDA receptors on cells in the ganglion cell layer of rat retina. J. Neurosci., 22, 2165-2173.

Chen, X. & Johnston, D. (2005) Constitutively active G-protein-gated inwardly rectifying K+ channels in dendrites of hippocampal CA1 pyramidal neurons. J. Neurosci., 25, 3787-3792.

Chen, X., Yuan, L.L., Zhao, C., Birnbaum, S.G., Frick, A., Jung, W.E., Schwarz, T.L., Sweatt, J.D. & Johnston, D. (2006) Deletion of Kv4.2 gene eliminates dendritic A-type K+ current and enhances induction of long-term potentiation in hippocampal CA1 pyramidal neurons. J. Neurosci., 26, 12143-12151.

Chiu, S.Y. & Ritchie, J.M. (1981) Evidence for the presence of potassium channels in the paranodal region of acutely demyelinated mammalian single nerve fibres. J. Physiol., 313, 415-437.

Clark, B.D., Kwon, E., Maffie, J., Jeong, H.Y., Nadal, M., Strop, P. & Rudy, B. (2008) DPP6 Localization in Brain Supports Function as a Kv4 Channel Associated Protein. Front. Mol. Neurosci., 1, 1-11.

Cobb, S.R., Buhl, E.H., Halasy, K., Paulsen, O. & Somogyi, P. (1995) Synchronization of neuronal activity in hippocampus by individual GABAergic interneurons. Nature, 378, 75-78.

Dani, A., Huang, B., Bergan, J., Dulac, C. & Zhuang, X. (2010) Superresolution imaging of chemical synapses in the brain. Neuron, 68, 843-856.

Dascal, N. (1997) Signalling via the G protein-activated K+ channels. Cell. Signal., 9, 551-573.

David, M., Richer, M., Mamarbachi, A.M., Villeneuve, L.R., Dupre, D.J. & Hebert, T.E. (2006) Interactions between GABA-B1 receptors and Kir 3 inwardly rectifying potassium channels. Cell. Signal., 18, 2172-2181.

Debanne, D., Guerineau, N.C., Gahwiler, B.H. & Thompson, S.M. (1997) Action-potential propagation gated by an axonal I(A)-like K+ conductance in hippocampus. Nature, 389, 286-289.

DeFelipe, J., Lopez-Cruz, P.L., Benavides-Piccione, R., Bielza, C., Larranaga, P., Anderson, S., Burkhalter, A., Cauli, B., Fairen, A., Feldmeyer, D., Fishell, G., Fitzpatrick, D., Freund, T.F., Gonzalez-Burgos, G., Hestrin, S., Hill, S., Hof,

P.R., Huang, J., Jones, E.G., Kawaguchi, Y., Kisvarday, Z., Kubota, Y., Lewis, D.A., Marin, O., Markram, H., McBain, C.J., Meyer, H.S., Monyer, H., Nelson, S.B., Rockland, K., Rossier, J., Rubenstein, J.L., Rudy, B., Scanziani, M., Shepherd, G.M., Sherwood, C.C., Staiger, J.F., Tamas, G., Thomson, A., Wang, Y., Yuste, R. & Ascoli, G.A. (2013) New insights into the classification and nomenclature of cortical GABAergic interneurons. Nat. Rev. Neurosci., 14, 202-216.

DiGregorio, D.A., Nusser, Z. & Silver, R.A. (2002) Spillover of glutamate onto synaptic AMPA receptors enhances fast transmission at a cerebellar synapse. Neuron, 35, 521-533.

Dodson, P.D. & Forsythe, I.D. (2004) Presynaptic K+ channels: electrifying regulators of synaptic terminal excitability. Trends Neurosci., 27, 210-217.

Doyle, D.A. (1998) The Structure of the Potassium Channel: Molecular Basis of K+ Conduction and Selectivity. Science, 280, 69-77.

Draguhn, A., Verdorn, T.A., Ewert, M., Seeburg, P.H. & Sakmann, B. (1990) Functional and molecular distinction between recombinant rat GABAA receptor subtypes by Zn2+. Neuron, 5, 781-788.

Drake, C.T., Bausch, S.B., Milner, T.A. & Chavkin, C. (1997) GIRK1 immunoreactivity is present predominantly in dendrites, dendritic spines, and somata in the CA1 region of the hippocampus. Proc. Natl. Acad. Sci. U. S. A., 94, 1007-1012.

Enyedi, P. & Czirjak, G. (2010) Molecular background of leak K+ currents: two-pore domain potassium channels. Physiol. Rev., 90, 559-605.

Essrich, C., Lorez, M., Benson, J.A., Fritschy, J.M. & Luscher, B. (1998) Postsynaptic clustering of major GABAA receptor subtypes requires the gamma 2 subunit and gephyrin. Nat. Neurosci., 1, 563-571.

Eyre, M.D., Kerti, K. & Nusser, Z. (2009) Molecular diversity of deep short-axon cells of the rat main olfactory bulb. Eur. J. Neurosci., 29, 1397-1407.

Eyre, M.D., Renzi, M., Farrant, M. & Nusser, Z. (2012) Setting the time course of inhibitory synaptic currents by mixing multiple GABA(A) receptor alpha subunit isoforms. J. Neurosci., 32, 5853-5867.

Farrant, M. & Nusser, Z. (2005) Variations on an inhibitory theme: phasic and tonic activation of GABA(A) receptors. Nat. Rev. Neurosci., 6, 215-229.

Ferando, I. & Mody, I. (2013) Altered gamma oscillations during pregnancy through loss of delta subunit-containing GABA(A) receptors on parvalbumin interneurons. Front. Neural Circuits, 7, 144.

Fernandez-Alacid, L., Aguado, C., Ciruela, F., Martin, R., Colon, J., Cabanero, M.J., Gassmann, M., Watanabe, M., Shigemoto, R., Wickman, K., Bettler, B., Sanchez-Prieto, J. & Lujan, R. (2009) Subcellular compartment-specific molecular diversity of pre- and post-synaptic GABA-activated GIRK channels in Purkinje cells. J. Neurochem., 110, 1363-1376.

Fernandez-Alacid, L., Watanabe, M., Molnar, E., Wickman, K. & Lujan, R. (2011) Developmental regulation of G protein-gated inwardly-rectifying K+ (GIRK/Kir3) channel subunits in the brain. Eur. J. Neurosci., 34, 1724-1736.

Fowler, C.E., Aryal, P., Suen, K.F. & Slesinger, P.A. (2007) Evidence for association of GABA(B) receptors with Kir3 channels and regulators of G protein signalling (RGS4) proteins. J. Physiol., 580, 51-65.

Frick, A., Magee, J. & Johnston, D. (2004) LTP is accompanied by an enhanced local excitability of pyramidal neuron dendrites. Nat. Neurosci., 7, 126-135.

Fritschy, J.M., Benke, D., Johnson, D.K., Mohler, H. & Rudolph, U. (1997) GABAA-receptor alpha-subunit is an essential prerequisite for receptor formation in vivo. Neuroscience, 81, 1043-1053.

Fritschy, J.M., Harvey, R.J. & Schwarz, G. (2008) Gephyrin: where do we stand, where do we go? Trends Neurosci., 31, 257-264.

Fritschy, J.M. & Mohler, H. (1995) GABAA-receptor heterogeneity in the adult rat brain: differential regional and cellular distribution of seven major subunits. J. Comp. Neurol., 359, 154-194.

Fritschy, J.M., Panzanelli, P. & Tyagarajan, S.K. (2012) Molecular and functional heterogeneity of GABAergic synapses. Cell. Mol. Life Sci., 69, 2485-2499.

Fritschy, J.M., Weinmann, O., Wenzel, A. & Benke, D. (1998) Synapse-specific localization of NMDA and GABA(A) receptor subunits revealed by antigen-retrieval immunohistochemistry. J. Comp. Neurol., 390, 194-210.

Fujimoto, K. (1995) Freeze-fracture replica electron microscopy combined with SDS digestion for cytochemical labeling of integral membrane proteins. Application to the immunogold labeling of intercellular junctional complexes. J. Cell Sci., 108 (Pt 11), 3443-3449.

Glykys, J. & Mody, I. (2006) Hippocampal network hyperactivity after selective reduction of tonic inhibition in GABA A receptor alpha5 subunit-deficient mice. J. Neurophysiol., 95, 2796-2807.

Glykys, J., Peng, Z., Chandra, D., Homanics, G.E., Houser, C.R. & Mody, I. (2007) A new naturally occurring GABA(A) receptor subunit partnership with high sensitivity to ethanol. Nat. Neurosci., 10, 40-48.

Golding, N.L. & Spruston, N. (1998) Dendritic sodium spikes are variable triggers of axonal action potentials in hippocampal CA1 pyramidal neurons. Neuron, 21, 1189-1200.

Gunther, U., Benson, J., Benke, D., Fritschy, J.M., Reyes, G., Knoflach, F., Crestani, F., Aguzzi, A., Arigoni, M., Lang, Y. & Bluethmann H., Mohler H. & Luscher B. (1995) Benzodiazepine-insensitive mice generated by targeted disruption of the gamma 2 subunit gene of gamma-aminobutyric acid type A receptors. Proc. Natl. Acad. Sci. U. S. A., 92, 7749-7753.

Gutman, G.A., Chandy, K.G., Adelman, J.P., Aiyar, J., Bayliss, D.A., Clapham, D.E., Covarriubias, M., Desir, G.V., Furuichi, K., Ganetzky, B., Garcia, M.L.,

Grissmer, S., Jan, L.Y., Karschin, A., Kim, D., Kuperschmidt, S., Kurachi, Y., Lazdunski, M., Lesage, F., Lester, H.A., McKinnon, D., Nichols, C.G., O'Kelly, I., Robbins, J., Robertson, G.A., Rudy, B., Sanguinetti, M., Seino, S., Stuehmer, W., Tamkun, M.M., Vandenberg, C.A., Wei, A., Wulff, H. & Wymore, R.S. (2003) International Union of Pharmacology. XLI. Compendium of voltage-gated ion channels: potassium channels. Pharmacol. Rev., 55, 583-586.

Hagiwara, A., Fukazawa, Y., Deguchi-Tawarada, M., Ohtsuka, T. & Shigemoto, R. (2005) Differential distribution of release-related proteins in the hippocampal CA3 area as revealed by freeze-fracture replica labeling. J. Comp. Neurol., 489, 195-216.

Hamann, M., Rossi, D.J. & Attwell, D. (2002) Tonic and spillover inhibition of granule cells control information flow through cerebellar cortex. Neuron, 33, 625-633.

Hamilton, D.L. & Abremski, K. (1984) Site-specific recombination by the bacteriophage P1 lox-Cre system. Cre-mediated synapsis of two lox sites. J. Mol. Biol., 178, 481-486.

Hammond, R.S., Lin, L., Sidorov, M.S., Wikenheiser, A.M. & Hoffman, D.A. (2008) Protein kinase A mediates activity-dependent Kv4.2 channel trafficking. J. Neurosci., 28, 7513-7519.

Herb, A., Wisden, W., Luddens, H., Puia, G., Vicini, S. & Seeburg, P.H. (1992) The third gamma subunit of the gamma-aminobutyric acid type A receptor family. Proc. Natl. Acad. Sci. U. S. A., 89, 1433-1437.

Hevers, W. & Luddens, H. (1998) The diversity of GABAA receptors. Pharmacological and electrophysiological properties of GABAA channel subtypes. Mol. Neurobiol., 18, 35-86.

Hille, B. (2001) Ion Channels of Excitable Membranes. Sinauer Associates, Inc., Sunderland, 2001: 1-21.

Hille, B., Armstrong, C.M. & MacKinnon, R. (1999) Ion channels: from idea to reality. Nat. Med., 5, 1105-1109.

Hodgkin, A.L. & Huxley, A.F. (1952) A quantitative description of membrane current and its application to conduction and excitation in nerve. J. Physiol., 117, 500-544.

Hoffman, D.A. & Johnston, D. (1998) Downregulation of transient K+ channels in dendrites of hippocampal CA1 pyramidal neurons by activation of PKA and PKC. J. Neurosci., 18, 3521-3528.

Hoffman, D.A., Magee, J.C., Colbert, C.M. & Johnston, D. (1997) K+ channel regulation of signal propagation in dendrites of hippocampal pyramidal neurons. Nature, 387, 869-875.

Homanics, G.E., DeLorey, T.M., Firestone, L.L., Quinlan, J.J., Handforth, A., Harrison, N.L., Krasowski, M.D., Rick, C.E., Korpi, E.R., Makela, R., Brilliant, M.H., Hagiwara, N., Ferguson, C., Snyder, K. & Olsen, R.W. (1997) Mice devoid of

gamma-aminobutyrate type A receptor beta3 subunit have epilepsy, cleft palate, and hypersensitive behavior. Proc. Natl. Acad. Sci. U. S. A., 94, 4143-4148.

Indriati, D.W., Kamasawa, N., Matsui, K., Meredith, A.L., Watanabe, M. & Shigemoto, R. (2013) Quantitative localization of Cav2.1 (P/Q-type) voltage-dependent calcium channels in Purkinje cells: somatodendritic gradient and distinct somatic coclustering with calcium-activated potassium channels. J. Neurosci., 33, 3668-3678.

Jacob, T.C., Bogdanov, Y.D., Magnus, C., Saliba, R.S., Kittler, J.T., Haydon, P.G. & Moss, S.J. (2005) Gephyrin regulates the cell surface dynamics of synaptic GABAA receptors. J. Neurosci., 25, 10469-10478.

Jacob, T.C., Moss, S.J. & Jurd, R. (2008) GABA(A) receptor trafficking and its role in the dynamic modulation of neuronal inhibition. Nat. Rev. Neurosci., 9, 331-343.

Jan, L.Y. & Jan, Y.N. (1997) Cloned potassium channels from eukaryotes and prokaryotes. Annu. Rev. Neurosci., 20, 91-123.

Jinno, S., Jeromin, A. & Kosaka, T. (2005) Postsynaptic and extrasynaptic localization of Kv4.2 channels in the mouse hippocampal region, with special reference to targeted clustering at gabaergic synapses. Neuroscience, 134, 483-494.

Johnston, J., Forsythe, I.D. & Kopp-Scheinpflug, C. (2010) Going native: voltage-gated potassium channels controlling neuronal excitability. J. Physiol., 588, 3187-3200.

Jones, A., Korpi, E.R., McKernan, R.M., Pelz, R., Nusser, Z., Makela, R., Mellor, J.R., Pollard, S., Bahn, S., Stephenson, F.A., Randall, A.D., Sieghart, W., Somogyi, P., Smith, A.J. & Wisden, W. (1997) Ligand-gated ion channel subunit partnerships: GABAA receptor alpha6 subunit gene inactivation inhibits delta subunit expression. J. Neurosci., 17, 1350-1362.

Kandel, E.R., Schwartz, J.H. & Jessel, T.M. Principles of Neural Science. The McGraw-Hill Companies, Inc., New York, 2000: 289.

Kasugai, Y., Swinny, J.D., Roberts, J.D., Dalezios, Y., Fukazawa, Y., Sieghart, W., Shigemoto, R. & Somogyi, P. (2010) Quantitative localisation of synaptic and extrasynaptic GABAA receptor subunits on hippocampal pyramidal cells by freeze-fracture replica immunolabelling. Eur. J. Neurosci., 32, 1868-1888.

Kaufmann, W.A., Kasugai, Y., Ferraguti, F. & Storm, J.F. (2010) Two distinct pools of large-conductance calcium-activated potassium channels in the somatic plasma membrane of central principal neurons. Neuroscience, 169, 974-986.

Kerti-Szigeti, K., Nusser, Z. & Eyre, M.D. (2014) Synaptic GABAA receptor clustering without the gamma2 subunit. J. Neurosci., 34, 10219-10233.

Kerti, K., Lorincz, A. & Nusser, Z. (2012) Unique somato-dendritic distribution pattern of Kv4.2 channels on hippocampal CA1 pyramidal cells. Eur. J. Neurosci., 35, 66-75.

Khom, S., Baburin, I., Timin, E.N., Hohaus, A., Sieghart, W. & Hering, S. (2006) Pharmacological properties of GABAA receptors containing gamma1 subunits. Mol. Pharmacol., 69, 640-649.

Kim, J. & Hoffman, D.A. (2008) Potassium channels: newly found players in synaptic plasticity. Neuroscientist, 14, 276-286.

Kim, J., Jung, S.C., Clemens, A.M., Petralia, R.S. & Hoffman, D.A. (2007) Regulation of dendritic excitability by activity-dependent trafficking of the A-type K+ channel subunit Kv4.2 in hippocampal neurons. Neuron, 54, 933-947.

Kim, S., Guzman, S.J., Hu, H. & Jonas, P. (2012) Active dendrites support efficient initiation of dendritic spikes in hippocampal CA3 pyramidal neurons. Nat. Neurosci., 15, 600-606.

Kirizs, T., Kerti-Szigeti, K., Lorincz, A. & Nusser, Z. (2014) Distinct axo-somato-dendritic distributions of three potassium channels in CA1 hippocampal pyramidal cells. Eur. J. Neurosci., 39, 1771-1783.

Kittel, R.J., Wichmann, C., Rasse, T.M., Fouquet, W., Schmidt, M., Schmid, A., Wagh, D.A., Pawlu, C., Kellner, R.R., Willig, K.I., Hell, S.W., Buchner, E., Heckmann, M. & Sigrist, S.J. (2006) Bruchpilot promotes active zone assembly, Ca2+ channel clustering, and vesicle release. Science, 312, 1051-1054.

Klausberger, T. & Somogyi, P. (2008) Neuronal diversity and temporal dynamics: the unity of hippocampal circuit operations. Science, 321, 53-57.

Knoflach, F., Rhyner, T., Villa, M., Kellenberger, S., Drescher, U., Malherbe, P., Sigel, E. & Mohler, H. (1991) The gamma 3-subunit of the GABAA-receptor confers sensitivity to benzodiazepine receptor ligands. FEBS Lett., 293, 191-194.

Knuesel, I., Mastrocola, M., Zuellig, R.A., Bornhauser, B., Schaub, M.C. & Fritschy, J.M. (1999) Short communication: altered synaptic clustering of GABAA receptors in mice lacking dystrophin (mdx mice). Eur. J. Neurosci., 11, 4457-4462.

Kofuji, P., Davidson, N. & Lester, H.A. (1995) Evidence that neuronal G-protein-gated inwardly rectifying K+ channels are activated by G beta gamma subunits and function as heteromultimers. Proc. Natl. Acad. Sci. U. S. A., 92, 6542-6546.

Kole, M.H., Letzkus, J.J. & Stuart, G.J. (2007) Axon initial segment Kv1 channels control axonal action potential waveform and synaptic efficacy. Neuron, 55, 633-647.

Kole, M.H. & Stuart, G.J. (2012) Signal processing in the axon initial segment. Neuron, 73, 235-247.

Konig, P., Engel, A.K. & Singer, W. (1996) Integrator or coincidence detector? The role of the cortical neuron revisited. Trends Neurosci., 19, 130-137.

Koyrakh, L., Lujan, R., Colon, J., Karschin, C., Kurachi, Y., Karschin, A. & Wickman, K. (2005) Molecular and cellular diversity of neuronal G-protein-gated potassium channels. J. Neurosci., 25, 11468-11478.

Kralic, J.E., Sidler, C., Parpan, F., Homanics, G.E., Morrow, A.L. & Fritschy, J.M. (2006) Compensatory alteration of inhibitory synaptic circuits in cerebellum and thalamus of gamma-aminobutyric acid type A receptor alpha1 subunit knockout mice. J. Comp. Neurol., 495, 408-421.

Kulik, A., Vida, I., Fukazawa, Y., Guetg, N., Kasugai, Y., Marker, C.L., Rigato, F., Bettler, B., Wickman, K., Frotscher, M. & Shigemoto, R. (2006) Compartment-dependent colocalization of Kir3.2-containing K+ channels and GABAB receptors in hippocampal pyramidal cells. J. Neurosci., 26, 4289-4297.

Kulik, A., Vida, I., Lujan, R., Haas, C.A., Lopez-Bendito, G., Shigemoto, R. & Frotscher, M. (2003) Subcellular localization of metabotropic GABA(B) receptor subunits GABA(B1a/b) and GABA(B2) in the rat hippocampus. J. Neurosci., 23, 11026-11035.

Ladera, C., del Carmen Godino, M., Jose Cabanero, M., Torres, M., Watanabe, M., Lujan, R. & Sanchez-Prieto, J. (2008) Pre-synaptic GABA receptors inhibit glutamate release through GIRK channels in rat cerebral cortex. J. Neurochem., 107, 1506-1517.

Lai, H.C. & Jan, L.Y. (2006) The distribution and targeting of neuronal voltage-gated ion channels. Nat. Rev. Neurosci., 7, 548-562.

Lambe, E.K. & Aghajanian, G.K. (2001) The role of Kv1.2-containing potassium channels in serotonin-induced glutamate release from thalamocortical terminals in rat frontal cortex. J. Neurosci., 21, 9955-9963.

Larkum, M.E. & Nevian, T. (2008) Synaptic clustering by dendritic signalling mechanisms. Curr. Opin. Neurobiol., 18, 321-331.

Lesage, F., Guillemare, E., Fink, M., Duprat, F., Heurteaux, C., Fosset, M., Romey, G., Barhanin, J. & Lazdunski, M. (1995) Molecular properties of neuronal G-protein-activated inwardly rectifying K+ channels. J. Biol. Chem., 270, 28660-28667.

Liao, Y.J., Jan, Y.N. & Jan, L.Y. (1996) Heteromultimerization of G-protein-gated inwardly rectifying K+ channel proteins GIRK1 and GIRK2 and their altered expression in weaver brain. J. Neurosci., 16, 7137-7150.

Long, S.B., Campbell, E.B. & Mackinnon, R. (2005) Crystal structure of a mammalian voltage-dependent Shaker family K+ channel. Science, 309, 897-903.

Lopez-Bendito, G., Shigemoto, R., Kulik, A., Vida, I., Fairen, A. & Lujan, R. (2004) Distribution of metabotropic GABA receptor subunits GABAB1a/b and GABAB2 in the rat hippocampus during prenatal and postnatal development. Hippocampus, 14, 836-848.

Lorincz, A., Notomi, T., Tamas, G., Shigemoto, R. & Nusser, Z. (2002) Polarized and compartment-dependent distribution of HCN1 in pyramidal cell dendrites. Nat. Neurosci., 5, 1185-1193.

Lorincz, A. & Nusser, Z. (2008) Specificity of immunoreactions: the importance of testing specificity in each method. J. Neurosci., 28, 9083-9086.

Lorincz, A. & Nusser, Z. (2010) Molecular identity of dendritic voltage-gated sodium channels. Science, 328, 906-909.

Losonczy, A., Makara, J.K. & Magee, J.C. (2008) Compartmentalized dendritic plasticity and input feature storage in neurons. Nature, 452, 436-441.

Losonczy, A., Zemelman, B.V., Vaziri, A. & Magee, J.C. (2010) Network mechanisms of theta related neuronal activity in hippocampal CA1 pyramidal neurons. Nat. Neurosci., 13, 967-972.

Lujan, R., Maylie, J. & Adelman, J.P. (2009) New sites of action for GIRK and SK channels. Nat. Rev. Neurosci., 10, 475-480.

Luscher, B., Fuchs, T. & Kilpatrick, C.L. (2011) GABAA receptor trafficking-mediated plasticity of inhibitory synapses. Neuron, 70, 385-409.

Luscher, C., Jan, L.Y., Stoffel, M., Malenka, R.C. & Nicoll, R.A. (1997) G protein-coupled inwardly rectifying K+ channels (GIRKs) mediate postsynaptic but not presynaptic transmitter actions in hippocampal neurons. Neuron, 19, 687-695.

Luscher, C. & Slesinger, P.A. (2010) Emerging roles for G protein-gated inwardly rectifying potassium (GIRK) channels in health and disease. Nat. Rev. Neurosci., 11, 301-315.

Ma, D., Zerangue, N., Raab-Graham, K., Fried, S.R., Jan, Y.N. & Jan, L.Y. (2002) Diverse trafficking patterns due to multiple traffic motifs in G protein-activated inwardly rectifying potassium channels from brain and heart. Neuron, 33, 715-729.

Maffie, J. & Rudy, B. (2008) Weighing the evidence for a ternary protein complex mediating A-type K+ currents in neurons. J. Physiol., 586, 5609-5623.

Magee, J.C. (1998) Dendritic hyperpolarization-activated currents modify the integrative properties of hippocampal CA1 pyramidal neurons. J. Neurosci., 18, 7613-7624.

Maglione, M. & Sigrist, S.J. (2013) Seeing the forest tree by tree: super-resolution light microscopy meets the neurosciences. Nat. Neurosci., 16, 790-797.

Makara, J.K., Losonczy, A., Wen, Q. & Magee, J.C. (2009) Experience-dependent compartmentalized dendritic plasticity in rat hippocampal CA1 pyramidal neurons. Nat. Neurosci., 12, 1485-1487.

Makara, J.K. & Magee, J.C. (2013) Variable dendritic integration in hippocampal CA3 pyramidal neurons. Neuron, 80, 1438-1450.

Maletic-Savatic, M., Lenn, N.J. & Trimmer, J.S. (1995) Differential spatiotemporal expression of K+ channel polypeptides in rat hippocampal neurons developing in situ and in vitro. J. Neurosci., 15, 3840-3851.

Mann, E.O. & Mody, I. (2010) Control of hippocampal gamma oscillation frequency by tonic inhibition and excitation of interneurons. Nat. Neurosci., 13, 205-212.

Margulis, M. & Tang, C.M. (1998) Temporal integration can readily switch between sublinear and supralinear summation. J. Neurophysiol., 79, 2809-2813.

Masugi-Tokita, M. & Shigemoto, R. (2007) High-resolution quantitative visualization of glutamate and GABA receptors at central synapses. Curr. Opin. Neurobiol., 17, 387-393.

Mathie, A., Al-Moubarak, E. & Veale, E.L. (2010) Gating of two pore domain potassium channels. J. Physiol., 588, 3149-3156.

Migliore, M., Hoffman, D.A., Magee, J.C. & Johnston, D. (1999) Role of an A-type K+ conductance in the back-propagation of action potentials in the dendrites of hippocampal pyramidal neurons. J. Comput. Neurosci., 7, 5-15.

Miles, R., Toth, K., Gulyas, A.I., Hajos, N. & Freund, T.F. (1996) Differences between somatic and dendritic inhibition in the hippocampus. Neuron, 16, 815-823.

Mortensen, M. & Smart, T.G. (2006) Extrasynaptic alphabeta subunit GABAA receptors on rat hippocampal pyramidal neurons. J. Physiol., 577, 841-856.

Nagy, A. (2000) Cre recombinase: the universal reagent for genome tailoring. Genesis, 26, 99-109.

Nagy, J.I., Dudek, F.E. & Rash, J.E. (2004) Update on connexins and gap junctions in neurons and glia in the mammalian nervous system. Brain Res. Brain Res. Rev., 47, 191-215.

Neher, E. & Sakaba, T. (2008) Multiple roles of calcium ions in the regulation of neurotransmitter release. Neuron, 59, 861-872.

Neher, E. & Sakmann, B. (1976) Single-channel currents recorded from membrane of denervated frog muscle fibres. Nature, 260, 799-802.

Nestor, M.W. & Hoffman, D.A. (2012) Differential cycling rates of Kv4.2 channels in proximal and distal dendrites of hippocampal CA1 pyramidal neurons. Hippocampus, 22, 969-980.

Notomi, T. & Shigemoto, R. (2004) Immunohistochemical localization of Ih channel subunits, HCN1-4, in the rat brain. J. Comp. Neurol., 471, 241-276.

Notter, T., Panzanelli, P., Pfister, S., Mircsof, D. & Fritschy, J.M. (2014) A protocol for concurrent high-quality immunohistochemical and biochemical analyses in adult mouse central nervous system. Eur. J. Neurosci., 39, 165-175.

Nusser, Z. (1999) A new approach to estimate the number, density and variability of receptors at central synapses. Eur. J. Neurosci., 11, 745-752.

Nusser, Z. (2012) Differential subcellular distribution of ion channels and the diversity of neuronal function. Curr. Opin. Neurobiol., 22, 366-371.

Nusser, Z. & Mody, I. (2002) Selective modulation of tonic and phasic inhibitions in dentate gyrus granule cells. J. Neurophysiol., 87, 2624-2628.

Nusser, Z., Naylor, D. & Mody, I. (2001) Synapse-specific contribution of the variation of transmitter concentration to the decay of inhibitory postsynaptic currents. Biophys. J., 80, 1251-1261.

Nusser, Z., Roberts, J.D., Baude, A., Richards, J.G., Sieghart, W. & Somogyi, P. (1995) Immunocytochemical localization of the alpha 1 and beta 2/3 subunits of the GABAA receptor in relation to specific GABAergic synapses in the dentate gyrus. Eur. J. Neurosci., 7, 630-646.

Nusser, Z., Sieghart, W. & Somogyi, P. (1998) Segregation of different GABAA receptors to synaptic and extrasynaptic membranes of cerebellar granule cells. J. Neurosci., 18, 1693-1703.

Olah, S., Fule, M., Komlosi, G., Varga, C., Baldi, R., Barzo, P. & Tamas, G. (2009) Regulation of cortical microcircuits by unitary GABA-mediated volume transmission. Nature, 461, 1278-1281.

Olsen, R.W. & Sieghart, W. (2008) International Union of Pharmacology. LXX. Subtypes of gamma-aminobutyric acid(A) receptors: classification on the basis of subunit composition, pharmacology, and function. Update. Pharmacol. Rev., 60, 243-260.

Panzanelli, P., Gunn, B.G., Schlatter, M.C., Benke, D., Tyagarajan, S.K., Scheiffele, P., Belelli, D., Lambert, J.J., Rudolph, U. & Fritschy, J.M. (2011) Distinct mechanisms regulate GABAA receptor and gephyrin clustering at perisomatic and axo-axonic synapses on CA1 pyramidal cells. J. Physiol., 589, 4959-4980.

Peng, Z., Hauer, B., Mihalek, R.M., Homanics, G.E., Sieghart, W., Olsen, R.W. & Houser, C.R. (2002) GABA(A) receptor changes in delta subunit-deficient mice: altered expression of alpha4 and gamma2 subunits in the forebrain. J. Comp. Neurol., 446, 179-197.

Pirker, S., Schwarzer, C., Wieselthaler, A., Sieghart, W. & Sperk, G. (2000) GABA(A) receptors: immunocytochemical distribution of 13 subunits in the adult rat brain. Neuroscience, 101, 815-850.

Ponce, A., Bueno, E., Kentros, C., Vega-Saenz de Miera, E., Chow, A., Hillman, D., Chen, S., Zhu, L., Wu, M.B., Wu, X., Rudy, B. & Thornhill, W.B. (1996) G-protein-gated inward rectifier K+ channel proteins (GIRK1) are present in the soma and dendrites as well as in nerve terminals of specific neurons in the brain. J. Neurosci., 16, 1990-2001.

Pouille, F. & Scanziani, M. (2001) Enforcement of temporal fidelity in pyramidal cells by somatic feed-forward inhibition. Science, 293, 1159-1163.

Poulopoulos, A., Aramuni, G., Meyer, G., Soykan, T., Hoon, M., Papadopoulos, T., Zhang, M., Paarmann, I., Fuchs, C., Harvey, K., Jedlicka, P., Schwarzacher, S.W., Betz, H., Harvey, R.J., Brose, N., Zhang, W. & Varoqueaux, F. (2009) Neuroligin 2 drives postsynaptic assembly at perisomatic inhibitory synapses through gephyrin and collybistin. Neuron, 63, 628-642.

Prenosil, G.A., Schneider Gasser, E.M., Rudolph, U., Keist, R., Fritschy, J.M. & Vogt, K.E. (2006) Specific subtypes of GABAA receptors mediate phasic and tonic

forms of inhibition in hippocampal pyramidal neurons. J. Neurophysiol., 96, 846-857.

Rhodes, K.J., Carroll, K.I., Sung, M.A., Doliveira, L.C., Monaghan, M.M., Burke, S.L., Strassle, B.W., Buchwalder, L., Menegola, M., Cao, J., An, W.F. & Trimmer, J.S. (2004) KChIPs and Kv4 alpha subunits as integral components of A-type potassium channels in mammalian brain. J. Neurosci., 24, 7903-7915.

Robenek, H. & Severs, N.J. (2008) Recent advances in freeze-fracture electron microscopy: the replica immunolabeling technique. Biol. Proced. Online, 10, 9-19.

Rovo, Z., Matyas, F., Bartho, P., Slezia, A., Lecci, S., Pellegrini, C., Astori, S., David, C., Hangya, B., Luthi, A. & Acsady, L. (2014) Phasic, Nonsynaptic GABA-A Receptor-Mediated Inhibition Entrains Thalamocortical Oscillations. J. Neurosci., 34, 7137-7147.

Royer, S., Zemelman, B.V., Losonczy, A., Kim, J., Chance, F., Magee, J.C. & Buzsaki, G. (2012) Control of timing, rate and bursts of hippocampal place cells by dendritic and somatic inhibition. Nat. Neurosci., 15, 769-775.

Schafer, D.P., Bansal, R., Hedstrom, K.L., Pfeiffer, S.E. & Rasband, M.N. (2004) Does paranode formation and maintenance require partitioning of neurofascin 155 into lipid rafts? J. Neurosci., 24, 3176-3185.

Schweizer, C., Balsiger, S., Bluethmann, H., Mansuy, I.M., Fritschy, J.M., Mohler, H. & Lüscher, B. (2003) The γ2 subunit of GABAA receptors is required for maintenance of receptors at mature synapses. Mol. Cell. Neurosci., 24, 442-450.

Scoville, W.B. & Milner, B. (1957) Loss of recent memory after bilateral hippocampal lesions. J. Neurol. Neurosurg. Psychiatry, 20, 11-21.

Sekirnjak, C., Martone, M.E., Weiser, M., Deerinck, T., Bueno, E., Rudy, B. & Ellisman, M. (1997) Subcellular localization of the K+ channel subunit Kv3.1b in selected rat CNS neurons. Brain Res., 766, 173-187.

Semyanov, A., Walker, M.C. & Kullmann, D.M. (2003) GABA uptake regulates cortical excitability via cell type-specific tonic inhibition. Nat. Neurosci., 6, 484-490.

Serodio, P. & Rudy, B. (1998) Differential expression of Kv4 K+ channel subunits mediating subthreshold transient K+ (A-type) currents in rat brain. J. Neurophysiol., 79, 1081-1091.

Shepherd, G.M. The Synaptic Organization of the Brain. Oxford University Press, New York, 2004: 499-524.

Shibasaki, K., Nakahira, K., Trimmer, J.S., Shibata, R., Akita, M., Watanabe, S. & Ikenaka, K. (2004) Mossy fibre contact triggers the targeting of Kv4.2 potassium channels to dendrites and synapses in developing cerebellar granule neurons. J. Neurochem., 89, 897-907.

Shu, Y., Yu, Y., Yang, J. & McCormick, D.A. (2007) Selective control of cortical axonal spikes by a slowly inactivating K+ current. Proc. Natl. Acad. Sci. U. S. A., 104, 11453-11458.

Sieghart, W. (1995) Structure and pharmacology of gamma-aminobutyric acidA receptor subtypes. Pharmacol. Rev., 47, 181-234.

Sieghart, W. & Sperk, G. (2002) Subunit composition, distribution and function of GABA(A) receptor subtypes. Curr. Top. Med. Chem., 2, 795-816.

Sigel, E. & Luscher, B.P. (2011) A closer look at the high affinity benzodiazepine binding site on GABAA receptors. Curr. Top. Med. Chem., 11, 241-246.

Signorini, S., Liao, Y.J., Duncan, S.A., Jan, L.Y. & Stoffel, M. (1997) Normal cerebellar development but susceptibility to seizures in mice lacking G protein-coupled, inwardly rectifying K+ channel GIRK2. Proc. Natl. Acad. Sci. U. S. A., 94, 923-927.

Simon, J., Wakimoto, H., Fujita, N., Lalande, M. & Barnard, E.A. (2004) Analysis of the set of GABA(A) receptor genes in the human genome. J. Biol. Chem., 279, 41422-41435.

Slesinger, P.A., Patil, N., Liao, Y.J., Jan, Y.N., Jan, L.Y. & Cox, D.R. (1996) Functional effects of the mouse weaver mutation on G protein-gated inwardly rectifying K+ channels. Neuron, 16, 321-331.

Smart, T.G., Moss, S.J., Xie, X. & Huganir, R.L. (1991) GABAA receptors are differentially sensitive to zinc: dependence on subunit composition. Br. J. Pharmacol., 103, 1837-1839.

Soltesz, I., Roberts, J.D., Takagi, H., Richards, J.G., Mohler, H. & Somogyi, P. (1990) Synaptic and Nonsynaptic Localization of Benzodiazepine/GABAA Receptor/Cl- Channel Complex Using Monoclonal Antibodies in the Dorsal Lateral Geniculate Nucleus of the Cat. Eur. J. Neurosci., 2, 414-429.

Somogyi, P., Fritschy, J.M., Benke, D., Roberts, J.D. & Sieghart, W. (1996) The gamma 2 subunit of the GABAA receptor is concentrated in synaptic junctions containing the alpha 1 and beta 2/3 subunits in hippocampus, cerebellum and globus pallidus. Neuropharmacology, 35, 1425-1444.

Somogyi, P. & Klausberger, T. (2005) Defined types of cortical interneurone structure space and spike timing in the hippocampus. J. Physiol., 562, 9-26.

Somogyi, P., Takagi, H., Richards, J.G. & Mohler, H. (1989) Subcellular localization of benzodiazepine/GABAA receptors in the cerebellum of rat, cat, and monkey using monoclonal antibodies. J. Neurosci., 9, 2197-2209.

Spruston, N., Schiller, Y., Stuart, G. & Sakmann, B. (1995) Activity-dependent action potential invasion and calcium influx into hippocampal CA1 dendrites. Science, 268, 297-300.

Steere, R.L. (1957) Electron microscopy of structural detail in frozen biological specimens. J. Biophys. Biochem. Cytol., 3, 45-60.

Stell, B.M., Brickley, S.G., Tang, C.Y., Farrant, M. & Mody, I. (2003) Neuroactive steroids reduce neuronal excitability by selectively enhancing tonic inhibition mediated by delta subunit-containing GABAA receptors. Proc. Natl. Acad. Sci. U. S. A., 100, 14439-14444.

Sumegi, M., Fukazawa, Y., Matsui, K., Lorincz, A., Eyre, M.D., Nusser, Z. & Shigemoto, R. (2012) Virus-mediated swapping of zolpidem-insensitive with zolpidem-sensitive GABA(A) receptors in cortical pyramidal cells. J. Physiol., 590, 1517-1534.

Sun, C., Sieghart, W. & Kapur, J. (2004) Distribution of alpha1, alpha4, gamma2, and delta subunits of GABAA receptors in hippocampal granule cells. Brain Res., 1029, 207-216.

Sun, W., Maffie, J.K., Lin, L., Petralia, R.S., Rudy, B. & Hoffman, D.A. (2011) DPP6 establishes the A-type K(+) current gradient critical for the regulation of dendritic excitability in CA1 hippocampal neurons. Neuron, 71, 1102-1115.

Sur, C., Farrar, S.J., Kerby, J., Whiting, P.J., Atack, J.R. & McKernan, R.M. (1999) Preferential coassembly of alpha4 and delta subunits of the gamma-aminobutyric acidA receptor in rat thalamus. Mol. Pharmacol., 56, 110-115.

Sur, C., Wafford, K.A., Reynolds, D.S., Hadingham, K.L., Bromidge, F., Macaulay, A., Collinson, N., O'Meara, G., Howell, O., Newman, R., Myers, J., Atack, J.R., Dawson, G.R., McKernan, R.M., Whiting, P.J. & Rosahl, T.W. (2001) Loss of the major GABA(A) receptor subtype in the brain is not lethal in mice. J. Neurosci., 21, 3409-3418.

Swartz, K.J. (2004) Towards a structural view of gating in potassium channels. Nat. Rev. Neurosci., 5, 905-916.

Takigawa, T. & Alzheimer, C. (1999) G protein-activated inwardly rectifying K+ (GIRK) currents in dendrites of rat neocortical pyramidal cells. J. Physiol., 517 (Pt 2), 385-390.

Takigawa, T. & Alzheimer, C. (2002) Phasic and tonic attenuation of EPSPs by inward rectifier K+ channels in rat hippocampal pyramidal cells. J. Physiol., 539, 67-75.

Tanaka, J., Matsuzaki, M., Tarusawa, E., Momiyama, A., Molnar, E., Kasai, H. & Shigemoto, R. (2005) Number and density of AMPA receptors in single synapses in immature cerebellum. J. Neurosci., 25, 799-807.

Tarusawa, E., Matsui, K., Budisantoso, T., Molnar, E., Watanabe, M., Matsui, M., Fukazawa, Y. & Shigemoto, R. (2009) Input-specific intrasynaptic arrangements of ionotropic glutamate receptors and their impact on postsynaptic responses. J. Neurosci., 29, 12896-12908.

Tempel, B.L., Papazian, D.M., Schwarz, T.L., Jan, Y.N. & Jan, L.Y. (1987) Sequence of a probable potassium channel component encoded at Shaker locus of Drosophila. Science, 237, 770-775.

Tretter, V., Hauer, B., Nusser, Z., Mihalek, R.M., Hoger, H., Homanics, G.E., Somogyi, P. & Sieghart, W. (2001) Targeted disruption of the GABA(A) receptor delta

subunit gene leads to an up-regulation of gamma 2 subunit-containing receptors in cerebellar granule cells. J. Biol. Chem., 276, 10532-10538.

Triller, A. & Choquet, D. (2005) Surface trafficking of receptors between synaptic and extrasynaptic membranes: and yet they do move! Trends Neurosci., 28, 133-139.

Trimmer, J.S. & Rhodes, K.J. (2004) Localization of voltage-gated ion channels in mammalian brain. Annu. Rev. Physiol., 66, 477-519.

Tyagarajan, S.K. & Fritschy, J.M. (2014) Gephyrin: a master regulator of neuronal function? Nat. Rev. Neurosci., 15, 141-156.

Vacher, H., Mohapatra, D.P. & Trimmer, J.S. (2008) Localization and targeting of voltage-dependent ion channels in mammalian central neurons. Physiol. Rev., 88, 1407-1447.

Varga, A.W. (2000) Input-Specific Immunolocalization of Differentially Phosphorylated Kv4.2 in the Mouse Brain. Learn. Mem., 7, 321-332.

Varoqueaux, F., Jamain, S. & Brose, N. (2004) Neuroligin 2 is exclusively localized to inhibitory synapses. Eur. J. Cell Biol., 83, 449-456.

Vicini, S., Ferguson, C., Prybylowski, K., Kralic, J., Morrow, A.L. & Homanics, G.E. (2001) GABA(A) receptor alpha1 subunit deletion prevents developmental changes of inhibitory synaptic currents in cerebellar neurons. J. Neurosci., 21, 3009-3016.

von Kriegstein, K. & Schmitz, F. (2003) The expression pattern and assembly profile of synaptic membrane proteins in ribbon synapses of the developing mouse retina. Cell Tissue Res., 311, 159-173.

Wang, K., Lin, M.T., Adelman, J.P. & Maylie, J. (2014) Distinct Ca2+ sources in dendritic spines of hippocampal CA1 neurons couple to SK and Kv4 channels. Neuron, 81, 379-387.

Watanabe, S., Hoffman, D.A., Migliore, M. & Johnston, D. (2002) Dendritic K+ channels contribute to spike-timing dependent long-term potentiation in hippocampal pyramidal neurons. Proc. Natl. Acad. Sci. U. S. A., 99, 8366-8371.

Wei, W., Zhang, N., Peng, Z., Houser, C.R. & Mody, I. (2003) Perisynaptic localization of delta subunit-containing GABA(A) receptors and their activation by GABA spillover in the mouse dentate gyrus. J. Neurosci., 23, 10650-10661.

Wickman, K., Karschin, C., Karschin, A., Picciotto, M.R. & Clapham, D.E. (2000) Brain localization and behavioral impact of the G-protein-gated K+ channel subunit GIRK4. J. Neurosci., 20, 5608-5615.

Wilson-Shaw, D., Robinson, M., Gambarana, C., Siegel, R.E. & Sikela, J.M. (1991) A novel gamma subunit of the GABAA receptor identified using the polymerase chain reaction. FEBS Lett., 284, 211-215.

Wisden, W., Laurie, D.J., Monyer, H. & Seeburg, P.H. (1992) The distribution of 13 GABAA receptor subunit mRNAs in the rat brain. I. Telencephalon, diencephalon, mesencephalon. J. Neurosci., 12, 1040-1062.

Wulff, P., Goetz, T., Leppa, E., Linden, A.M., Renzi, M., Swinny, J.D., Vekovischeva, O.Y., Sieghart, W., Somogyi, P., Korpi, E.R., Farrant, M. & Wisden, W. (2007) From synapse to behavior: rapid modulation of defined neuronal types with engineered GABAA receptors. Nat. Neurosci., 10, 923-929.

Yu, F.H. & Catterall, W.A. (2004) The VGL-chanome: a protein superfamily specialized for electrical signaling and ionic homeostasis. Sci. STKE, 2004, re15.

Yu, F.H., Yarov-Yarovoy, V., Gutman, G.A. & Catterall, W.A. (2005) Overview of molecular relationships in the voltage-gated ion channel superfamily. Pharmacol. Rev., 57, 387-395.

Yuan, L.L., Adams, J.P., Swank, M., Sweatt, J.D. & Johnston, D. (2002) Protein kinase modulation of dendritic K+ channels in hippocampus involves a mitogen-activated protein kinase pathway. J. Neurosci., 22, 4860-4868.

Zhang, D., Pan, Z.H., Awobuluyi, M. & Lipton, S.A. (2001) Structure and function of GABA(C) receptors: a comparison of native versus recombinant receptors. Trends Pharmacol. Sci., 22, 121-132.

DOI:10.14753/SE.2015.1809

10. LIST OF OWN PUPLICATIONS

Publications that formed the basis of the dissertation:

Kerti-Szigeti K., Nusser Z., Eyre M.D. (2014) Synaptic clustering without the γ2 subunit. J. Neurosci., 34: 10219-10233.

Kirizs T., **Kerti-Szigeti K.**, Lorincz A., Nusser Z. (2014) Distinct axo-somato-dendritic distributions of three potassium channels in CA1 hippocampal pyramidal cells. Eur. J. Neurosci., 39: 1771-1783.

Kerti K, Lorincz A, Nusser Z. (2012) Unique somato-dendritic distribution pattern of K_V4.2 channels on hippocampal CA1 pyramidal cells. Eur. J. Neurosci., 35: 66-75.

Other publications:

Eyre MD, **Kerti K**, Nusser Z.s (2009) Molecular diversity of deep short-axon cells of the rat main olfactory bulb. Eur. J. Neurosci., 29: 1397-1407.

DOI:10.14753/SE.2015.1809

11. ACKNOWLEDGEMENTS

I would like to thank my supervisor, Prof. Zoltán Nusser for giving me the opportunity to join his research group, and work in a stimulating atmosphere during my graduate years. He provided a good example of precision and perseverance in science; his patient guidance enabled me to complete my work successfully. I am extremely indebted to Dr. Andrea Lőrincz for introducing me in the beauty of the 'SDS-digested freeze-fracture replica labelling' method and for her continuous advice during my work. I would like to express my special thanks to Dr. Mark D. Eyre for his altruistic support during our longstanding collaborations.

I thank all my colleagues in the Laboratory of Cellular Neurophysiology, Dr. Noémi Holderith, Dr. Máté Sümegi, Dr. Nóra Lenkey, Dr. Tekla Kirizs, Dr. Timea Szabadi and Miklós Szoboszlay for providing a motivating environment. I am thankful to Éva Dóbai, Bence Kókay and Dóra Rónaszéki for their technical assistance during many years.

I am grateful to my parents for their support in my choice, and last but not least, to my husband András, for his patience, understanding and unceasing support.